

Magnetic structure and phase formation of magnetocaloric Mn-Fe-P-X compounds

PROEFSCHRIFT

ter verkrijging van de graad van doctor

aan de Technische Universiteit Delft,

op gezag van de Rector Magnificus prof. ir. K.C.A.M. Luyben,

voorzitter van het College voor Promoties,

in het openbaar te verdedigen op woensdag 10 juli 2013 om 10:00 uur

door

Zhiqiang Ou

Master of Science in Condensed Matter Physics, Inner Mongolia Normal University

geboren te Inner Mongolia, China

Dit proefschrift is goedgekeurd door de promotor:

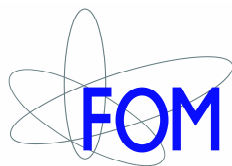
Prof. dr. E. H. Brück

Copromotor: Dr. ir. N. H. van Dijk

Samenstelling promotiecommissie:

Rector Magnificus,	voorzitter
Prof. dr. E. H. Brück,	Technische Universiteit Delft, promotor
Dr. ir. N. H. van Dijk,	Technische Universiteit Delft, copromotor
Prof. dr. F. M. Mulder,	Technische Universiteit Delft
Prof. dr. R.A. de Groot,	Radboud University Nijmegen
Prof. dr. K. H. J. Buschow,	University of Amsterdam
Prof. dr. O. Tegusi,	Inner Mongolia Normal Univerisity
Prof. dr. P. Nordblad,	Uppsala university
Prof. dr. P. Dorenbos,	Technische Universiteit Delft, reservelid

The work presented in this PhD thesis is financially supported by the Foundation for Fundamental Research on Matter (FOM), the Netherlands, via the Industrial Partnership Program IPP I18 and co-financed by BASF Future Business, carried out at the section of Fundamental Aspects of Materials and Energy, Faculty of Applied Sciences, Delft University of Technology (TUD).



ISBN: 978-90-8891-667-0

Copyright © 2013 by Zhiqiang Ou

Published by: Uitgeverij BOXPress, 's-Hertogenbosch

Dedicated to my wife Juanjuan and my parents

Contents

Chapter 1 Introduction	1
1.1 Magnetocaloric effect and magnetic refrigeration	1
1.2 Magnetocaloric materials	2
1.3 Thesis outline	3
References	4
Chapter 2 Theoretical aspects	7
2.1 Thermodynamics.....	7
2.2 Bean-Rodbell model.....	8
2.3 Determination of the magnetic entropy change	10
2.4 Magnetic neutron diffraction.....	11
References	14
Chapter 3 Experimental	17
3.1 Introduction	17
3.2 Sample preparation.....	17
3.2.1 High-energy ball-milling	17
3.2.2 Melt-spinning technique.....	19
3.3 Sample characterization and magnetization measurements	19
3.3.1 X-ray powder diffraction.....	19
3.3.2 Neutron powder diffraction.....	20
3.3.3 SQUID magnetometer.....	20
3.3.4 Differential scanning calorimeter.....	21
References	21
Chapter 4 Interstitial boron in MnFe(P,As) giant-magnetocaloric alloy	23
4.1 Introduction	23
4.2 Materials and methods	24
4.3 X-ray diffraction results	24

4.4 Magnetic properties and magnetocaloric effect	26
4.5 Conclusions	30
References	30
Chapter 5 Transition metal substitution in Fe₂P-based MnFe_{0.95}P_{0.50}Si_{0.50}	
magnetocaloric compounds	33
5.1 Introduction	33
5.2 Sample preparation.....	34
5.3 Structural, magnetic and magnetocaloric properties	35
5.3.1 MnFe _{0.95-x} Co _x P _{0.50} Si _{0.50} compounds	35
5.3.2 Mn _{1-y} Co _y Fe _{0.95} P _{0.50} Si _{0.50} compounds	37
5.3.3 (Mn,Fe,Ni) _{1.95} P _{0.50} Si _{0.50} and (Mn,Fe,Cu) _{1.95} P _{0.50} Si _{0.50} compounds	41
5.4 Discussion	42
5.5 Summary	43
References	44
Chapter 6 Structure, magnetism and magnetocalorics of Fe-rich (Mn,Fe)_{1.95}P_{1-x}Si_x	
melt-spun ribbons.....	47
6.1 Introduction	47
6.2 Sample preparation.....	48
6.3 Structure and phase formation.....	48
6.4 Magnetism and magnetocaloric effect	52
6.5 Conclusions	56
References	57
Chapter 7 Structure, magnetism and magnetocalorics of Fe-rich Mn_{1.95-x}Fe_xP_{2/3}Si_{1/3}	
compounds	59
7.1 Introduction	59
7.2 Sample preparation.....	60
7.3 Structure and phase formation.....	60
7.4 Magnetism and magnetocaloric effect	63
7.5 Conclusions	66
References	67
Chapter 8 Neutron diffraction study on the magnetic structure of Fe₂P-based	
(Mn,Fe)_{1.95}P_{1-x}Si_x melt-spun ribbons	69
8.1 Introduction	69

8.2 Experimental details	70
8.3 Structural parameters.....	70
8.4 Alignment of magnetic moment.....	73
8.5 Valence state and interatomic distances.....	77
8.6 Conclusions	81
References	81
Chapter 9 Neutron diffraction study on the Fe₂P-type Mn_{1.95-x}Fe_xP_{2/3}Si_{1/3} compounds	83
9.1 Introduction	83
9.2 Experimental details.....	84
9.3 Structural parameters.....	85
9.4 Alignment of magnetic moment.....	87
9.5 Influence of site disorder on the stability of the crystal structure	93
9.6 Conclusions	93
References	94
Summary	97
Samenvatting	100
List of publications	103
Acknowledgements.....	105
Curriculum Vitae	107

Chapter 1

Introduction

1.1 Magnetocaloric effect and magnetic refrigeration

The magnetocaloric effect (MCE) is defined as the thermal response of a magnetic material due to the application of a magnetic field [1, 2]. Modern society shows a large interest in using the MCE as an alternative technology for the conventional vapor-compression refrigeration, as ~15% of the total world wide energy consumption involves the use of refrigeration (air conditioning, refrigeration, freezing, chilling, etc.) [3].

Magnetic refrigeration is based on the MCE, which was discovered in pure nickel in 1917 by P. Weiss and A. Piccard [4]. Compared to the conventional vapor-compression, the major differences are: (i) that magnetic refrigeration employs a solid refrigerant instead of gases, (ii) magnetic refrigeration is an environmentally friendly technology since it eliminates ozone depleting gases, reduces the need for global warming greenhouse effect gases, and other hazardous gaseous refrigerants. Besides, it has been indicated that the cooling efficiency in magnetic refrigerants can reach a theoretical limit of 60%, compared to only 40% in gas-compression refrigerators [5]. The schematic demonstration of a magnetic refrigeration cycle is shown in Figure 1.1.

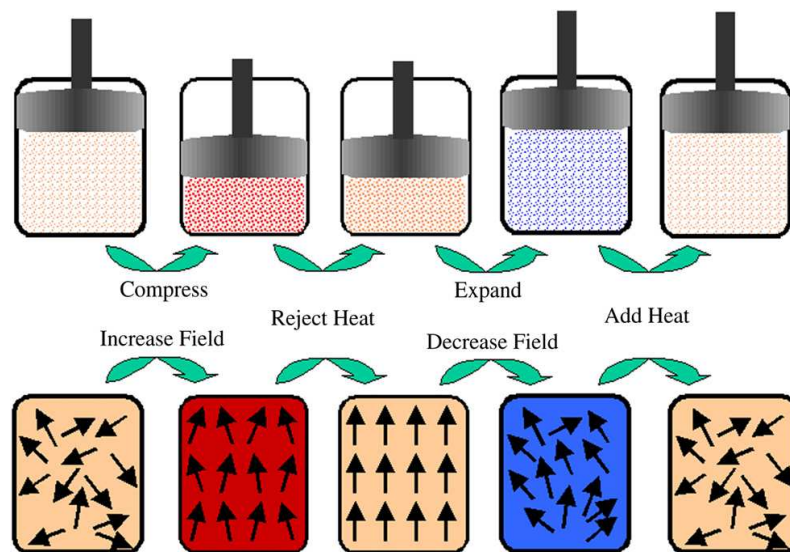


Figure 1.1 Schematic demonstration of a magnetic refrigeration cycle, which is analogous to the conventional vapor-compression cycle [3].

1.2 Magnetocaloric materials

Magnetocaloric materials are essential to the magnetic refrigeration. Among all the magnetocaloric materials, Fe₂P-based Mn-Fe-P-Si compounds show the most promising properties for magnetic refrigeration applications.

In 1926 Debye [6] and 1927 Giauque [7] proposed independently that the MCE could be used to achieve ultra-low temperatures below 1 K. Later in 1933, Giauque and MacDougall demonstrated the first operating adiabatic demagnetization refrigerator that reached 0.25 K [8]. The material they used was the paramagnetic salt (Gd₂(SO₄)₃·8H₂O). In 1976, Brown [9] constructed a magnetic heat pump operating at room temperature using the rare-earth metal Gd.

In 1997 Pecharsky and Gschneidner [10] discovered that Gd₅Ge₂Si₂ behaves as a giant MCE material, pointing people's attention into magnetic refrigeration. Since then, several magnetocaloric materials were reported, most prominent are MnAs_{1-x}Sb_x [11], La(Fe_{1-x}Si_x)₁₃ and their hydrides [12, 13], MnFeP_{1-x}As_x [14], Ni_{0.50}Mn_{0.50-x}Sn_x [15] and MnCoGeB_x [16]. All these materials show a large MCE due to the first-order nature of their phase transitions. Some other factors that need to be addressed, to achieve magnetic refrigeration, are thermal/field hysteresis, thermal/electrical conductivity, corrosion resistance, mechanical properties, etc.

1.3 Thesis outline

The work presented in this thesis is a study of the crystal and magnetic structure, the magnetocaloric effect and related physical properties in the Mn-Fe-P-X compounds.

In Chapter 2, some theoretical aspects of the MCE are discussed. The phenomenological Bean-Rodbell model, that is commonly used to describe first-order phase transitions, is briefly introduced. Also the magnetic form factor, which is relevant for Chapter 8 and Chapter 9, is introduced.

In Chapter 3, a short review is given on experimental techniques used for the sample preparation, the structural characterization and the determination of the magnetic properties.

In Chapter 4, it is shown that boron atoms in the Mn-Fe-P-As system occupy interstitial rather than substitutional positions. The effects of interstitial boron on T_C and the magnetic moments in the Mn-Fe-P-As system are described. The influence on the magnetocaloric properties is also discussed.

In Chapter 5, the effect of the transition metal substitution with Co, Ni and Cu on the $\text{MnFe}_{0.95}\text{P}_{0.5}\text{Si}_{0.5}$ compound has been studied. Due to the different magnetic behaviors on the $3g$ and $3f$ layers, substitution for Mn($3g$) or Fe($3f$) atoms results in a rather different behavior on the thermal and/or field hysteresis, although the ferromagnetic ordering temperature reduces in all the cases.

In Chapter 6, the tuneability of the thermal hysteresis in Fe-rich alloys is addressed. By varying the non-metal P/Si ratio, a small thermal hysteresis is achieved, while retaining a large MCE. Besides, the structure, magnetism and magnetocaloric effect of Fe-rich $(\text{Mn,Fe})_{1.95}\text{P}_{1-x}\text{Si}_x$ melt-spun ribbons were systematically studied.

In Chapter 7, a phase diagram of the crystal structure and magnetic transition as a function of temperature and Fe content for the $\text{Mn}_{1.95-x}\text{Fe}_x\text{P}_{2/3}\text{Si}_{1/3}$ compounds has been established. The magnitude of the thermal hysteresis and the magnitude of the relative lattice parameter changes $|\Delta a/a|$ and $|\Delta c/c|$ at the transition appear to be correlated.

In Chapter 8, high-resolution neutron diffraction has been employed to determine the crystal and magnetic structure, the magnetic moment and the interatomic distances in the $\text{Mn}_{0.66}\text{Fe}_{1.29}\text{P}_{1-x}\text{Si}_x$ melt-spun ribbons. With increasing Si content, the alignment of the

magnetic moment has changed from the c -axis towards the a - b plane. The magnetic moment on both the $3g$ and $3f$ sites slightly decrease with increasing Si content from $x = 0.34$ to 0.42 .

Chapter 9 is dedicated to the effect of varying the Mn/Fe ratio in the $\text{Mn}_{1.95-x}\text{Fe}_x\text{P}_{2/3}\text{Si}_{1/3}$ compounds using high-resolution neutron diffraction. For increasing iron content, the magnetic moment at the pyramidal $3g$ site is unaffected (about $2.8 \mu_B$), while the magnetic moment on the tetrahedral $3f$ site is gradually reduced from $1.6 \mu_B$ for $x = 1.0$ to $0.9 \mu_B$ for $x = 1.4$. The development of the magnetic moment and microstrain for decreasing Mn/Fe ratio in the system is discussed based on the changes in the interlayer, intralayer and interatomic distances.

References

- [1] A.M. Tishin and Y.I. Spichkin, *The magnetocaloric effect and its application*, Institute of Physics Publishing, Bristol (2003).
- [2] K.A. Gschneidner and V.K. Pecharsky, Magnetocaloric materials, *Annual Review of Materials Science* 30 (2000) 387-429.
- [3] S.L. Russek and C.B. Zimm, Potential for cost effective magnetocaloric air conditioning systems, *International Journal of Refrigeration* 29 (2006) 1366-1373.
- [4] P. Weiss and A. Piccard, Le phénomène magnétocalorique, *Journal de Physique Théorique et Appliquée* 7 (1917) 103-109.
- [5] C. Zimm, A. Jastrab, A. Sternener, V. Pcharpreky, K. Gschneidner, M. Osborne and I. Anderson, Description and performance of a near-room temperature magnetic refrigerator, *Advances in Cryogenic Engineering* 43 (1998) 1759-1766.
- [6] P. Debye, Some observations on magnetisation at a low temperature, *Annalen Der Physik* 81 (1926) 1154-1160.
- [7] W.F. Giaque, A thermodynamic treatment of certain magnetic effects. A proposed method of producing temperatures considerably below 1° absolute, *Journal of the American Chemical Society* 49 (1927) 1864-1870.
- [8] W.F. Giaque and D.P. MacDougall, Attainment of temperatures below 1 degrees absolute by demagnetization of $\text{Gd}_2(\text{SO}_4)_3 \cdot 8\text{H}_2\text{O}$, *Physical Review* 43 (1933) 768-768.
- [9] G.V. Brown, Magnetic heat pumping near room temperature, *Journal of Applied Physics* 47 (1976) 3673-3680.

-
- [10] V.K. Pecharsky, K.A. Gschneidner, Giant magnetocaloric effect in $\text{Gd}_5(\text{Si}_2\text{Ge}_2)$, *Physical Review Letters* 78 (1997) 4494-4497.
- [11] H. Wada and Y. Tanabe, Giant magnetocaloric effect of $\text{MnAs}_{1-x}\text{Sb}_x$, *Applied Physics Letters* 79 (2001) 3302-3304.
- [12] F.X. Hu, B.G. Shen, J.R. Sun, Z.H. Cheng, G.H. Rao and X.X. Zhang, Influence of negative lattice expansion and metamagnetic transition on magnetic entropy change in the compound $\text{LaFe}_{11.4}\text{Si}_{1.6}$, *Applied Physics Letters* 78 (2001) 3675-3677.
- [13] A. Fujita, S. Fujieda, Y. Hasegawa and K. Fukamichi, Itinerant-electron metamagnetic transition and large magnetocaloric effects in $\text{La}(\text{Fe}_x\text{Si}_{1-x})_{13}$ compounds and their hydrides, *Physical Review B* 67 (2003) 104416.
- [14] O. Tegus, E. Brück, K.H.J. Buschow and F.R. de Boer, Transition-metal-based magnetic refrigerants for room-temperature applications, *Nature* 415 (2002) 150-152.
- [15] T. Krenke, E. Duman, M. Acet, E.F. Wassermann, X. Moya, L. Manosa and A. Planes, Inverse magnetocaloric effect in ferromagnetic Ni-Mn-Sn alloys, *Nature Materials* 4 (2005) 450-454.
- [16] N.T. Trung, L. Zhang, L. Caron, K.H.J. Buschow and E. Brück, Giant magnetocaloric effects by tailoring the phase transitions, *Applied Physics Letters* 96 (2010) 172504.

Chapter 2

Theoretical aspects

2.1 Thermodynamics

Generally, the Gibbs free energy G is used to describe the magnetocaloric properties of magnetic systems [1]. In a system with a magnetic material in an external magnetic field B under a pressure p , the Gibbs free energy G is given by:

$$G = U - TS + pV - MB \quad (2.1)$$

where U is the internal energy of the system, T the absolute temperature, S the entropy, M the magnetization of the magnetic material and V the volume.

Correspondingly, the total differential of G can be written as:

$$dG = Vdp - SdT - MdB \quad (2.2)$$

For the Gibbs free energy G , the internal parameters M , S , V and (generalized thermodynamic quantities), conjugated to the external variables T , B and p , can be determined by the following equations of state:

$$V(T, B, p) = \left(\frac{\partial G}{\partial p} \right)_{T, B} \quad (2.3a)$$

$$S(T, B, p) = - \left(\frac{\partial G}{\partial T} \right)_{B, p} \quad (2.3b)$$

$$M(T, B, p) = - \left(\frac{\partial G}{\partial B} \right)_{T, p} \quad (2.3c)$$

Using the second law of thermodynamics, the specific heat C_p can be represented as

$$C_p(T, B) = T \left(\frac{\partial S}{\partial T} \right)_{B, p} \quad (2.4)$$

2.2 Bean-Rodbell model

Bean and Rodbell proposed a model to describe the magneto-structural first-order phase transition in MnAs [2, 3]. The framework of the model was extended to explain the first-order phase transitions occurring in $\text{MnFeP}_{1-x}\text{As}_x$ [4, 5], $\text{Gd}_5(\text{Ge}_{1-x}\text{Si}_x)_4$ [6], $\text{MnAs}_{1-x}\text{Sb}_x$ [7, 8] and $\text{LaFe}_{13-x}\text{Si}_x$ [9] compounds. The Bean-Rodbell model is based on the molecular-field approximation. The central consideration of the model is that the exchange interaction parameter (or the Curie temperature) is a strong function of lattice spacing. In this model, the dependence of the Curie temperature on the volume is described as:

$$T_C = T_0 \left(1 + \beta \frac{V - V_0}{V_0} \right) \quad (2.5)$$

where T_C is the Curie temperature, T_0 the Curie temperature in the absence of deformation, β the slope of the Curie temperature dependence on the lattice deformation and can be positive or negative, V the equilibrium volume and V_0 the volume in the absence of exchange interactions.

In the molecular field approximation, the Gibbs free energy for a magnetic system, consists of the exchange interaction, the elastic energy and the Zeeman energy, and is described as:

$$G(T, B) = -\frac{3}{2} \left(\frac{J}{J+1} \right) N k_B T_C \sigma^2 + \frac{1}{2K} \left(\frac{V - V_0}{V_0} \right)^2 + P \left(\frac{V - V_0}{V_0} \right) - TS - B g \mu_B J N \sigma \quad (2.6)$$

where J is the ion total angular momentum, N the number of magnetic ions per unit volume, k_B the Boltzmann's constant, σ ($M / g \mu_B J N$) the normalized magnetization per magnetic ion, K the compressibility, S the entropy, B the external magnetic field, g the Landé factor and μ_B the Bohr magneton.

Substituting Eq. (2.5) into Eq. (2.6) and minimizing the free energy G with respect to equilibrium volume, we obtain:

$$\frac{V - V_0}{V_0} = \frac{3}{2V_0} \frac{J}{J(J+1)} N k_B \beta K T_0 \sigma^2 - PK + \alpha T \quad (2.7)$$

where α is the coefficient of thermal expansion.

Substituting Eq. (2.5) and Eq. (2.7) into Eq. (2.6), and minimizing the free energy G with respect to σ , the magnetic state equation is obtained:

$$\sigma = B_J(Y) = \frac{2J+1}{2J} \coth \left[\frac{(2J+1)}{2J} Y \right] - \frac{1}{2J} \coth \left(\frac{1}{2J} Y \right) \quad (2.8)$$

Where $B_J(Y)$ is the Brillouin function and [6]

$$Y = \frac{1}{T} \left[3T_0 \left(\frac{J}{J+1} \right) \sigma + \frac{g\mu_B J}{k_B} B + \frac{9}{5} \left(\frac{(2J+1)^4 - 1}{[2(J+1)]^4} \right) T_0 \eta \sigma^3 - 3 \frac{J\beta p K}{J+1} T_0 \sigma \right]$$

Here, η , involving the parameters K and β that are related to the volume change, is the parameter controlling the order of the magnetic phase transition:

$$\eta = \frac{5}{2} \frac{[4J(J+1)]^2}{[(2J+1)^4 - 1]V_0} N k_B K T_0 \beta^2 \quad (2.9)$$

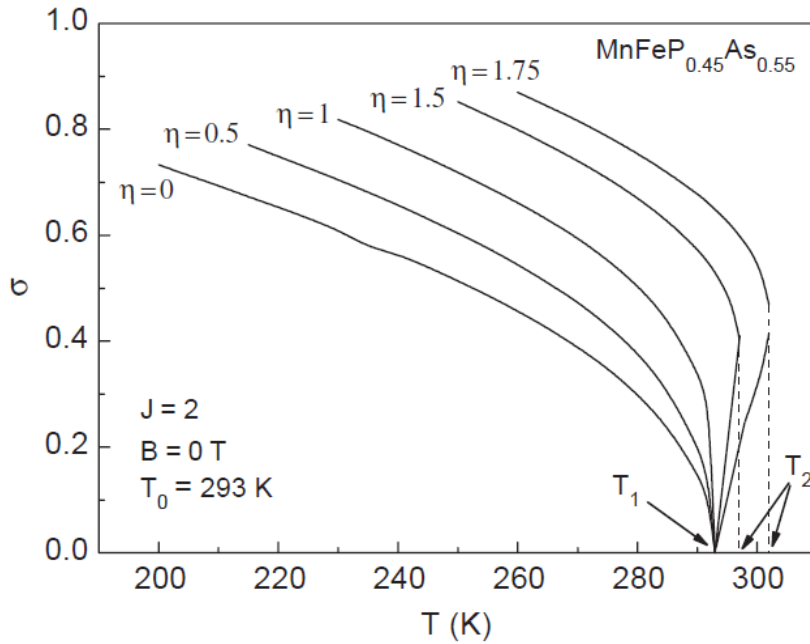


Figure 2.1 Temperature dependence of the relative magnetization of the $\text{MnFeP}_{0.45}\text{As}_{0.55}$ compound calculated in zero field with different values of parameter η . ([5])

$\eta = 1$ is the critical value to separate the first-order and the second-order phase transition [6]. Figure 2.1 shows the relative magnetization of $\text{MnFeP}_{0.45}\text{As}_{0.55}$ compound as a function of temperature, in which the $\sigma(T)$ curves have been calculated in zero field for different η values.

For $\eta < 1$, the magnetic system undergoes a second-order phase transition and the curves show a continuous change in the magnetization. For $\eta > 1$, the magnetic system undergoes a first-order phase transition and a discontinuous change occurs in the magnetization (indicated by dashed vertical lines).

2.3 Determination of the magnetic entropy change

Entropy can be changed by varying of the magnetic field, temperature and pressure for given system parameters. The magnetic entropy and its change are closely related to the MCE value and the magnetic contribution to the heat capacity.

The total entropy of a magnetic material can in general be described as:

$$S(T, B, p) = S_l(T, B, p) + S_e(T, B, p) + S_m(T, B, p) \quad (2.10)$$

where S_l , S_e and S_m are the lattice, electron and magnetic contributions to the total entropy, respectively.

The full differential of the total entropy of a closed system is given by

$$dS = \left(\frac{\partial S}{\partial T} \right)_{p,B} dT + \left(\frac{\partial S}{\partial p} \right)_{T,B} dp + \left(\frac{\partial S}{\partial B} \right)_{T,p} dB \quad (2.11)$$

If both the magnetization and entropy are continuous functions of the temperature and magnetic field, then the infinitesimal isobaric-isothermal magnetic entropy change can be related to the magnetization (M), the magnetic field strength (H), and the absolute temperature (T) using one of the Maxwell relations:

$$\left(\frac{\partial S_M(T, B)}{\partial B} \right)_T = \left(\frac{\partial M(T, B)}{\partial T} \right)_B \quad (2.12)$$

After integration this yields

$$\Delta S_M(T)_{\Delta B} = \int_{B_i}^{B_f} dS_M(T, B)_T = \int_{B_i}^{B_f} \left(\frac{\partial M(T, B)}{\partial T} \right)_B dB \quad (2.13)$$

From the second law of thermodynamics (2.4), the integration yields

$$S(T, B) = S_0 + \int_0^T \frac{c_p(T', B)}{T'} dT' \quad (2.14)$$

Neglecting the configurational entropy, then the entropy will be zero at $T = 0$ K. That means we can rewrite the Eq. (2.10) as

$$S(T, B) = \int_0^T \frac{c_p(T', B)}{T'} dT' \quad (2.15)$$

Therefore, the entropy change corresponding to a field change ΔB is given by

$$\Delta S(T)_{\Delta B} = \int_0^T \frac{c_p(T', B_f) - c_p(T', B_i)}{T'} dT' \quad (2.16)$$

where $c_p(T', B_f)$ and $c_p(T', B_i)$ represent the specific heat at constant pressure p in the magnetic field B_f and B_i , respectively.

Considering constant pressure, Eq. 2.6 can be rewritten as

$$dS = \left(\frac{\partial S(T, B)}{\partial T} \right)_B dT + \left(\frac{\partial S(T, B)}{\partial B} \right)_T dB \quad (2.17)$$

By combining the Eqs. 2.7, 2.9 and 2.13, the infinitesimal adiabatic ($TdS = 0$) temperature rise for the reversible adiabatic-isobaric process can be obtained

$$dT(T, B) = - \left(\frac{T}{C_p(T, B)} \right)_B \left(\frac{\partial M(T, B)}{\partial T} \right)_B dB \quad (2.18)$$

where $C_p(T, B)$ is the temperature and magnetic field dependent heat capacity at constant pressure p . The adiabatic temperature change $\Delta T_{ad}(T)_{\Delta B}$ is then found by integration of Eq. 2.14:

$$\Delta T_{ad}(T)_{\Delta B} = \int_{B_i}^{B_f} dT(T, B) = - \int_{B_i}^{B_f} \left(\frac{T}{C_p(T, B)} \right)_B \left(\frac{\partial M(T, B)}{\partial T} \right)_B dB \quad (2.19)$$

2.4 Magnetic neutron diffraction

Neutrons have zero charge and a negligible electric dipole and therefore they can easily approach the point-like atomic nuclei in a material before the nuclear scattering occurs. The rather weak interaction of neutrons with materials enables the high penetration depth and therefore is a non-destructive probe. Thermal neutrons have wavelengths of about 10^{-8} cm, which is appropriate for diffraction by an atomic or molecular lattice [10, 11].

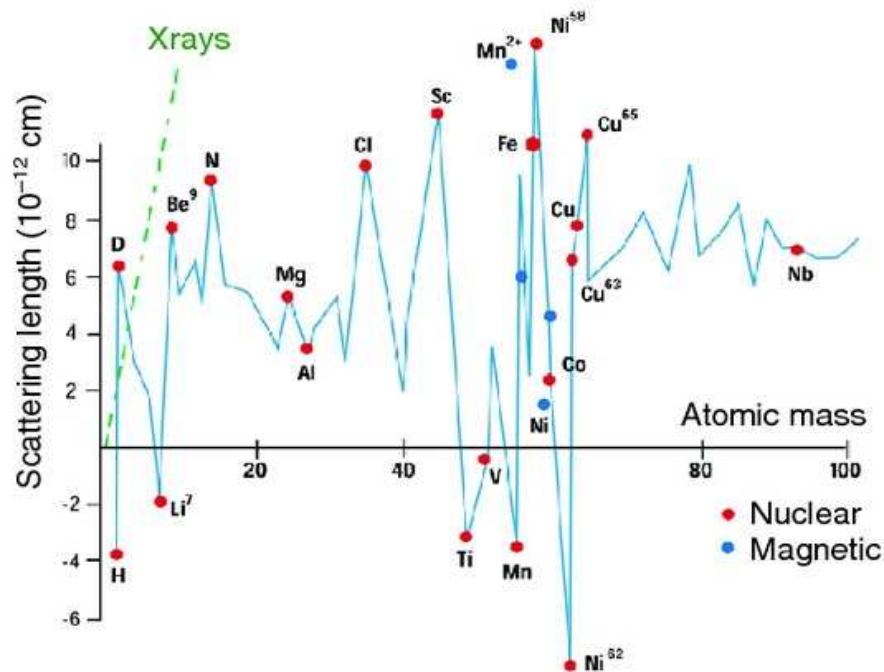


Figure 2.2 Atomic coherent scattering length for thermal neutrons, the dashed line shows the corresponding trend for X-ray scattering. A much smaller contrast is observed from one atom to the following atom in the periodic table using X-rays [11].

Neutron diffraction, based on constructive elastic neutron scattering, is a powerful tool for studying the atomic and/or magnetic structure of a material. The technique is similar to X-ray diffraction but the different type of radiation gives complementary information due to a difference in sensitivity. The scattering length varies from isotope to isotope rather than linearly with the atomic number. The atomic coherent scattering length as a function of atomic mass for thermal neutrons is shown in Figure 2.2. A major difference from X-rays is that the scattering is mostly due to the tiny nuclei of the atoms. As a result, there is no need for an atomic form factor for the nuclear scattering of neutrons in contrast to X-rays. Therefore, the neutron diffraction peaks at high angles still show a relatively high intensity, particularly if the experiment is done at low temperatures [12].

In magnetic neutron scattering, the interaction is between the spin moment of the neutron and the magnetic moments of unpaired electrons and nuclei. Considering the size of the magnetic moment distribution of the electrons, it is comparable to the wavelength of thermal neutrons and thus an angle-dependent magnetic form factor is caused due to the interference. Figure 2.3 shows the magnetic form factor of the Mn^{2+} atom as a function of the inverse d -spacing. The magnetic form factor for neutron diffraction falls off rapidly with angle like X-rays. The magnetic form factor can be calculated from theoretical electron densities, or

determined experimentally [13]. Note that, the magnetic form factor also depends on the valence state of the atom or ion as it defines the radial extends of the moment distribution.

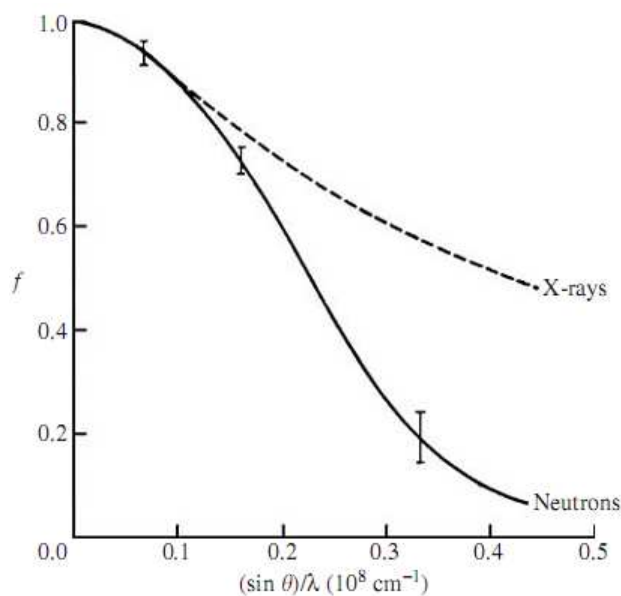


Figure 2.3 The magnetic neutron form factor of Mn^{2+} compared with the (normalized) X-ray form factor [12] as a function of $\text{Sin}\theta/\lambda$.

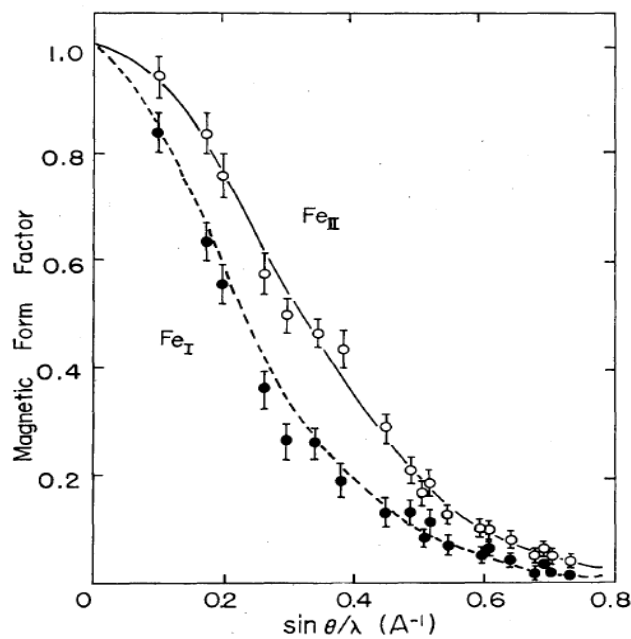


Figure 2.4 Magnetic form factor of $\text{Fe}_I(3f)^0$ and $\text{Fe}_{II}(3g)^{4+}$ atoms as a function of $\text{Sin}\theta/\lambda$ obtained from polarized neutron diffraction [14]. The dashed curve is a spherical form factor for free Fe atom state calculated by Watson and Freeman, the full curve is a calculated one for Fe^{4+} atom state by Watson and Freeman [15].

Figure 2.4 shows the difference in magnetic form factor between Fe^0 and Fe^{4+} ions. In magnetic scattering, the cross section is sensitive to the orientation and the size of the atomic magnetic moment and the scattering vector as the neutrons only scatter from the moment component oriented perpendicular to the wave vector transfer \vec{Q} . This allows us to determine the magnetic structures from the intensities of magnetic neutron diffraction peaks [16].

References

- [1] A.M. Tishin and Y.I. Spichkin, *The magnetocaloric effect and its application*, Institute of Physics Publishing, Bristol (2003).
- [2] C.P. Bean and D.S. Rodbell, Magnetic disorder as a first-order phase transformation, *Physical Review*, 126 (1962) 104-115.
- [3] R.W. de Blois and D.S. Rodbell, Magnetic first-order phase transition in single-crystal MnAs, *Physical Review* 130 (1963) 1347-1360.
- [4] R. Zach, M. Guillot and J. Tobola, Semiquantitative analysis of magnetic phase transitions in the $\text{MnFeP}_{1-x}\text{As}_x$ series of compounds, *Journal of Applied Physics* 83 (1998) 7237-7239.
- [5] O. Tegus, G.X. Lin, W. Dagula, B. Fuquan, L. Zhang, E. Brück, F.R. de Boer and K.H.J. Buschow, A model description of the first-order phase transition in $\text{MnFeP}_{1-x}\text{As}_x$, *Journal of Magnetism and Magnetic Materials* 290 (2005) 658-660.
- [6] P.J. von Ranke, N.A. de Oliveira and S. Gama, Understanding the influence of the first-order magnetic phase transition on the magnetocaloric effect: application to $\text{Gd}_5(\text{Si}_x\text{Ge}_{1-x})_4$, *Journal of Magnetism and Magnetic Materials* 277 (2004) 78-83.
- [7] P.J. von Ranke, N.A. de Oliveira and S. Gama, Theoretical investigations on giant magnetocaloric effect in $\text{MnAs}_{1-x}\text{Sb}_x$, *Physics Letters A* 320 (2004) 302-306.
- [8] P.J. von Ranke, S. Gama, A.A. Coelho, A. de Campos, A.M.G. Carvalho, F.C.G. Gandra and N.A. de Oliveira, Theoretical description of the colossal entropic magnetocaloric effect: Application to MnAs, *Physical Review B*, 73 (2006) 014415.
- [9] L. Jia, J.R. Sun, H.W. Zhang, F.X. Hu, C. Dong and B.G. Shen, Magnetovolume effect in intermetallics $\text{LaFe}_{13-x}\text{Si}_x$, *Journal of Physics: Condensed Matter*, 18 (2006) 9999-10007.
- [10] *Neutron scattering for magnetic materials*, Elsevier B.V., Edited by T. Chatterji (2006).
- [11] *Nanoscale Magnetic Materials and Applications*, Springer Publishing, US, Edited by J.P. Liu, E. Fullerton, O. Gutfleisch and D.J. Sellmyer, Chapter 5 (2009) 123-157.

- [12] E.H. Kisi and C.J. Howard, *Applications of neutron powder diffraction*, Oxford Science publications, Chapter 1 and 2 (2008) 1-64.
- [13] H. Fujii, S. Komura, T. Takeda, T. Okamoto, Y. Ito, J. Akimitsu, Polarized neutron diffraction study of Fe₂P single crystal, *Journal of the Physical Society of Japan*, 46 (1979) 1616-1621.
- [14] R.E. Watson, A.J. Freeman, Hartree-Fock atomic scattering factors for iron transition series, *Acta Crystallographica*, 14 (1961) 27-37.
- [15] M.R. Yearian and R. Hofstadter, Magnetic form factor of the neutron, *Physical Review*, 110 (1958) 552-564.
- [16] J. Rodriguez-Carvajal, Recent advances in magnetic-structure determination by neutron powder diffraction, *Physica B* 192 (1993) 55-69.

Chapter 3

Experimental

3.1 Introduction

The materials presented in this thesis were prepared at the section Fundamental Aspects of Materials and Energy (FAME), Faculty of Applied Sciences, Delft University of Technology (TU Delft). Most of the structural and the magnetic characterizations were carried out at FAME, such as X-ray diffraction (XRD), magnetization measurements using Superconducting Quantum Interference Device (SQUID) magnetometer, Differential Scanning Calorimetry (DSC) measurements. The neutron diffraction measurements were carried out outside FAME. A brief description on sample preparation and characterizations is given in this chapter.

3.2 Sample preparation

3.2.1 High-energy ball-milling

A ball mill, a type of grinder, is used in grinding (or mixing) materials. During the milling process solid-state reactions are initiated through repeated deformation, cold welding and fracture of the raw powder particles.

Vibratory ball mill: The vibratory ball mill and its cross section are shown in Figure 3.1 [1, 2]. The device consists of a stainless-steel jar with a hardened-steel bottom, the central part of which is a tungsten-carbide disk. Inside the vial, a single hardened-steel ball

with a diameter of 6 cm and weight of 800 g is kept in motion by a water-cooled vibrating frame. The vacuum of the system is less than 10^{-6} mbar. The vibration amplitude and the milling time can be adjusted. The materials presented in Chapter 4 were prepared by using this mill.

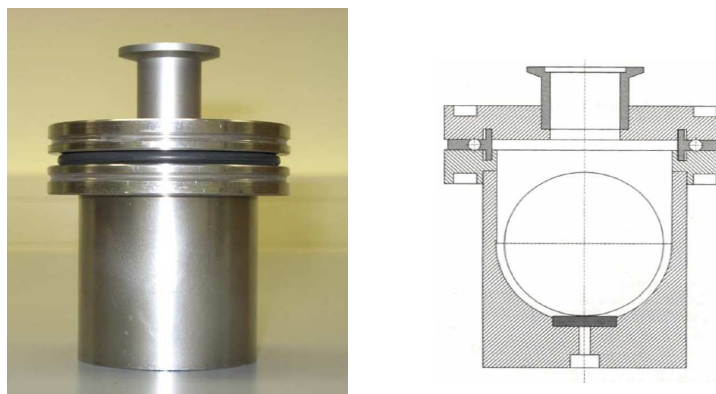


Figure 3.1 Ball mill and its cross section picture.

Planetary ball mill: A PULVERISETTE 5 *classic line* planetary ball mill has also been employed for the sample synthesis [3]. The schematic drawing of the planetary ball mill is shown in Figure 3.2 [4]. 15 grinding balls (10 mm diameter and 4 g each) and a typical amount of 15 gram starting materials with appropriate proportions were mixed. During the milling process, the sample material is primarily crushed by the high-energy impact of grinding balls together with friction between the balls and the wall of the grinding bowl. The grinding bowls with material and balls rotate around their own axis on a counter-rotating supporting disc. The centrifugal forces caused by the double rotation of the grinding bowls and supporting discs work on the contents of the grinding bowls. The force, which can reach 10 times the earth's gravitational force, causes the rotating balls to crash against the inside wall of the bowl and thus crushing the material. The grinding process take place in an argon gas atmosphere with the adjustable rotation speed (30 - 400 rpm) and milling time. The materials presented in Chapter 5, 7 and 9 were prepared by using this mill.

The obtained fine powder was then pressed into small tablets and sealed in quartz ampoules with an Ar gas atmosphere of 200 mbar. Then, the samples were sintered at 1273/1373 K for 2 hours and annealed at 1123 K for 20 hours before being furnace cooled to room temperature.

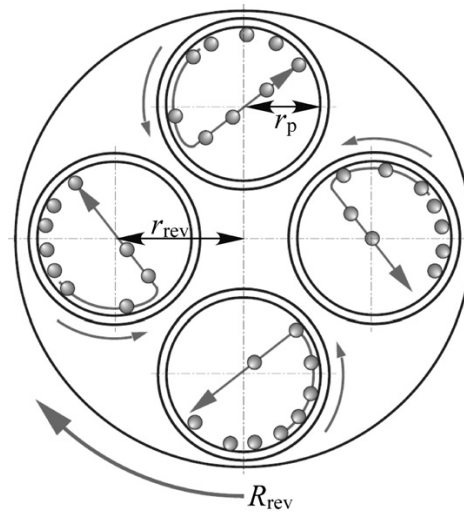


Figure 3.2 Schematic drawing of planetary ball milling. ([3])

3.2.2 Melt-spinning technique

Melt-spinning is an important technique that is used for rapid cooling of melts [5]. The melt-spinner used in this thesis is produced by the Edmund Bühler Company (Article No. 2460019) [6].

An as-cast ingot obtained by the induction-melting is inserted into a quartz tube with a nozzle. The ingot is induction melted under an Ar gas atmosphere (~ 800 mbar). By applying a pressure difference the obtained liquid is ejected through the nozzle onto the polished surface of the rotating Cu wheel, which traverses with ~ 38 m/s surface speed. In this way melt-spun ribbons are prepared. Cooling rates of $10^5 - 10^6$ K/s can be achieved, that guaranty the formation of nanocrystalline or glassy materials. The as-spun ribbons were subsequently annealed before being quenched into water at room temperature. The materials presented in Chapter 6 and 8 were prepared by this technique.

3.3 Sample characterization and magnetization measurements

3.3.1 X-ray powder diffraction

X-ray diffraction (XRD) patterns of the studied polycrystalline samples were collected using a PANalytical X-pert Pro diffractometer with Cu $K\alpha$ radiation, a secondary-beam flat-crystal monochromator and a multichannel X'celerator detector. An Anton Paar TTK450

Low-Temperature Chamber with a flat sample holder and a Pt 100 temperature sensor was employed to perform the temperature-dependent XRD measurement [7]. Short cooling and heating cycles (~80 K to 723 K) are guaranteed by the combination of the LNC Liquid Nitrogen Control Unit and the TCU 100 temperature control unit. Measurements may be carried out either under vacuum, air or inert gas. The X-ray diffraction patterns were analyzed by means of the Rietveld method [8] using the Fullprof program [9].

3.3.2 Neutron powder diffraction

Neutron diffraction data were collected at the Bragg Institute of the Australian Nuclear Science and Technology Organization (ANSTO) on the ECHIDNA high-resolution powder diffractometer [10] with an incident wavelength of 1.622 Å and at the Institut Laue-Langevin (ILL) on the D2B high-resolution powder diffractometer [11] with an incident wavelength of 1.595 Å. The sample powder was contained in a vanadium can which was mounted in an Orange cryostat. The measurements were carried out at fixed temperatures between 5 and 400 K in zero field. The crystal and magnetic structure were obtained by means of the Rietveld method [8] using the Fullprof program [9].

3.3.3 SQUID magnetometer

Magnetic measurements were carried out using superconducting quantum interference devices (SQUID) MPMS-XL and MPMS-5S magnetometer. The temperature range is from 1.7 to 400 K and the applied magnetic field up to 5 T. The lowest temperature of 1.7 K can be reached by continuous pumping on a capillary connected to the liquid helium (LHe) reservoir.

All samples were inserted in a gelatin capsule and mounted in a plastic straw with diamagnetic contribution of the order of 10^{-8} Am² in 1 T external magnetic field. Since the SQUID utilizes an extremely sensitive detection system, the smallest moments that can be detected are 10^{-12} Am², the largest 10^3 Am², with an accuracy of 0.1 % [12]. Thus, for a magnetic material with strong magnetic signal, like ferromagnetic materials, the empty-sample holder signal can be ignored; for a magnetic material with weak signal, like diamagnetic materials, the sample holder was measured separately and the contribution is subtracted from the total magnetization.

3.3.4 Differential scanning calorimeter

The differential scanning calorimetry (DSC) measurements were carried out using a TA-Q2000 instrument (TA Instrument Company) equipped with a liquid nitrogen cooling system. Employing the so-called Tzero™ DSC technology, this equipment allows to measure the heat capacity and latent heat directly with a high precision.

The heat flux was measured as a function of temperature. The temperatures can vary from 90 to 820 K, with variable temperature sweep rates. The sweep rate selected for the measurements in this thesis is 20 K/min.

References

- [1] H. Bakker, G.F. Zhou and H. Yang, Mechanically driven disorder and phase-transformations in alloys, *Progress in Materials Science* 39 (1995) 159-241.
- [2] H.L. Castricum, *Mechanically induced chemical and structural changes in materials*, PhD thesis, University of Amsterdam 2001.
- [3] <http://www.fritsch.de/Produkt/mahlen/planetenmuehlen/pulverisette-54-classic-line>.
- [4] K. Asano, H. Enoki and E. Akiba, Synthesis of HCP, FCC and BCC structure alloys in the Mg-Ti binary system by means of ball milling, *Journal of Alloys and Compounds* 480 (2009) 558-563.
- [5] A. Yan, K.H. Müller, L. Schultz and O. Gutfleisch, Magnetic entropy change in melt-spun MnFePGe, *Journal of Applied Physics* 99 (2006) 08K903.
- [6] <http://www.edmund-buehler.de/english/i-rascherstarrungstechnologie.pml>.
- [7] http://www.anto-paar.com/Low-Temperature-Chamber-TTk-450/XRD/60_Corporate_en?product_id=134.
- [8] H.M. Rietveld, A profile refinement method for nuclear and magnetic structures. *Journal of Applied Crystallography* 2 (1969) 65-71.
- [9] J. Rodriguez-Carvajal, Recent advances in magnetic-structure determination by neutron powder diffraction, *Physica B: Condensed Matter* 192 (1993) 55-69.
- [10] K.D. Liss, B. Hunter, M. Hagen, T. Noakes and S. Kennedy, Echidna - the new high-resolution powder diffractometer being built at OPAL, *Physica B: Condensed*

Matter 385 (2006) 1010-1012.

[11] A.W. Hewat, D2B, a new high-resolution neutron powder diffractometer, Materials Science Forum 9 (1986) 69-80.

[12] <http://www.qdusa.com/products/mpms.html>.

Chapter 4

Interstitial boron in MnFe(P,As)

giant-magnetocaloric alloy

4.1 Introduction

Magnetic refrigeration is a cooling technology which takes advantage of the entropy difference between the magnetized and demagnetized states of magnetic refrigerant materials. It represents an energy efficient and environmentally friendly alternative for the vapor-cycle refrigeration technology in use today. Recently magnetocaloric materials have been intensively investigated, especially materials undergoing a first order magnetic phase transition [1-5]. The (Mn,Fe)₂(P,As) compounds are known for their good magnetocaloric properties: small thermal hysteresis, high magnetic entropy change and large adiabatic temperature changes. Another favorable point of this family of compounds is the tuneability of the working temperatures [6]. This is done by changing the Mn:Fe and/or P:As ratios, thus changing the lattice parameters, electron concentration and Curie temperatures (T_C). However, small changes in composition result in rather large changes in T_C . Additionally, this often results in slightly changed magnetocaloric properties, which need to be optimized composition by composition. It is known that the magnetic and the magnetocaloric properties can be affected by the application of physical pressure [7, 8]. Since physical pressure is an impractical technique for applications, chemical pressure is often used by the introduction of interstitial elements. Thus, we searched for interstitial elements, which would play the role of gradually displacing the phase transition without changing the magnetocaloric properties.

4.2 Materials and methods

Polycrystalline $\text{Mn}_{0.95}\text{Fe}_{1.05}\text{P}_{0.5}\text{As}_{0.5}\text{B}_x$ compounds ($x = 0, 0.01, 0.02$ and 0.04) were synthesized using a high-energy ball-milling and solid state reaction. Appropriate proportions of starting materials, pure Mn chips (purity 99.99%), B pieces (purity 99.9%), red-P (purity 99.99%), and the binary compounds Fe_2P and FeAs_2 (purity 99.5%), were ball milled for 7 days under vacuum (about 10^{-7} mbar) in a vibrating ball mill. During the milling process solid-state reactions are initiated through repeated deformation and fracture of the powder particles. The obtained mixtures were pressed into tablets and sealed in quartz ampoules under an Ar atmosphere of ~ 200 mbar. All the samples were sintered at 1000°C for 2 hours, and then homogenized at 850°C for 20 hours and finally oven-cooled to room temperature. Powder x-ray diffraction (XRD) was performed in a PANalytical X'pert Pro diffractometer with Cu $K\alpha$ radiation, secondary flat crystal monochromator, and X'celerator real time multiple strip (RTMS) detector system. The magnetic measurements were carried out in a Quantum Design MPMS-5XL SQUID magnetometer in the temperature range 5 – 400 K and magnetic fields up to 5 T. The magnetic entropy change is derived from isothermal magnetization measurements using the equation

$$\Delta S_m(T, \Delta B) = \sum_i \frac{M(T + \Delta T/2, B_i) - M(T - \Delta T/2, B_i)}{\Delta T} B_i \quad (1)$$

where ΔB is the sum of ΔB_i , $M(T + \Delta T/2, B_i)$ and $M(T - \Delta T/2, B_i)$ represent the values of the magnetization in a magnetic field B_i at the temperatures $T + \Delta T/2$ and $T - \Delta T/2$, respectively.

4.3 X-ray diffraction results

It is known that the lattice parameters change discontinuously during the first-order magnetoelastic transition [9-11]. Thus, to separate the influence on the lattice parameters due to the magnetic phase transition and the addition of interstitial elements, the powder X-ray diffraction patterns of the $\text{Mn}_{0.95}\text{Fe}_{1.05}\text{P}_{0.5}\text{As}_{0.5}\text{B}_x$ compounds ($x = 0, 0.01, 0.02$ and 0.04) were collected at both 250 and 330 K (in the ferromagnetic and paramagnetic states, respectively, for all the compounds shown in Figure 4.1). The results show that the reflections can be identified with the hexagonal Fe_2P -type phase. There is a minor MnO impurity phase with a peak indicated by the arrow. Lattice parameters have been obtained from careful refinement of the XRD data by Rietveld refinement [12] using the Fullprof [13] program, the results are

summarized in Table 4.1. Due to thermal expansion the cell volume V increases about 0.6% from 250 to 340 K, the volume change at T_C due to the magnetoelastic transition is less than 0.1%. The boron addition mainly influences the lattice parameter a resulting in an increase of 0.2% (at both 250 and 340 K) when increasing boron concentration from $x = 0$ to $x = 0.04$. The lattice parameter c is rather unaffected by the boron concentration. The expansion of the lattice volume with increasing boron concentration, observed in this study, indicates that the boron atoms are entering the lattice as an interstitial element rather than a substitutional element. Note that, small B atoms replacing P in Fe_2P reduce the unit-cell volume and alter both lattice parameters a and c [14], as shown in Table 4.1.

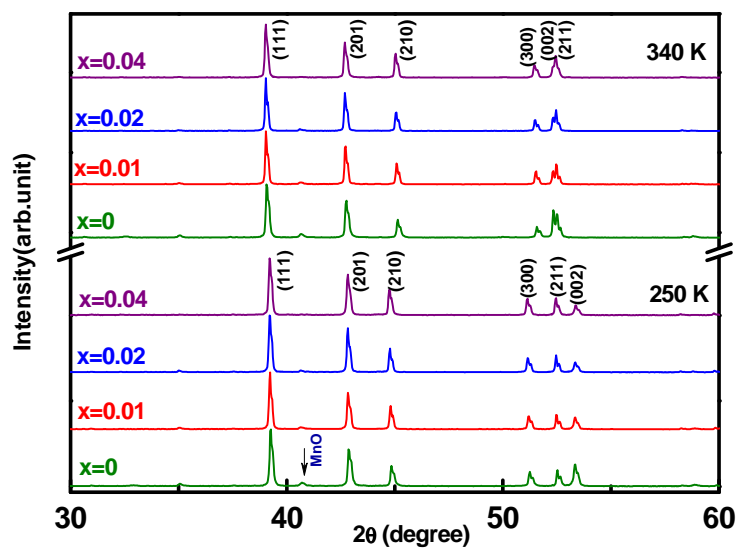


Figure 4.1 X-ray diffraction patterns of $\text{Mn}_{0.95}\text{Fe}_{1.05}\text{P}_{0.5}\text{As}_{0.5}\text{B}_x$ compounds ($x = 0, 0.01, 0.02$ and 0.04) collected at 250 and 340 K (in ferromagnetic and paramagnetic state for all the samples, respectively). The arrow indicates the presence of minor impurity phase MnO.

There are several possible Wyckoff positions that may be occupied by boron atoms as there are several sites with a sufficiently large open volumes in the MnFe(P,As) unit cell. The distinct difference between the response of lattice parameters a and c suggests that boron, as an interstitial element, prefers to occupy interstitial sites within the a - b plane. Introducing boron as an interstitial atom, thus, results in a negative pressure. This negative pressure is primarily parallel to the basal plane and raises T_C . Concerning the application of pressure, one generally distinguishes hydrostatic and uniaxial pressures. The effect of both types of pressure on the parent compound Fe_2P have been explored earlier: positive hydrostatic pressure reduces the size of the unit cell, changing the lattice parameters a and c simultaneously, with

the basal plane being more compressible than the c -axis [15,16]; uniaxial pressure on Fe_2P single crystal (parallel to the c -axis or perpendicular to the c -axis) can provide a pressure perpendicular or parallel to the basal plane, which leads to increase or decrease of T_C , respectively [17].

Table 4.1 Variation of lattice parameters a , c , V (volume) and c/a ratio (at 250 and 340 K), Curie temperature (T_C), maximal isothermal magnetic entropy change ($-\Delta S_M$) and the relative cooling power $\text{RCP}(S)$ under the magnetic field change $\Delta B = 0 - 2$ T of $\text{Mn}_{0.95}\text{Fe}_{1.05}\text{P}_{0.5}\text{As}_{0.5}\text{B}_x$ compounds ($x = 0, 0.01, 0.02$ and 0.04). For comparison, some results for Gd and $\text{Fe}_2\text{P}_{1-x}\text{B}_x$ ($x = 0, 0.04, 0.08$ and 0.15) from Ref. [1] and Ref. [14], respectively, are presented as well.

Compounds	a (Å)	c (Å)	V (Å ³)	c/a	T_C (K)	$-\Delta S_{M, \max}$ (J kg ⁻¹ K ⁻¹)	$\text{RCP}(S)$ (J kg ⁻¹)
$\text{Mn}_{0.95}\text{Fe}_{1.05}\text{P}_{0.5}\text{As}_{0.5}\text{B}_x$	(250 /340 K)	(250 /340 K)	(250 /340 K)	(250 /340 K)			
$x = 0$	6.178/6.142	3.437/3.498	113.61/114.29	0.5563/0.5695	290	11.3	131
$x = 0.01$	6.182/6.146	3.436/3.498	113.70/114.46	0.5558/0.5692	295	15.2	146
$x = 0.02$	6.187/6.151	3.436/3.499	113.88/114.65	0.5553/0.5688	301	13.4	149
$x = 0.04$	6.190/6.154	3.434/3.498	113.97/114.74	0.5548/0.5684	305	14.3	162
Gadolinium*					293	4.2	166
$\text{Fe}_2\text{P}_{1-x}\text{B}_x$ **							
$x = 0$	5.872	3.442	102.78	0.5862	216		
$x = 0.04$	5.897	3.410	102.70	0.5782	358		
$x = 0.08$	5.916	3.370	102.14	0.5695	440		
$x = 0.15$	5.936	3.325	101.45	0.5602	528		

*Reference [1] and **Reference [14].

4.4 Magnetic properties and magnetocaloric effect

Figure 4.2 shows the temperature dependence of the magnetization of the $\text{Mn}_{0.95}\text{Fe}_{1.05}\text{P}_{0.5}\text{As}_{0.5}\text{B}_x$ compounds ($x = 0, 0.01, 0.02$ and 0.04) measured in a field of 0.05 T with increasing and followed by decreasing temperature. The thermal hysteresis, between the heating and cooling curves, indicates the magnetic transition is of first order, which is accompanied by a large magnetic entropy change due to latent heat. The thermal hysteresis (ΔT_{hys}) is hardly influenced by boron doping and the values are in the order of 1 or 2 K for all compounds. The Curie temperature, derived from M - T curves, increases about 15 K with increasing boron concentration from $x = 0$ to $x = 0.04$. Note that, B substitution in the $\text{Fe}_2\text{P}_{1-x}\text{B}_x$ compounds ($x < 0.15$) rapidly raises the T_C (from 216 to 358 K when increase B

content from 0 up to 0.04) [14]. Magnetic field induced phase transitions are at the basis of the giant magnetocaloric effect. For all boron concentrations a strong magnetic field-induced transition with small magnetic hysteresis is observed, as depicted in Figure 4.3. The magnetic hysteresis is slightly reduced with increasing boron concentration.

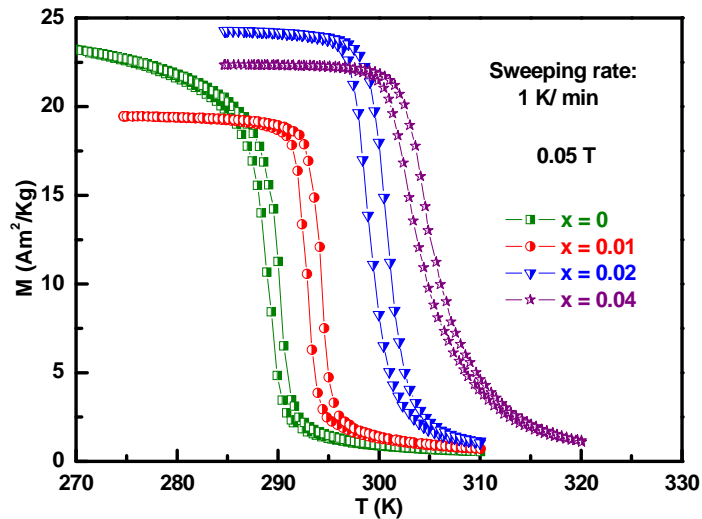


Figure 4.2 Temperature dependence of magnetization of $\text{Mn}_{0.95}\text{Fe}_{1.05}\text{P}_{0.5}\text{As}_{0.5}\text{B}_x$ compounds ($x = 0, 0.01, 0.02$ and 0.04) in a field of 0.05 T with temperature increasing and decreasing.

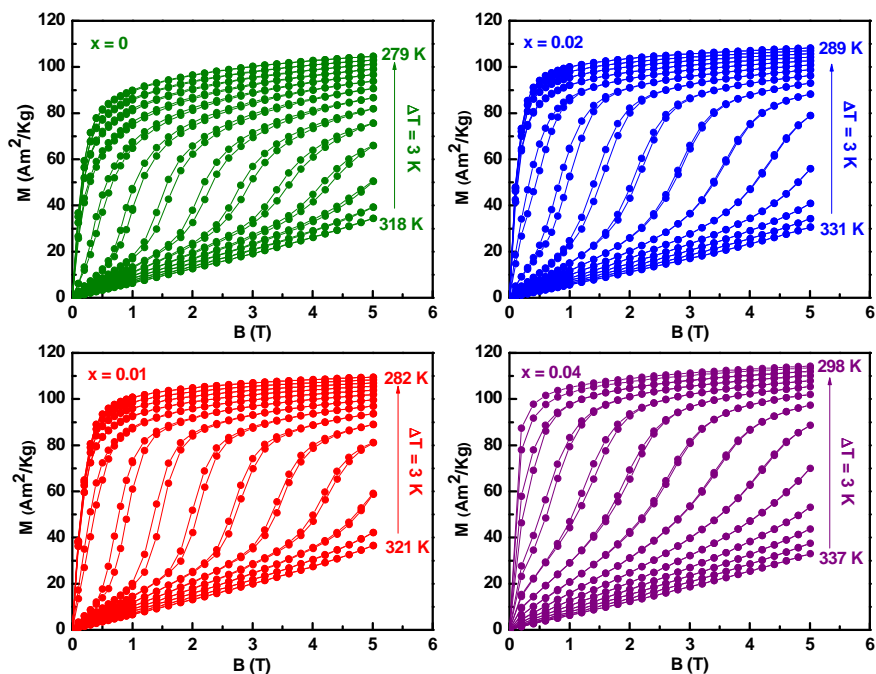


Figure 4.3 Isothermal magnetization curves of the $\text{Mn}_{0.95}\text{Fe}_{1.05}\text{P}_{0.5}\text{As}_{0.5}\text{B}_x$ compounds ($x = 0, 0.01, 0.02$ and 0.04) measured in vicinity of T_C with increasing and decreasing magnetic field.

The Arrott plot [18], which is obtained by plotting the magnetization M measured in the field $\mu_0 H$ as a function of M^2 versus H/M , is an effective tool to determine the order of the phase transition. Figure 4.4 shows the Arrott plots for the $\text{Mn}_{0.95}\text{Fe}_{1.05}\text{P}_{0.5}\text{As}_{0.5}\text{B}_x$ compounds with $x = 0, 0.01, 0.02$ and 0.04 in the vicinity of their respective T_C 's. The S-shaped curves confirm the occurrence of a first-order magnetic phase transition (FOMT) in all compounds [19]. However, the S shape is less pronounced for the compound with the highest boron concentration.

The isothermal magnetic entropy changes derived from the magnetization data are shown in Figure 4.5. A small amount of boron addition slightly enhances the magnetic entropy change, the values of maximum magnetic entropy changes in a field change of 2 T are shown in table 4.1. The relative cooling power (RCP) [20], a parameter which evaluates the magnetic cooling efficiency of magnetocaloric materials increases with increasing boron content. The full width at half maximum (δT_{FWHM}) of the entropy change also increases with increasing boron content. The increase of RCP(S) values is probably caused by the widening of δT_{FWHM} due to the less pronounced FOMT for the higher boron content compounds.

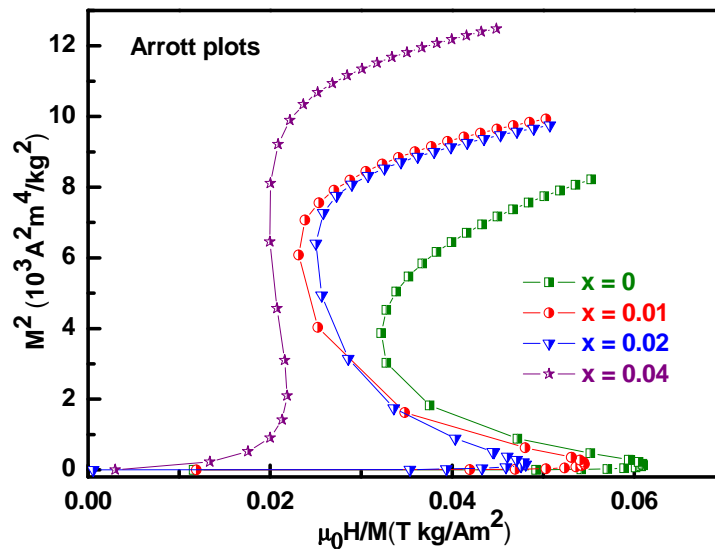


Figure 4.4 Arrott plots of the $\text{Mn}_{0.95}\text{Fe}_{1.05}\text{P}_{0.5}\text{As}_{0.5}\text{B}_x$ compounds ($x = 0, 0.01, 0.02$ and 0.04) obtained from magnetized isothermal magnetization data measured in the vicinity of their critical temperatures.

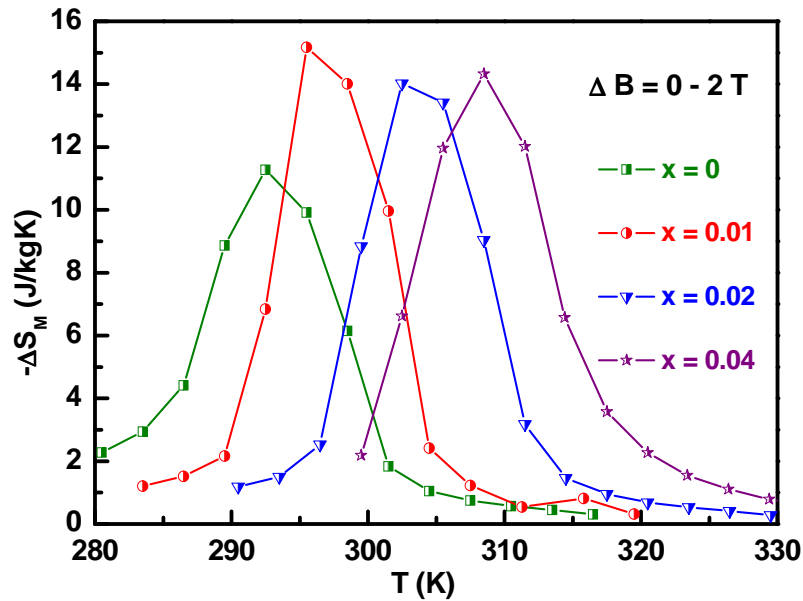


Figure 4.5 Isothermal magnetic entropy changes of the $\text{Mn}_{0.95}\text{Fe}_{1.05}\text{P}_{0.5}\text{As}_{0.5}\text{B}_x$ compounds ($x = 0, 0.01, 0.02$ and 0.04) in a field change of 2 T.

The competition between the intra-layer (a - b plane) and the inter-layer (parallel to a - b plane) exchange interactions can be characterized by as the c/a ratio, resulting in the change of the Curie temperature [7, 8, 14 and 21]. Uniaxial pressure studies on the parent compound Fe_2P show that, a change on either lattice parameter a or c will alter the Curie temperature: it increases by applying pressure along c , while it decreases applying pressure perpendicular to c [17]. With hydrostatic pressure both lattice parameters contract simultaneously. The change in Curie temperature is associated with a change of both a and c and is therefore best characterized by the c/a ratio. It is claimed that the strongest ferromagnetic exchange interactions are the ones between the different nearest-neighbor $3g$ intra-plane atoms and affected the most by the c/a ratio, while the ferromagnetic exchange interactions between the inter-layer ($3g$ - $3f$ sites) are less affected by the c/a ratio [11, 21]. In other words, a change of the c/a ratio will cause a shift in T_C . In the case of hydrostatic positive pressure in Fe_2P , a is much more compressible and goes down much faster than c , thus decreasing c/a and resulting in a decrease of T_C [22]. If the c/a ratio remains constant, a constant T_C would be expected. In our study, the boron doping expands the a - b plane, having little influence on the lattice parameter c , which makes the c/a ratio decrease, resulting in the upward shift of T_C .

4.5 Conclusions

The $(\text{Mn,Fe})_2(\text{P,As})\text{B}_x$ compounds ($x = 0, 0.01, 0.02$ and 0.04) crystallize in the hexagonal Fe_2P -type structure and boron atoms occupy interstitial sites within the basal plane. First-order magnetoelastic phase-transitions with small thermal and magnetic hysteresis are observed in all these compounds. The ferromagnetic ordering temperatures increase by boron addition. The optimal working temperatures can be finely adjusted by varying the boron content without losing the good magnetocaloric properties. Both the maximal magnetic entropy changes and the RCP are slightly enhanced for all boron concentrations. All these features make boron addition a good tool to tune and improve magnetic and magnetocaloric properties in $(\text{Mn,Fe})_2(\text{P,As})$ compounds.

References

- [1] V.K. Pecharsky and K.A. Gschneidner, Giant magnetocaloric effect in $\text{Gd}_5(\text{Si}_2\text{Ge}_2)$, *Physical Review Letters* 78 (1997) 4494-4997.
- [2] F.X. Hu, B.G. Shen, J.R. Sun and Z.H. Cheng, G.H. Rao and X.X. Zhang, Influence of negative lattice expansion and metamagnetic transition on $\text{LaFe}_{11.4}\text{Si}_{1.6}$, *Applied Physics Letters* 78 (2001) 3675-3677.
- [3] O. Tegus, E. Brück, K.H.J. Buschow and F.R. de Boer, Transition-metal-based magnetic refrigerants for room-temperature applications, *Nature* 415 (2002) 150-152.
- [4] H. Wada and Y. Tanabe, Giant magnetocaloric effect of $\text{MnAs}_{1-x}\text{Sb}_x$, *Applied Physics Letters* 79 (2001) 3302-3304.
- [5] A. Fujita, S. Fujieda, Y. Hasegawa and K. Fukamichi, Itinerant-electron metamagnetic transition and large magnetocaloric effects in $\text{La}(\text{Fe}_x\text{Si}_{1-x})_{13}$ compounds and their hydrides, *Physical Review B* 67 (2003) 104416.
- [6] O. Tegus, E. Brück, L. Zhang, Dagula, K.H.J. Buschow and F.R. de Boer, Magnetic-phase transitions and magnetocaloric effects, *Physica B* 319 (2002) 174-192.
- [7] E. Brück, J. Kamarad, V. Sechovsky, Z. Arnold, O. Tegus and F.R. de Boer, Pressure effects on the magnetocaloric properties of $\text{MnFeP}_{1-x}\text{As}_x$, *Journal of Magnetism and Magnetic Materials* 310 (2007) e1008-e1009.

- [8] H. Yabuta, K. Umeo, T. Takabatake, L. Chen, Y. Uwatoko, Pressure effects on the first order transition in MnFe(P,As) and MnFe(P,Ge), *Journal of Magnetism and Magnetic Materials* 310 (2007) 1826-1828.
- [9] E. Brück, Developments in magnetocaloric refrigeration, *Journal of Physics D: Applied Physics* 38 (2005) R381-R391.
- [10] N.T. Trung, Z.Q. Ou, T.J. Gortenmulder, O. Tegus, K.H.J. Buschow, and E. Brück, Tunable thermal hysteresis in MnFe(P,Ge) compounds, *Applied Physics Letters* 94 (2009) 102513.
- [11] N.H. Dung, L. Zhang, Z.Q. Ou and E. Brück, From first-order magneto-elastic to magneto-structural transition in $(\text{Mn,Fe})_{1.95}\text{P}_{0.50}\text{Si}_{0.50}$ compounds, *Applied Physics Letters* 99 (2011) 092511.
- [12] H.M. Rietveld, A profile refinement method for nuclear and magnetic structures, *Journal of Applied Crystallography* 2 (1969) 65-71.
- [13] J. Rodríguez-Carvajal, Recent advances in magnetic structure determination by neutron powder diffraction, *Physica B* 192 (1993) 55-69.
- [14] R. Chandra, S. Bjarman, T. Ericsson, L. Häggström, C. Wilkinson and R. Wäppling, A Mössbauer and X-Ray study of $\text{Fe}_2\text{P}_{1-x}\text{B}_x$ Compounds ($x \leq 0.15$), *Journal of Solid State Chemistry* 34 (1980) 389-396.
- [15] H. Fujiwara, M. Nomura, H. Kadomatsu, N. Nakagiri, T. Nishizaka, Y. Yamamoto, H. Fujii and T. Okamoto, Anisotropic lattice compression in Fe_2P , *Journal of the Physical Society of Japan* 50 (1981) 3533-3534.
- [16] D.M. Liu, Q.Z. Huang, M. Yue, J.W. Lynn, L.J. Liu, Y. Chen, Z.H. Wu and J.X. Zhang, Temperature, magnetic field, and pressure dependence of the crystal and magnetic structures of the magnetocaloric compound $\text{Mn}_{1.1}\text{Fe}_{0.9}(\text{P}_{0.8}\text{Ge}_{0.2})$ *Physical Review B* 80 (2009) 174415.
- [17] H. Fujiwara, H. Kadomatsu and K. Tohma, Effect of uniaxial stress on the Curie temperature in Fe_2P , *Journal of the Physical Society of Japan* 51 (1982) 1401-1405.
- [18] A. Arrott, Criterion for ferromagnetism from observations of magnetic isotherms *Physical Review* 108 (1957) 1394-1396.
- [19] A. Yan, K.H. Müller, L. Schultz and O. Gutfleisch, Magnetic entropy change in melt-spun MnFePGe, *Journal of Applied Physics* 99 (2006) 08K903.
- [20] K.A. Gschneidner and V.K. Pecharsky, Magnetocaloric materials, *Annual Review of Materials Science* 30 (2000) 387-429.

-
- [21] E.K. Delczeg-Czirjak, Z. Gercsi, L. Bergqvist, O. Eriksson, L. Szunyogh, P. Nordblad, B. Johansson, and L. Vitos, Magnetic exchange interactions in B-, Si-, and As-doped Fe₂P from first-principles theory, *Physical Review B* 85 (2012) 224435.
- [22] H. Kadomatsu, M. Isoda and K. Tohma, H. Fujii, T. Okamoto and H. Fujiwara, Pressure induced antiferromagnetism of Fe₂P, *Journal of the Physical Society of Japan* 54 (1985) 2690-2699.

Chapter 5

Transition metal substitution in Fe₂P-based MnFe_{0.95}P_{0.50}Si_{0.50} magnetocaloric compounds

5.1 Introduction

Magnetic refrigeration has attracted much attention in recent years as a promising and environmentally friendly alternative to conventional gas-compression cooling [1-6]. Magnetocaloric materials that undergo a first-order magnetic phase transition (FOMT) are being intensively investigated. However, the thermal hysteresis, which is a characteristic feature of a FOMT, is unfavorable for thermal cycles. The reduction of thermal hysteresis (ΔT_{hys}) is an essential issue to practical refrigeration applications.

Fe₂P-based MnFeP_{1-x}As_x compounds are known as promising materials for magnetic cooling, presenting small thermal hysteresis (less than 2 K), a large magnetocaloric effect and easy tuneability of the optimal operating temperature (from ~200 to ~340 K) by varying the P/As ratio [4, 7]. However, the toxicity of arsenic hampers the use of this material in practical applications. Following studies on both MnFe(P,Ge) [8] and MnFe(P,Si) [9] compounds have shown the successful replacement of the toxic element arsenic, at the expense of a large ΔT_{hys} of ~ 10 K and 35 K, respectively. The limited availability of Ge puts the Mn-Fe-P-Si compound as the best candidate among Fe₂P-based compounds so far. It is found that a large

temperature span and small ΔT_{hys} can be achieved by varying the Mn/Fe and/or P/Ge(Si) ratios [10, 11]. Moreover, Co and Ni substitutions for Fe in Mn-Fe-P-Ge compounds reduce the thermal hysteresis, while retaining good magnetocaloric properties [12].

In the Mn-Fe-P-Si compound, Mn and Fe atoms preferably occupy the 3g and 3f sites, respectively, where ions in the 3g sites show much larger magnetic moments than that of the 3f sites [9]. First-principle electronic structure calculations suggest that the high and low-moment sites show a different magnetic behavior: the 3g sites show a more localized magnetism, while 3f sites show weak itinerant magnetism [11]. Thus, the substitution of different elements on 3g or 3f sites may have different effects on the magnetic and magnetocaloric properties. In this chapter, we show the sensitivity of T_C and the thermal hysteresis on the replacement of Fe(3f)/Mn(3g) by transition metals, *e.g.* Co, Ni and Cu, in the $\text{MnFe}_{0.95}\text{P}_{0.50}\text{Si}_{0.50}$ compound.

5.2 Sample preparation

Polycrystalline Fe_2P -based $(\text{Mn,Fe,T})_{1.95}\text{P}_{0.50}\text{Si}_{0.50}$ ($T = \text{Co, Ni and Cu}$) compounds were prepared by ball-milling and solid-state reactions. Appropriate amounts of starting materials of Mn (99.9%), Si (99.999%) chips, binary compound Fe_2P (99.5%), red-P (99.7%), Co (99.8%), Ni (99.9%) and Cu (99.9%) powder were mixed and ball-milled for 10 h. The ball-milled powder was then pressed into small tablets and sealed in quartz ampoules in an Ar atmosphere of ~ 200 mbar. The samples were sintered at 1373 K for 2 h and then annealed at 1123 K for 20 h before being furnace cooled to room temperature. For a better homogeneity, the obtained bulk samples were re-annealed at 1373 K for 20 h and finally quenched into water. X-ray diffraction patterns were collected in zero field using a PANalytical X-pert Pro diffractometer using Cu $K\alpha$ radiation, a secondary-beam flat-crystal monochromator and a multichannel X'celerator detector. A superconducting quantum interference device (SQUID) magnetometer (Quantum Design MPMS 5XL) with the reciprocating sample option (RSO) mode was employed for magnetic measurements in the temperature range of 5 - 400 K and in magnetic fields up to 5 T. Differential scanning calorimetry (DSC) measurements were carried out using a TA-Q2000 DSC calorimeter in a temperature range of 90 K to 820 K.

5.3 Structural, magnetic and magnetocaloric properties

The $(Mn,Fe)_{1.95}P_{0.50}Si_{0.50}$ compound shows a T_C of 395 K and ΔT_{hys} of 16 K, as obtained from the DSC measurements. The X-ray diffraction pattern shows that the sample crystallizes in the hexagonal Fe_2P -type structure (space group $P-62m$). Due to the site preferences of Fe and Mn, the $3f$ and $3g$ sites will be occupied by Fe and Mn, respectively.

5.3.1 $MnFe_{0.95-x}Co_xP_{0.50}Si_{0.50}$ compounds

X-ray diffraction patterns collected at 473 K, which is a temperature at which all the compounds are in the paramagnetic state, indicate that all the samples crystallize in the hexagonal Fe_2P -type structure. The cell volume decreases with increasing Co content, as Co (1.26 Å) has a smaller covalent radius than Fe (1.32 Å). The lattice parameter a decreases and c increases with increasing Co content, as shown in Figure 5.1. We find that the c/a value increases linearly with increasing Co content.

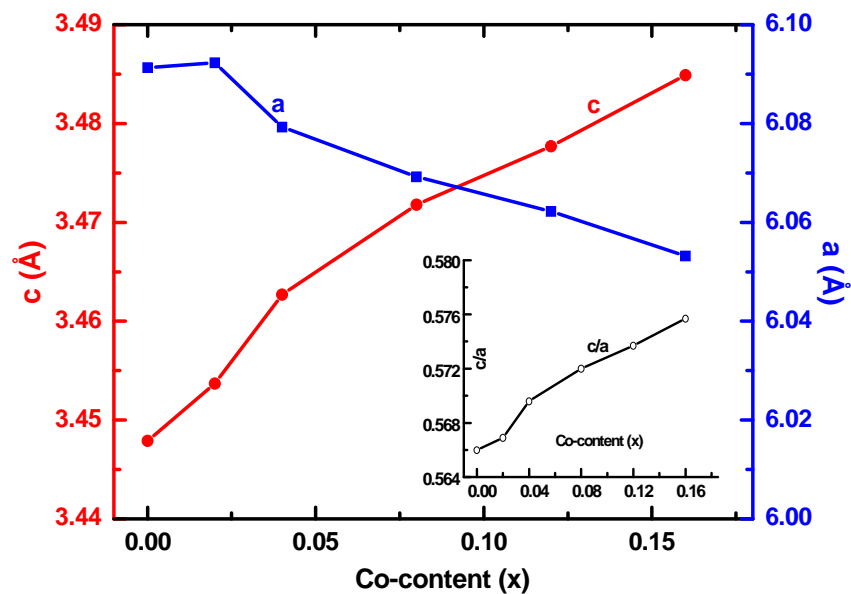


Figure 5.1 Variation of lattice parameters obtained from XRD patterns measured at 473 K for $MnFe_{0.95-x}Co_xP_{0.50}Si_{0.50}$ ($x = 0, 0.02, 0.04, 0.08, 0.12$ and 0.16).

The temperature dependence of the magnetization for the $MnFe_{0.95-x}Co_xP_{0.50}Si_{0.50}$ ($x = 0.04, 0.08, 0.12$ and 0.16) compounds measured in a field of 1 T is shown in Figure 5.2. The temperature dependence of the magnetization shows very sharp first-order ferromagnetic to

paramagnetic phase transitions accompanied by a large temperature hysteresis ΔT_{hys} of ~ 15 K between heating and cooling curves. T_C decreases almost linearly with increasing Co content (see the insert in Figure 5.2). The reduction of T_C suggests that the replacement of Fe(3f) by Co weakens the ferromagnetic (FM) ordering, which is consistent with the results for similar substitutions in Mn-Fe-P-X (X = As, Ge) compounds. The ΔT_{hys} value is rather constant when Fe(3f) is replaced by Co up to 0.16 at. %, implying that the FOMT is retained and the energy barrier for nucleation [13] is hardly changed. This behavior is unexpected since it is found that Co substitution on the Fe(3f) site in Mn-Fe-P-Ge compounds reduces both T_C and ΔT_{hys} , while retaining a sharp magnetic transition at T_C [12].

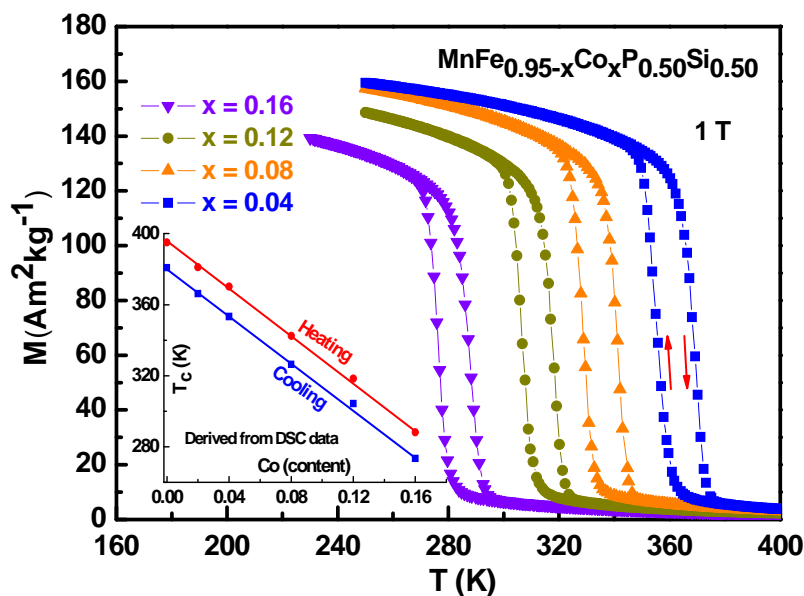


Figure 5.2 Temperature dependence of the magnetization of $\text{MnFe}_{0.95-x}\text{Co}_x\text{P}_{0.50}\text{Si}_{0.50}$ ($x = 0.04, 0.08, 0.12$ and 0.16) compounds measured in a magnetic field of 1 T. The insert shows the transition temperatures obtained from DSC experiments.

Figure 5.3a shows the isothermal magnetization loops measured for increasing and decreasing magnetic field in the vicinity of T_C for the $x = 0.16$ sample. Due to the large ΔT_{hys} , the isothermal magnetization has been measured by the method discussed by Caron *et al.* [14]. A strong magnetic field-induced transition and a large field hysteresis confirm the first-order nature of the transition. All these results imply that the FOMT is retained when Fe(3f) is replaced by Co in $\text{MnFe}_{0.95-x}\text{Co}_x\text{P}_{0.50}\text{Si}_{0.50}$ compounds. The corresponding magnetic entropy

changes ($-\Delta S_M$) can be derived using the Maxwell relation. The values are shown in Figure 5.3b.

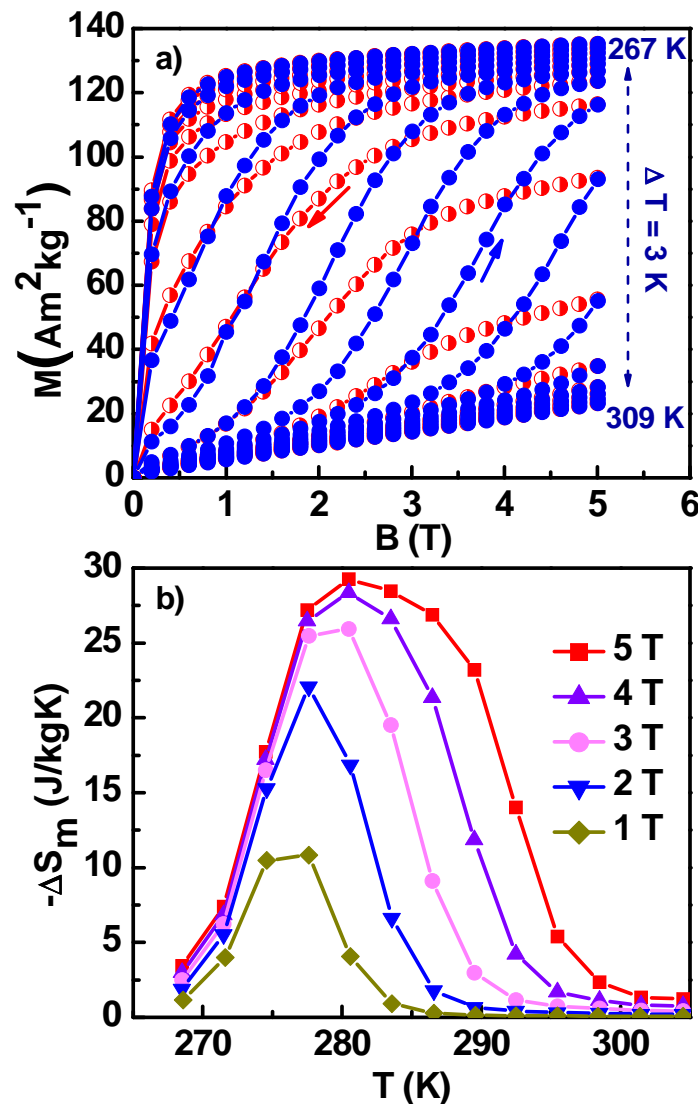


Figure 5.3 Isothermal magnetization curves of the $MnFe_{0.79}Co_{0.16}P_{0.50}Si_{0.50}$ compound measured in vicinity of its T_C with increasing and decreasing magnetic field up to 5 T (a) and its corresponding magnetic entropy changes as a function of temperature in different fields (b).

5.3.2 $Mn_{1-y}Co_yFe_{0.95}P_{0.50}Si_{0.50}$ compounds

As shown above, the replacement of Fe by Co on the Fe(3f) site in $MnFe_{0.95}P_{0.50}Si_{0.50}$ results in different behavior compared with the effect of the same substitution in Mn-Fe-P-Ge compounds [12]. Therefore, we have investigated another series of compounds, the $Mn_{1-y}Co_yFe_{0.95}P_{0.50}Si_{0.50}$ ($y = 0, 0.04, 0.08, 0.12, 0.16, 0.20, 0.24$ and 0.28), where Mn(3g) is

replaced by Co. The variation in lattice parameters with Co content is shown in Figure 5.4. It is found that Co substitution reduces the a lattice parameter while it increases the c lattice parameter and the c/a ratio. Replacement of Mn(3g) by Co reduces the Curie temperature and broadens the ferro-paramagnetic phase transition. Moreover, the thermal hysteresis is gradually reduced with increasing Co content, as shown in Figure 5.5, suggesting that the energy barrier for nucleation is reduced when Mn(3g) is replaced by Co.

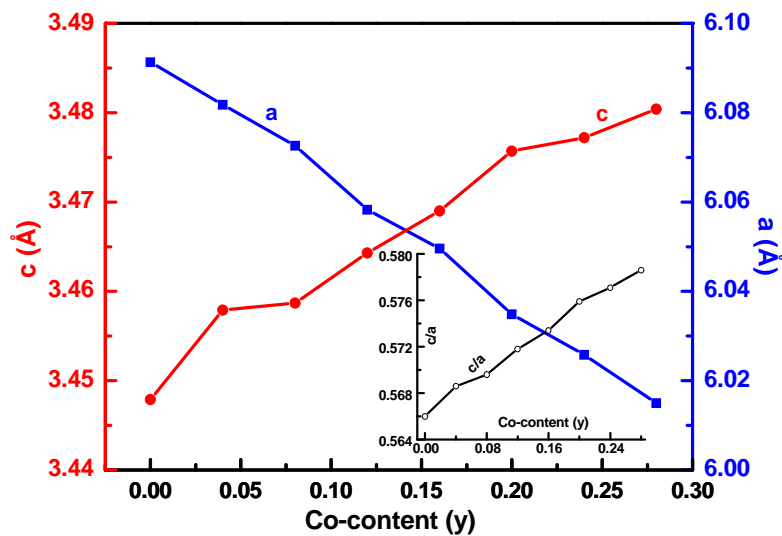


Figure 5.4 Variation of lattice parameters obtained from XRD patterns measured in zero-field for $\text{Mn}_{1-y}\text{Co}_y\text{Fe}_{0.95}\text{P}_{0.50}\text{Si}_{0.50}$ ($y = 0, 0.04, 0.08, 0.12, 0.16, 0.20, 0.24$ and 0.28).

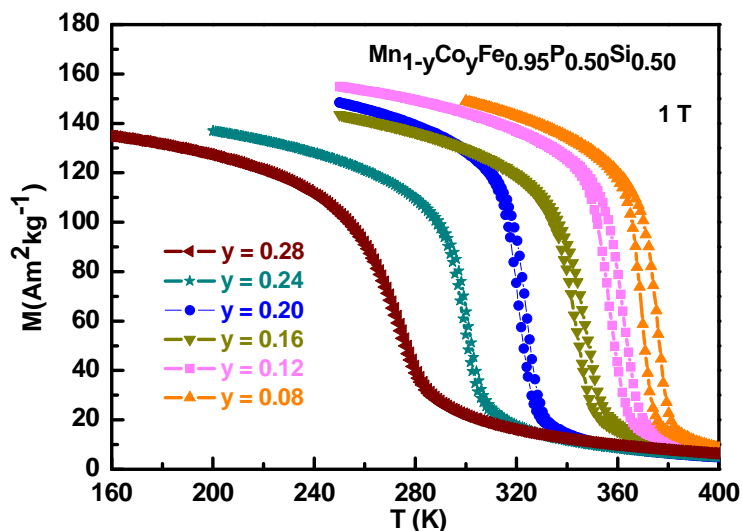


Figure 5.5 Temperature dependence of the magnetization of $\text{Mn}_{1-y}\text{Co}_y\text{Fe}_{0.95}\text{P}_{0.50}\text{Si}_{0.50}$ ($y = 0.08, 0.12, 0.16, 0.20, 0.24$ and 0.28) compounds measured in a magnetic field of 1 T.

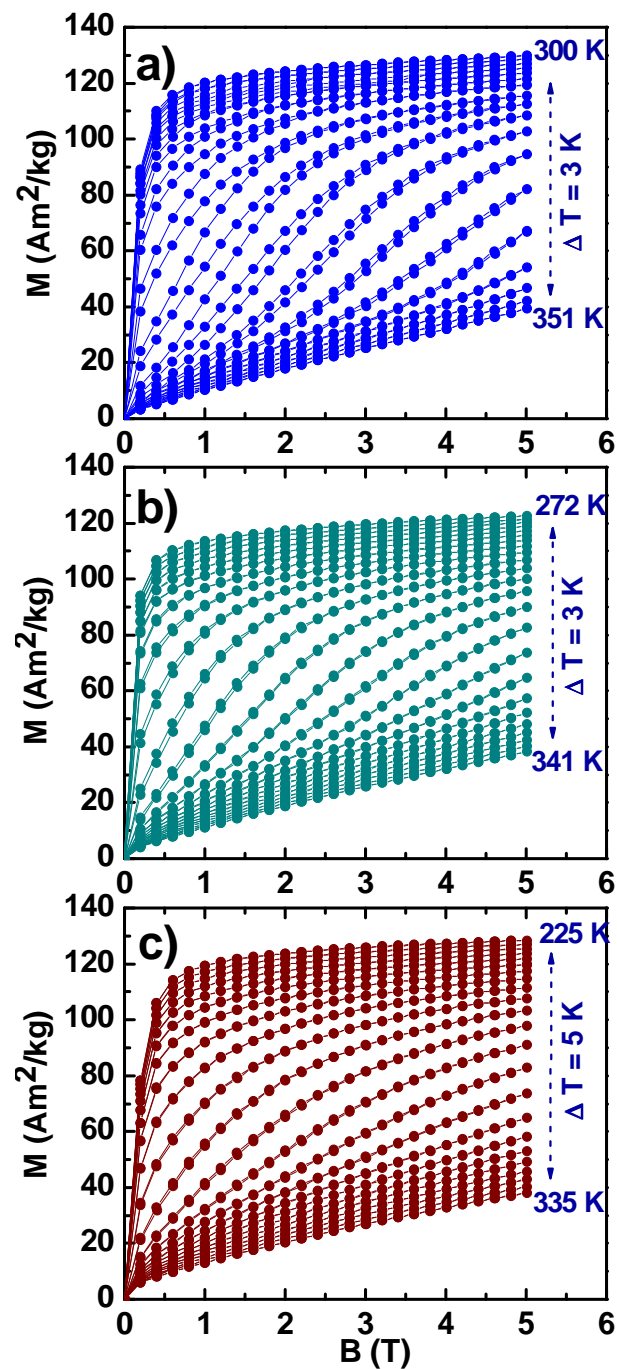


Figure 5.6 Isothermal magnetization curves of the $Mn_{1-y}Co_yFe_{0.95}P_{0.50}Si_{0.50}$ ($y = 0.20, 0.24$ and 0.28) compounds measured in vicinity of their T_C s with increasing and decreasing magnetic field up to 5 T.

Isothermal magnetization data of the compounds $Mn_{1-y}Co_yFe_{0.95}P_{0.50}Si_{0.50}$ ($y = 0.20, 0.24$ and 0.28) was measured in the vicinity of their T_C 's for increasing and decreasing magnetic field up to 5 T, as shown in Figure 5.6. A magnetic field induced transition and small field hysteresis are observed for the sample with $y = 0.20$, suggesting that the first-order nature of

the transition is kept when Mn(3g) is replaced by Co up to 0.20 at.%. Samples with a higher Co content (up to 0.28 at.%) display a second order-like phase transition, where field induced transitions and magnetic hysteresis are hardly observed, suggesting that the first-order nature of the transition is suppressed.

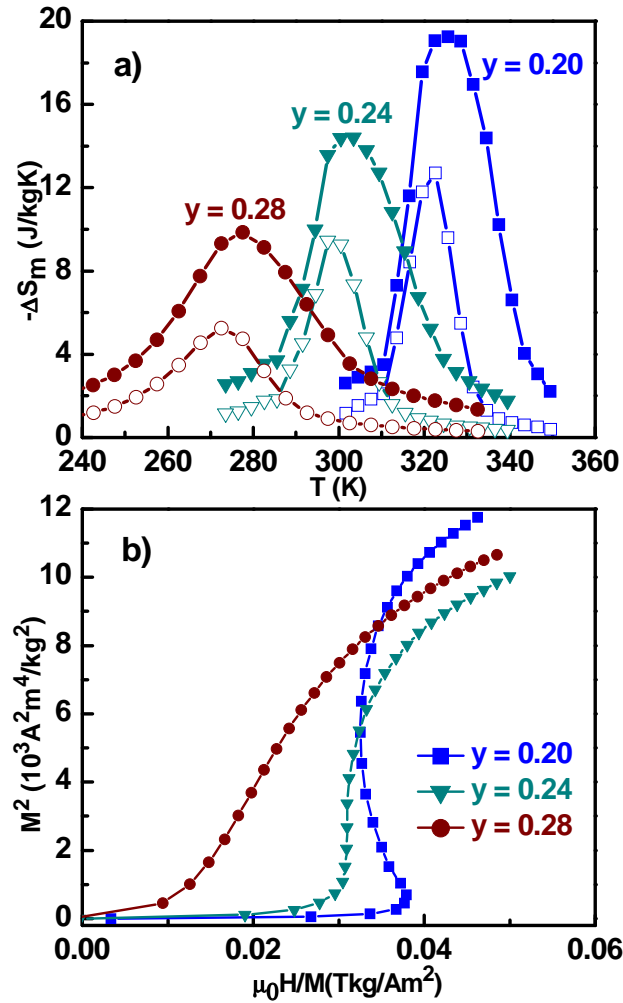


Figure 5.7 (a) Magnetic entropy changes under field changes of 0-2 T (open symbols) and 0-5 T (solid symbols). (b) Arrott plots obtained from increasing field magnetization isotherms in vicinity of the transition temperature for the $\text{Mn}_{1-y}\text{Co}_y\text{Fe}_{0.95}\text{P}_{0.50}\text{Si}_{0.50}$ ($y = 0.20, 0.24$ and 0.28) compounds.

Figure 5.7a, shows the isothermal magnetic entropy changes ($-\Delta S_M$) of the compounds $\text{Mn}_{1-y}\text{Co}_y\text{Fe}_{0.95}\text{P}_{0.50}\text{Si}_{0.50}$ ($y = 0.20, 0.24$ and 0.28) for a field change of 2 and 5 T, the maximum values of $-\Delta S_M$ decreases with increasing Co content. The Arrott plot [15], which is obtained by plotting the magnetization M measured in a field $\mu_0 H$ as M^2 versus H/M , is an

effective tool to determine the order of the phase transition. Figure 5.7b shows the Arrott plots for $Mn_{1-y}Co_yFe_{0.95}P_{0.50}Si_{0.50}$ with $y = 0.20, 0.24$ and 0.28 in vicinity of their respective T_C 's. The S-shaped curve for the $y = 0.20$ sample confirms the occurrence of a FOMT. Further increasing the Co content, yields a less pronounced S-shape curve, while it retains a small thermal hysteresis (< 1 K), suggesting that the transition is still of first-order. Thus, a small ΔT_{hys} and a large MCE can be obtained when the magnetic transition is controlled to be close to the border separating the first- and second-order magnetic transition regimes.

5.3.3 $(Mn,Fe,Ni)_{1.95}P_{0.50}Si_{0.50}$ and $(Mn,Fe,Cu)_{1.95}P_{0.50}Si_{0.50}$ compounds

Figures 5.8a and 5.8b show the temperature dependence of the magnetization for the compounds where Fe(3f) and Mn(3g), respectively, are substituted by Ni. Ni substitutions on

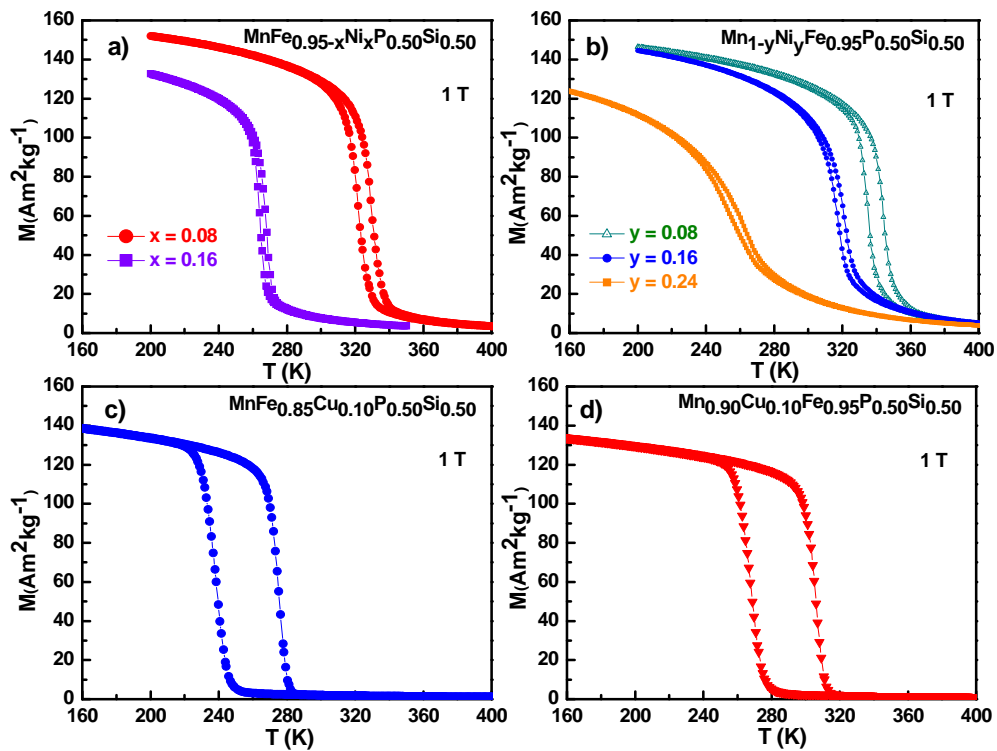


Figure 5.8 Temperature dependence of the magnetization measured in a magnetic field of 1 T of compounds: (a) $MnFe_{0.95-x}Ni_xP_{0.50}Si_{0.50}$ ($x = 0.08$ and 0.16), (b) $Mn_{1-y}Ni_yFe_{0.95}P_{0.50}Si_{0.50}$ ($y = 0.08, 0.16$ and 0.24), (c) $MnFe_{0.85}Cu_{0.10}P_{0.50}Si_{0.50}$, (d) $Mn_{0.90}Cu_{0.10}Fe_{1.95}P_{0.50}Si_{0.50}$.

both the Fe(3f) and Mn(3g) sites in the $(Mn,Fe)_{1.95}P_{0.50}Si_{0.50}$ compound result in similar magnetic properties. The ΔT_{hys} decreases with increasing Ni content. T_C is strongly reduced with increasing Ni content, while the reduction of T_C is faster with a Ni substitution on the Fe(3f) site than with Ni substitution on the Mn(3g) site. Figures 5.8c and 5.8d show the

temperature dependence of the magnetization for the compounds with 0.1 at.% Cu substitution on the Fe(3f) and Mn(3g) sites, respectively. Interestingly, with increasing Cu content the ΔT_{hys} increases markedly, while T_{C} strongly decreases.

5.4 Discussion

Figure 5.9a shows the transition-metal content dependence of T_{C} with substitutions on the Fe(3f) and Mn(3g) sites, respectively. The reduction in T_{C} for an increasing transition-metal content is independent of the transition metal species and independent on the site (Fe(3f)/Mn(3g)) they have been replaced, indicating that the ferromagnetic interaction is weakened with transition-metal substitution. However, the slopes of the curves are different. T_{C} is the most sensitive to Cu substitution and the least sensitive to Co substitution. As for the same transition-metal substitution on different sites, T_{C} is more sensitive when a transition-metal is substituted on the Fe(3f) than on the Mn(3g) site. Additionally, we found that an increase in the transition-metal content leads to an increase in the lattice parameter ratio c/a , which changes at the same rate as T_{C} . The exchange interaction between the nearest Fe(3f)-Mn(3g) inter-layer is known to be responsible for ferromagnetic ordering in Mn-Fe-P-Si compounds and is more sensitive to changes in c/a ratio than to changes in the lattice parameters a and c itself. Substitution essentially alters the interatomic distances, indicating a strong distance dependence of the exchange interactions.

Figure 5.9b shows the dependence of ΔT_{hys} on the transition-metal content when substituted on the Fe(3f) and Mn(3g) sites, respectively. It is found that the substitution of Fe(3f)/Mn(3g) by Ni reduces ΔT_{hys} , while the substitution by Cu increases ΔT_{hys} . Interestingly, the slopes of the composition dependence of ΔT_{hys} are the same for the same transition-metal substituted on different crystallographic sites.

Substitution of Fe(3f)/Mn(3g) by Co results in inconsistent behavior of the thermal and field hysteresis. Replacement of Fe(3f) by Co results in hardly any change on the ΔT_{hys} and the large field hysteresis suggests, that the first-order nature of the phase transition retains. Replacing Mn(3g) by Co reduces the ΔT_{hys} and field hysteresis, indicating that replacing Mn(3g) by Co can lower the energy barrier for nucleation in the FOMT and gradually pushes

the FOMT towards the SOMT. The large MCE is retained with the substitution of Fe(3f) by Co and is slightly reduced with the substitution of Mn(3g) by Co, implying that the weakened FOMT reduces both the hysteresis (thermal and field) and the MCE.

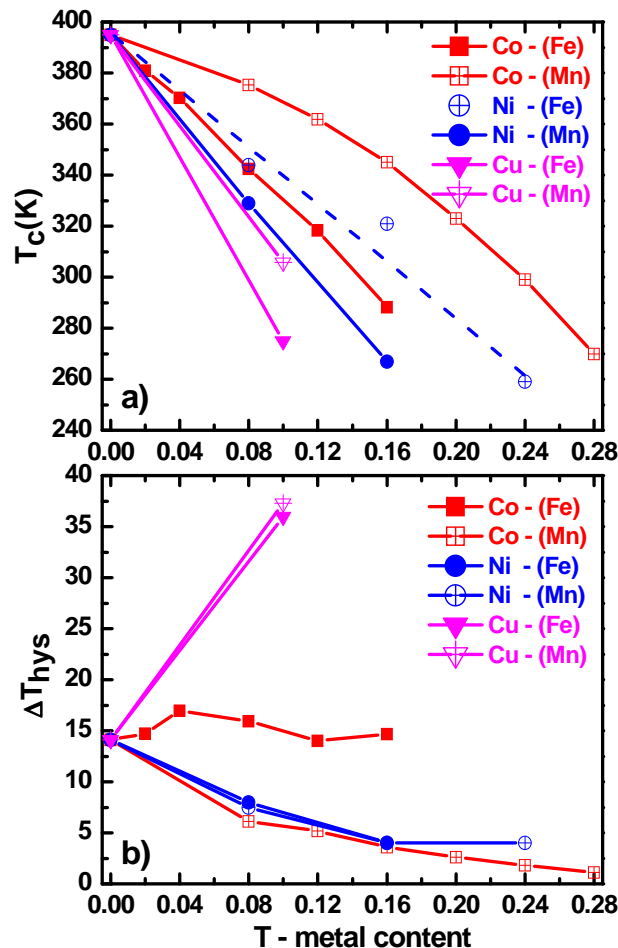


Figure 5.9 Overview of T_C and ΔT_{hys} as function of the transition metal content in $(Mn,Fe,T)_{1.95}P_{0.50}Si_{0.50}$ compounds .

5.5 Summary

The effect of transition metal substitution on T_C and ΔT_{hys} has been studied in $(Mn,Fe,T)_{1.95}P_{0.50}Si_{0.50}$ ($T = Co, Ni$ and Cu) compounds. X-ray diffraction patterns imply that all the compounds crystallize in the hexagonal Fe_2P type of structure. It is found that all these transition metal substitutions for Mn(3g)/Fe(3f) weaken the ferromagnetic ordering. Ni substitutions reduce the thermal hysteresis, while the Cu substitutions enhance the thermal hysteresis. Moreover, the Co substitutions for Mn(3g) reduce thermal hysteresis, while the Co substitutions for Fe(3f) result in hardly any change in thermal hysteresis.

References:

- [1] V.K. Pecharsky, K.A. Gschneidner, Giant magnetocaloric effect in $\text{Gd}_5(\text{Si}_2\text{Ge}_2)$, *Physical Review Letters* 78 (1997) 4494-4497.
- [2] F.X. Hu, B.G. Shen, J.R. Sun, Z.H. Cheng, G.H. Rao, X.X. Zhang, Influence of negative lattice expansion and metamagnetic transition on magnetic entropy change in the compound $\text{LaFe}_{11.4}\text{Si}_{1.6}$, *Applied Physics Letters* 78 (2001) 3675-3677.
- [3] H. Wada, Y. Tanabe, Giant magnetocaloric effect of $\text{MnAs}_{1-x}\text{Sb}_x$, *Applied Physics Letters* 79 (2001) 3302-3304.
- [4] O. Tegus, E. Brück, K.H.J. Buschow, F.R. de Boer, Transition-metal-based magnetic refrigerants for room-temperature applications, *Nature* 415 (2002) 150-152.
- [5] T. Krenke, E. Duman, M. Acet, E.F. Wassermann, X. Moya, L. Manosa and A. Planes, Inverse magnetocaloric effect in ferromagnetic Ni-Mn-Sn alloys, *Nature Materials* 4 (2005) 450-454.
- [6] O. Gutfleisch, M.A. Willard, E. Brück, C.H. Chen, S.G. Sankar and J.P. Liu, Magnetic materials and devices for the 21st Century: stronger, lighter, and more energy efficient, *Advanced Materials* 23 (2011) 821-842.
- [7] E. Brück, M. Ilyn, A.M. Tishin, O. Tegus, Magnetocaloric effects in $\text{MnFeP}_{1-x}\text{As}_x$ -based compounds, *Journal of Magnetism and Magnetic Materials* 290 (2005) 8-13.
- [8] W. Dagula, O. Tegus, B. Fuquan, L. Zhang, P.Z. Si, M. Zhang, W.S. Zhang, E. Brück, F.R. de Boer and K.H.J. Buschow, Magnetic-entropy change in $\text{Mn}_{1.1}\text{Fe}_{0.9}\text{P}_{1-x}\text{Ge}_x$ compounds. *IEEE Transactions on Magnetics* 41 (2005) 2778-2780.
- [9] L. Zhang, O. Može, K. Prokešc, O. Tegus, E. Brück, Neutron diffraction study of history dependence in $\text{MnFeP}_{0.6}\text{Si}_{0.4}$, *Journal of Magnetism and Magnetic Materials* 290 (2005) 679-681.
- [10] N.T. Trung, Z.Q. Ou, T.J. Gortenmulder, O. Tegus, K.H.J. Buschow, and E. Brück, Tunable thermal hysteresis in $\text{MnFe}(\text{P,Ge})$ compounds, *Applied Physics Letters* 94 (2009) 102513.

-
- [11] N.H. Dung, Z.Q. Ou, L. Caron, L. Zhang, D.T.C. Thanh, G.A. de Wijs, R.A. de Groot, K.H.J. Buschow, E. Brück, Mixed magnetism for refrigeration and energy conversion, *Advanced Energy Materials* 1 (2011) 1215-1219.
- [12] E. Brück, N.T. Trung, Z.Q. Ou and K.H.J. Buschow, Enhanced magnetocaloric effects and tunable thermal hysteresis in transition metal pnictides, *Scripta Materialia* 67 (2012) 590-593.
- [13] O. Tegus, G.X. Lin, W. Dagula, B. Fuquan, L. Zhang, E. Brück, F.R. de Boer and K.H.J. Buschow, A model description of the first-order phase transition in $MnFeP_{1-x}As_x$, *Journal of Magnetism and Magnetic Materials* 290 (2005) 658-660.
- [14] L. Caron, Z.Q. Ou, T.T. Nguyen, D.T. Cam Thanh, O. Tegus and E. Brück, On the determination of the magnetic entropy change in materials with first-order transitions, *Journal of Magnetism and Magnetic Materials* 321 (2009) 3559-3566.
- [15] A. Arrott, Criterion for ferromagnetism from observations of magnetic isotherms, *Physical Review* 108 (1957) 1394-1396.

Chapter 6

Structure, magnetism and magnetocalorics of Fe-rich $(\text{Mn,Fe})_{1.95}\text{P}_{1-x}\text{Si}_x$ melt-spun ribbons

6.1 Introduction

As described in chapter 4 $\text{MnFeP}_{1-x}\text{As}_x$ compounds are known for their good magnetocaloric and magnetic properties. However, the toxic element arsenic can be an obstacle for applications in household refrigeration appliances. In various studies As was successfully replaced by Ge and/or Si retaining the characteristics of the GMCE [1-5]. As discussed in the previous chapter for Si, the thermal and field hysteresis may markedly increase.

It has been shown, that the thermal hysteresis in the Mn-Fe-P-Ge compounds can be strongly reduced by adjusting the ratio of Mn/Fe and/or P/Ge, the heat treatment and the synthesis method [6]. In the Mn-Fe-P-Si system there appears to be also a metallurgical issue: it is difficult to avoid the formation of impurity phases. In most cases this impurity phase is the $(\text{Mn,Fe})_3\text{Si}$ phase [4]. A strong reduction of the impurity phase has been observed on adjusting the metal to non-metal ratio in the Mn-rich Mn-Fe-P-Si compounds [7]. As we observed that the amount of impurity phase strongly depends on the quality of the starting materials, a melt segregation may help to avoid impurity phases in the final sample. Melt-spinning combines liquid phase segregation and rapid solidification, which may result in fine grained single phase materials. In this chapter, the structural, magnetic and

magnetocaloric properties of the Fe-rich $\text{Mn}_{0.66}\text{Fe}_{1.29}\text{P}_{1-x}\text{Si}_x$ melt-spun ribbons have been investigated.

6.2 Sample preparation

Polycrystalline Fe-rich $(\text{Mn,Fe})_{1.95}(\text{P,Si})$ melt-spun ribbons were prepared using the melt spinning technique. Appropriate proportions of starting materials, pure Mn chips (purity 99.99%), Fe granules (purity 99.98%), Si pieces (purity 99.99%) and the binary compounds $\text{Fe}_{1.21}\text{P}$ (purity 97%), were put in a quartz crucible and melted by radio-frequency induction heating in an argon atmosphere. The obtained ingots were then put into a quartz tube with a nozzle at the bottom, melted and ejected through the nozzle on to the Cu wheel rotating at a surface speed of 40 m/s. The as-spun ribbons were annealed at 1100 °C for 2 hours before quenching into water. A total of 11 compositions of $\text{Mn}_{0.66}\text{Fe}_{1.29}\text{P}_{1-x}\text{Si}_x$ were studied, with $x = 0, 0.12, 0.18, 0.24, 0.30, 0.33, 0.34, 0.36, 0.37, 0.40$ and 0.42 . The X-ray diffraction patterns were collected at various temperatures with a PANalytical X-pert Pro diffractometer using Cu $K\alpha$ radiation, a secondary-beam flat-crystal monochromator and a multichannel X'celerator detector.

A superconducting quantum interference device (SQUID) magnetometer (Quantum Design MPMS 5XL) with the reciprocating sample option (RSO) mode was employed for magnetic measurements in the temperature range of 5 - 400 K and in magnetic fields up to 5 T. Measurements are performed on 1 - 2 mg of powder samples and temperature scans are performed at a sweep rate of 2 K/min. The differential scanning calorimetry (DSC) measurements were carried out using a TA-Q2000 DSC instrument in the temperature range from 90 to 820 K.

6.3 Structure and phase formation

The room-temperature X-ray diffraction patterns indicate that all Si containing quaternary samples studied crystallize in the hexagonal Fe_2P -type structure (space group $P-62m$). Only the ternary sample $\text{Mn}_{0.66}\text{Fe}_{1.29}\text{P}$ crystallizes in the orthorhombic Co_2P -type structure (space group $Pnma$), in good agreement with earlier results [8]. X-ray diffraction patterns are frequently used to determine the amount of impurity phases. In the Mn-Fe-P-Si system this is not straightforward, because the strongest characteristic reflection of the cubic $(\text{Mn,Fe})_3\text{Si}$ phase, a well-known impurity phase of Mn-Fe-P-Si compounds, usually overlaps with the (210) peak of the main phase in the ferromagnetic state [4, 9, 10]. This implies that X-ray

patterns below and above T_C need to be analyzed. As indicated by the dashed lines in Figure 6.1, no secondary phases were detected.

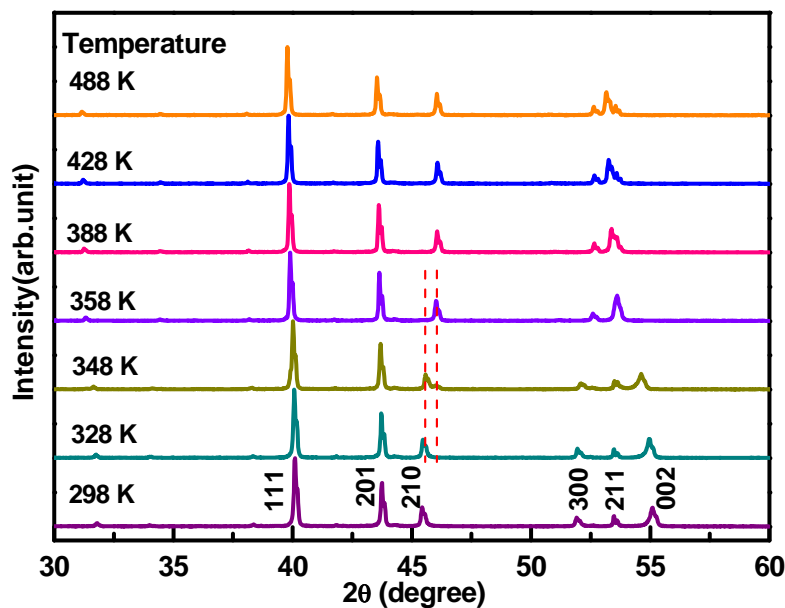


Figure 6.1 X-ray diffraction patterns of $\text{Mn}_{0.66}\text{Fe}_{1.29}\text{P}_{0.66}\text{Si}_{0.34}$ recorded at different temperatures. The lines indicate the (210) peak positions before and after the phase transition.

Figure 6.1 depicts the evolution of X-ray diffraction patterns with temperature in the 2θ range $30^\circ - 60^\circ$ for the $x = 0.34$ sample in the temperature range of 298 - 488 K recorded upon heating. Within this temperature range the $x = 0.34$ sample undergoes a ferromagnetic (FM) - paramagnetic (PM) phase transition without change in the crystal structure. The X-ray pattern at 348 K shows the coexistence of both the FM and PM phase, a characteristic feature of a first-order phase transition. With increasing temperature the (300) and (002) peaks shift towards each other, indicating the lattice constants a and c change in opposite sense.

Figure 6.2 shows the temperature dependence of the lattice parameters for the $\text{Mn}_{0.66}\text{Fe}_{1.29}\text{P}_{1-x}\text{Si}_x$ compounds with $x = 0.33, 0.37, 0.40$ and 0.42 . For all these compositions, the thermal evolution of the lattice parameters c resembles an S-shape rather than a linear response. An inverted S-shape is observed for the lattice parameter a . Thus, while the c parameter shows the expected increase with increasing temperature the a parameter shows a contraction upon heating over a wide range of temperatures. For an increasing Si content, the discontinuous change in lattice parameter at T_C becomes less pronounced. Besides, T_C is shifted to higher temperature with increasing Si content. Finally, the lattice parameter a increases while c decreases with increasing Si content.

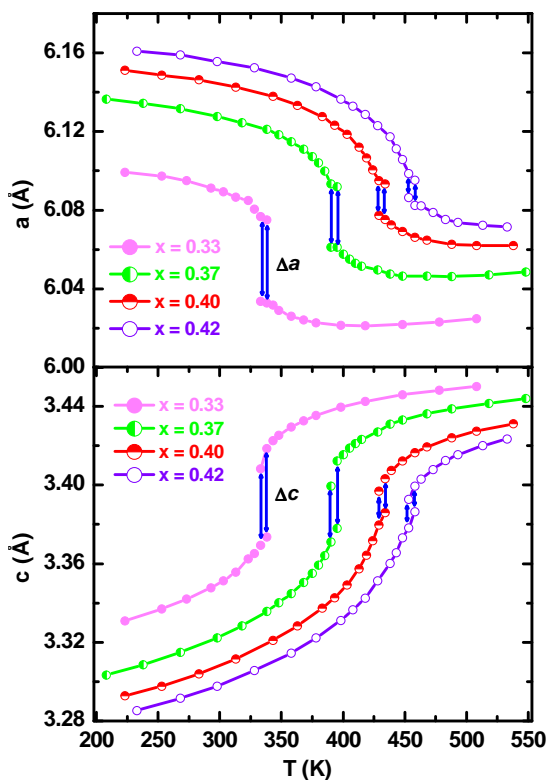


Figure 6.2 Temperature dependence of the lattice parameters a and c of the $\text{Mn}_{0.66}\text{Fe}_{1.29}\text{P}_{1-x}\text{Si}_x$ compounds with $x = 0.33, 0.37, 0.40$ and 0.42 derived from X-ray diffraction patterns measured upon heating. (arrows indicate the jump in lattice parameter in the two-phase region)

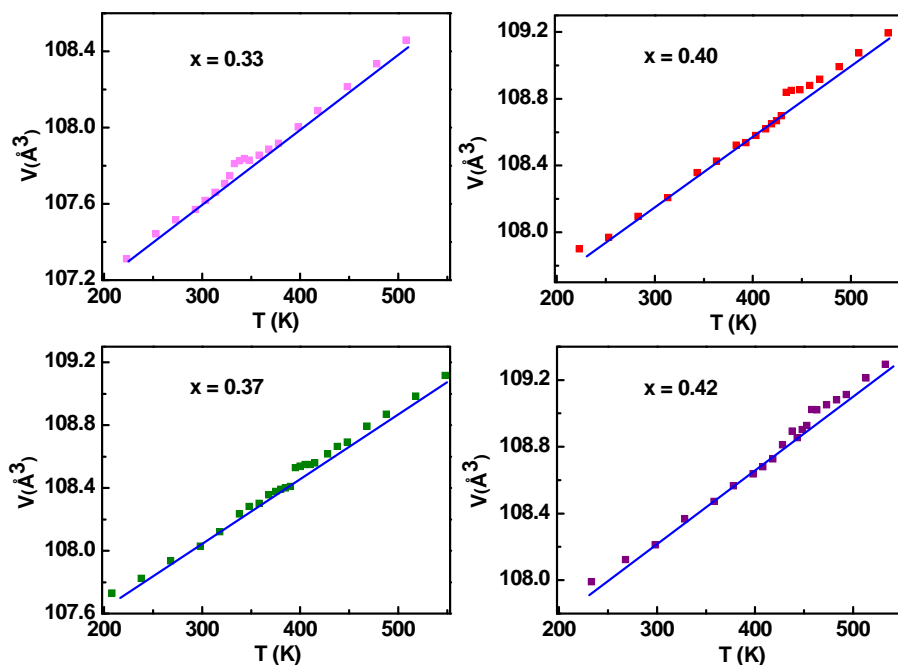


Figure 6.3 Temperature dependence of the volume of the $\text{Mn}_{0.66}\text{Fe}_{1.29}\text{P}_{1-x}\text{Si}_x$ compounds with $x = 0.33, 0.37, 0.40$ and 0.42 derived from X-ray diffraction patterns measured in nitrogen atmospheres upon heating.

These observations strongly support an exceptional coupling between the magnetism and the elastic properties of the lattice in these compounds. Obviously, this is not limited to the direct vicinity of T_C , but a rather broad temperature range above and below T_C is affected by this coupling. The width of this temperature range of this anomalous behavior appears to be inversely correlated with the size of the discontinuous change in lattice parameter at T_C . In other words the transition is smeared out over a larger temperature interval with increasing Si content, while the nature of the transition retains first-order.

Table 6.1 Structural and magnetization data for Mn_{0.66}Fe_{1.29}P_{1-x}Si_x compounds.

x	Struc.	Type of the magnetic transition	T_N (K)	T_C (K)	μ_s (μ_B)	ΔT_{hys} (K)	$-\Delta S_M$ (J/kgK) $\Delta B = 2$ T	Density** (g cm ⁻³)
0	O	AFM-PM	208					
0.12	H	AFM-PM	138					
0.18	H	AFM-PM	134					
0.24	H	FM-PM		195	3.97	61	12	6.55
0.30	H	FM-PM		258	4.27	14	15	6.51
0.33	H	FM-PM		338	4.38	2	10	6.48
0.34	H	FM-PM		350	4.57	3	11	6.49
0.36	H	FM-PM		375	4.42	1	12	6.48
0.37	H	FM-PM		392*	4.47	2*		6.47
0.40	H	FM-PM		427*	4.43	2*		6.46
0.42	H	FM-PM		451*	3.86	1*		6.45

μ_s is spontaneous magnetic moment given in μ_B /f.u., H = hexagonal, O = orthorhombic, AFM = anti-ferromagnetic, PM = paramagnetic, FM = ferromagnetic, the T_C values are determined from the heating M vs. T curves, the thermal hysteresis is measured at 1 T. *The values are obtained from zero-field DSC measurements with sweeping rate of 20 K/min. **The density is estimated from X-ray diffraction pattern measured at room temperature.

Discontinuous changes and nonlinear variations in lattice constants at and around the FM-PM phase transition, confirm the presence of a first-order magneto-elastic transition (FOMET). The coexistence of two phases at the transition is confirmed, as two sets of lattice parameters

are obtained. It is interesting to note that, although the changes in lattice parameters a and c at the phase transition are of the order of a percent, as they are in the opposite sense, they result in a rather small volume change ($< 0.1\%$), as depicted in Figure 6.3. The overall thermal volume expansion is linear and the coefficient of volume expansion is $3.7 \times 10^{-5} \text{ K}^{-1}$, in the same order of magnitude as pure Fe and Ni.

6.4 Magnetism and magnetocaloric effect

The temperature dependence of the magnetization of the $\text{Mn}_{0.66}\text{Fe}_{1.29}\text{P}_{1-x}\text{Si}_x$ compounds with $0 \leq x \leq 0.36$ measured in an applied magnetic field of 1 T is plotted in Figure 6.4. For the compounds with $x = 0, 0.12$ and 0.18 , an antiferromagnetic (AFM) – paramagnetic phase transition is observed, the Néel temperatures (T_N) are 208, 138 and 134 K, respectively. For the compounds with higher Si content, a FM-PM phase transition is observed and the T_C increases from 195 K for $x = 0.24$ to 375 K for $x = 0.36$, as shown in Table 6.1. All the magnetization curves plotted were chosen from the second cooling-heating cycle. The so called “virgin-effect” [2, 11] curves are excluded and all the magnetization curves are reproducible in subsequent cycles. For the compounds with $x \geq 0.37$, the T_C values are not measurable using the SQUID magnetometer due to the limitation of the accessible temperature range. The thermal hysteresis (ΔT_{hys}) between the cooling and heating transitions drastically reduces from ~ 61 K for $x = 0.24$ to ~ 2 K for $x = 0.33$ and the small thermal hysteresis is retained when further increasing Si content upto 0.42 wt.% (see Figure 6.5). The existence of ΔT_{hys} confirms the first-order nature of the transition, which is usually associated with the large MCE [12].

Figure 6.5 shows the temperature dependence of the specific heat (C_p) for the $\text{Mn}_{0.66}\text{Fe}_{1.29}\text{P}_{1-x}\text{Si}_x$ compounds with $x = 0.37, 0.40$ and 0.42 measured in zero-field using a Differential Scanning Calorimeter (DSC). A small thermal hysteresis between the cooling (dashed lines) and heating (solid lines) is observed. The transition temperature (T_C), determined from the peak position upon heating, are 392, 427 and 451 K for $x = 0.37, 0.40$ and 0.42 , respectively. The pronounced thermal effects confirm the first-order nature of the transitions.

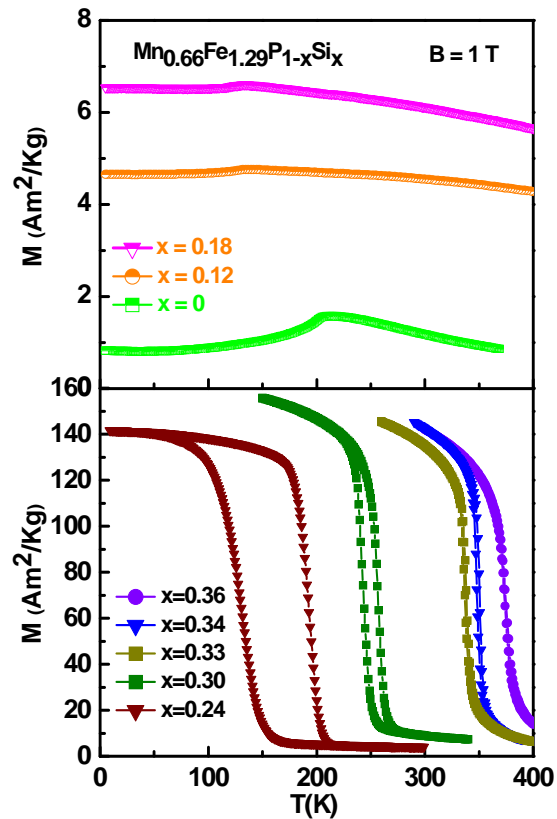


Figure 6.4 Temperature dependence of the magnetization of the $\text{Mn}_{0.66}\text{Fe}_{1.29}\text{P}_{1-x}\text{Si}_x$ compounds with $x = 0, 0.12$ and 0.18 , measured in a field of 1 T upon cooling. For the compounds with $x = 0.24, 0.30, 0.33, 0.34$ and 0.36 , measurements were performed in a field of 1 T upon both cooling and heating.

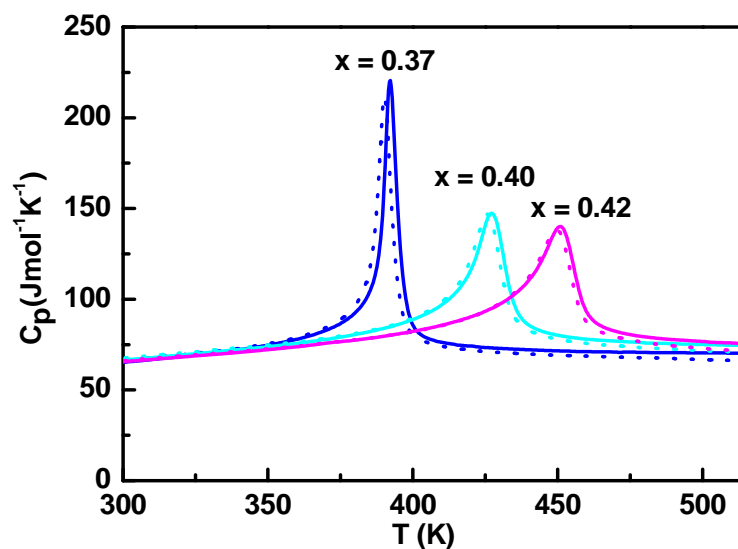


Figure 6.5 Temperature dependence of the specific heat of the $\text{Mn}_{0.66}\text{Fe}_{1.29}\text{P}_{1-x}\text{Si}_x$ compounds with $x = 0.37, 0.40$ and 0.42 measured in zero-field upon cooling (dashed lines) and heating (solid lines).

Figure 6.6 shows the magnetic field dependence of the magnetization of the $\text{Mn}_{0.66}\text{Fe}_{1.29}\text{P}_{1-x}\text{Si}_x$ compounds with $x = 0, 0.12, 0.18, 0.24, 0.30, 0.33, 0.34, 0.36, 0.37, 0.40$ and 0.42 at 5 K. The compounds with a Si content from 0.24 to 0.42 are ferromagnetic and their spontaneous magnetic moments (M_s) are between 3.86 and $4.57 \mu_B/\text{f.u.}$. These values are in agreement with those obtained from our neutron diffraction results (see Chapter 8). Note that, the M_s values of Fe-rich $\text{Mn}_{0.66}\text{Fe}_{1.29}\text{P}_{1-x}\text{Si}_x$ compounds are the largest among all the Fe_2P -based Mn-Fe-P-X (X = As, Ge and Si) compounds.[2, 4, 13-16]

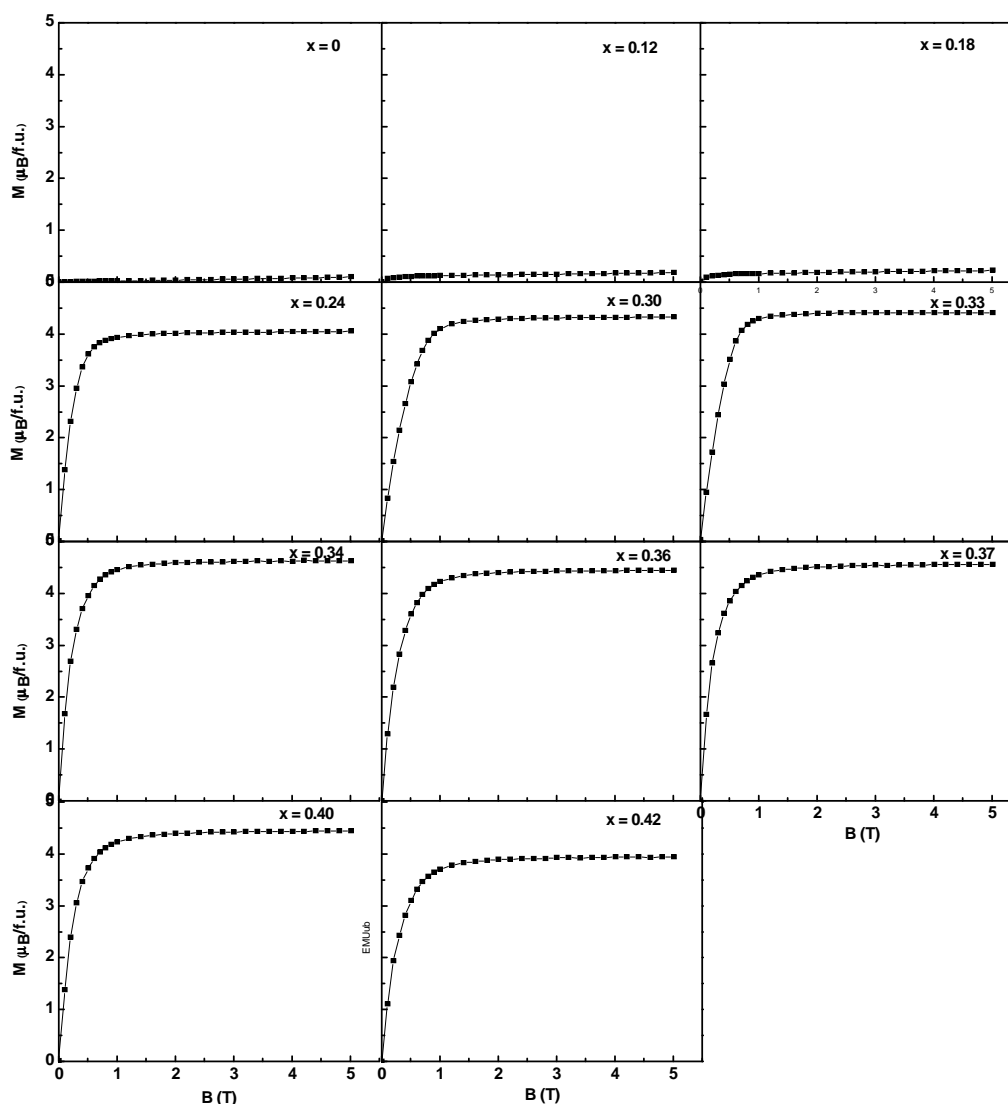


Figure 6.6 Field dependence of the magnetization of the $\text{Mn}_{0.66}\text{Fe}_{1.29}\text{P}_{1-x}\text{Si}_x$ compounds measured at 5 K.

Figure 6.7 (a) shows the isothermal magnetization loops measured in the vicinity of T_C for the sample with $x = 0.33$. A pronounced magnetic field-induced PM-FM transition is observed,

which is accompanied by a small magnetic field hysteresis between the field increasing and decreasing magnetization curves. These results from the first-order nature of the magnetic phase transition. For the samples with a large thermal hysteresis, the isothermal magnetization curves were measured following the method discussed by Caron *et al.* [17]. The isothermal magnetic entropy change $(-\Delta S_m)$ has been derived from the magnetic isotherms using the Maxwell equation (2.12). Figure 6.7 (b) shows the temperature dependence of the isothermal magnetic entropy change of the $x = 0.33$ sample in different magnetic field changes.

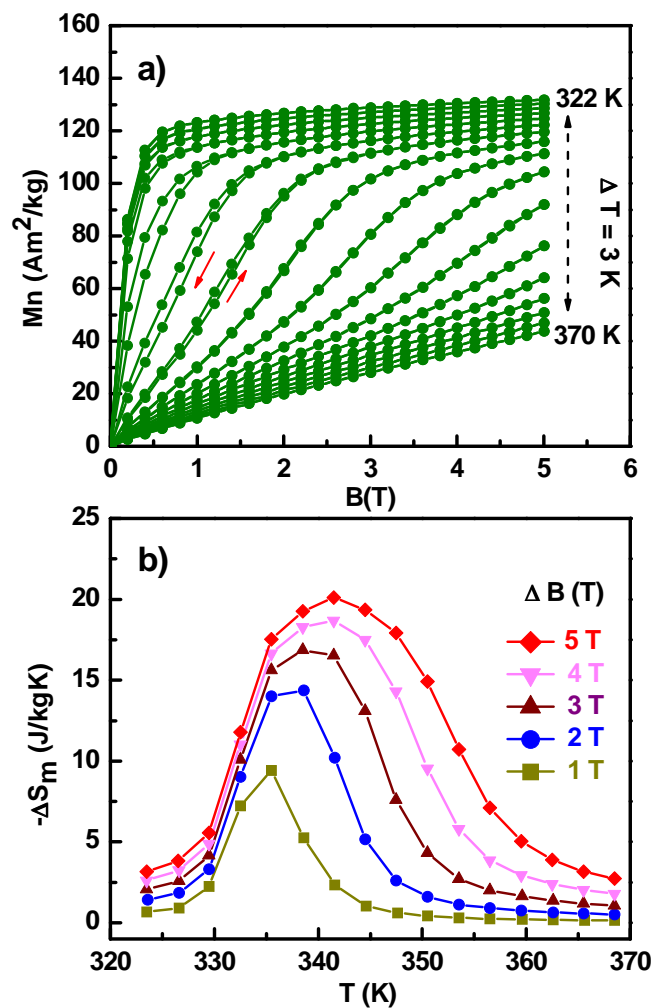


Figure 6.7 Magnetic isotherms of the $\text{Mn}_{0.66}\text{Fe}_{1.29}\text{P}_{0.67}\text{Si}_{0.33}$ compound in the vicinity of its T_C (a) and the magnetic entropy changes for different magnetic field change (b).

Figure 6.8 shows the temperature dependence of the magnetization curves $M(T)$ in different magnetic fields upon cooling and heating. T_C and the thermal hysteresis are field dependent. The T_C values on heating shift to higher temperatures with increasing field, indicating enhanced ferromagnetic interactions. The magnetic field induced PM-FM transition observed

in the Figure 6.7 (a), is triggered by this enhanced FM interaction. The insert in Figure 6.8 shows a linear increase of T_C with applied magnetic field. The rate ($\Delta T_C/\Delta B$) is about 4.4 K/T. ΔT_{hys} shows a slight reduction for increasing magnetic field.

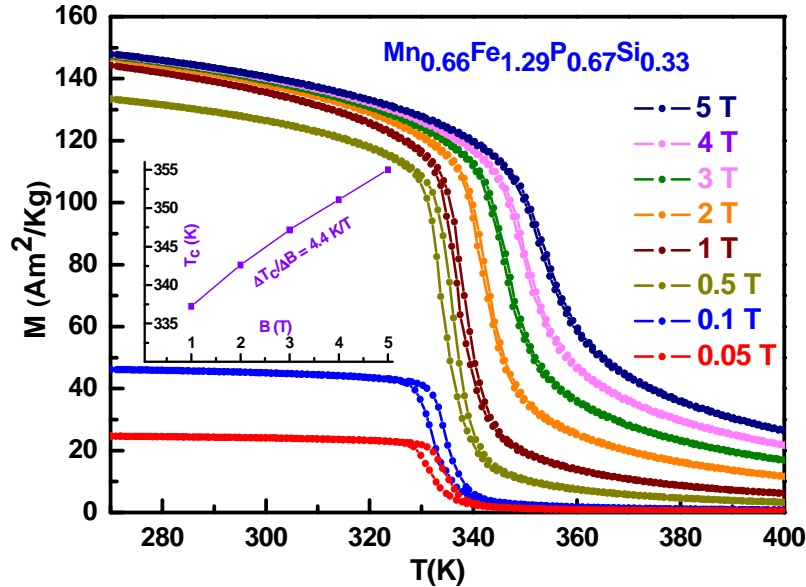


Figure 6.8 Temperature dependence of the magnetization of the $\text{Mn}_{0.66}\text{Fe}_{1.29}\text{P}_{0.67}\text{Si}_{0.33}$ compound measured with increasing temperature and then decreasing temperature.

6.5 Conclusions

We have synthesized the $\text{Mn}_{0.66}\text{Fe}_{1.29}\text{P}_{1-x}\text{Si}_x$ ($0 \leq x \leq 0.42$) single phase compounds using the melt-spinning (rapid solidification) technique. All the compounds form in the Fe_2P -type hexagonal structure, except a Co_2P -type orthorhombic structure of the Si-free $\text{Mn}_{0.66}\text{Fe}_{1.29}\text{P}$ compound. The compounds with $0.24 \leq x \leq 0.42$ present a FM-PM phase transition, while the compounds with lower Si content show an AFM-PM phase transition.

In the $\text{Mn}_{0.66}\text{Fe}_{1.29}\text{P}_{1-x}\text{Si}_x$ compounds, T_C and ΔT_{hys} are not only Si content dependent, but also magnetic field dependent. By increasing the Si content from $x = 0.24$ to 0.42 , T_C increases from 195 to 451 K and ΔT_{hys} is strongly reduced from ~ 61 to ~ 1 K. T_C increases and ΔT_{hys} decreases with increasing magnetic field, $\Delta T_C/\Delta B$ is about 4.4 K/T. $\text{Mn}_{0.66}\text{Fe}_{1.29}\text{P}_{1-x}\text{Si}_x$ compounds show large spontaneous magnetic moments with values up to $4.57 \mu_B/\text{f.u.}$. A large MCE with a small thermal hysteresis is obtained simultaneously in Fe-rich $\text{Mn}_{0.66}\text{Fe}_{1.29}\text{P}_{1-x}\text{Si}_x$ melt-spun ribbons. The compounds with a high working temperature may also be useful for other applications, *e.g.* thermomagnetic generators and heat pumps.

References:

- [1] A. Yan, K.H. Müller, L. Schultz and O. Gutfleisch, Magnetic entropy change in melt-spun MnFePGe (invited), *Journal of Applied Physics* 99 (2006) 08K903.
- [2] Z.Q. Ou, G.F. Wang, S. Lin, O. Tegus, E. Brück and K.H.J. Buschow, Magnetic properties and magnetocaloric effects in $\text{Mn}_{1.2}\text{Fe}_{0.8}\text{P}_{1-x}\text{Ge}_x$ compounds, *Journal of Physics: Condensed Matter* 18 (2006) 11577-11584.
- [3] D.T. Cam Thanh, E. Brück, J.C.P. Klaasse and K.H.J. Buschow, Influence of Si and Ge on the magnetic phase transition and magnetocaloric properties of MnFe(P,Si,Ge), *Journal of Magnetism and Magnetic Materials* 310 (2007) E1012-E1014.
- [4] D.T. Cam Thanh, E. Brück, N.T. Trung, J.C.P. Klaasse, K.H.J. Buschow, Z.Q. Ou, O. Tegus and L. Caron, Structure, magnetism, and magnetocaloric properties of $\text{MnFeP}_{1-x}\text{Si}_x$ compounds, *Journal of Applied Physics* 103 (2008) 07B318.
- [5] L. Song, G.F. Wang, Z.Q. Ou, O. Haschaolu, O. Tegus, E. Brück and K.H.J. Buschow, Magnetic properties and magnetocaloric effect of $\text{MnFeP}_{0.5}\text{Ge}_{0.5-x}\text{Si}_x$ compounds, *Journal of Alloys and Compounds* 474 (2009) 388-390.
- [6] N.T. Trung, Z.Q. Ou, T.J. Gortenmulder, O. Tegus, K.H.J. Buschow and E. Brück, Tunable thermal hysteresis in MnFe(P,Ge) compounds, *Applied Physics Letters* 94 (2009) 102513.
- [7] N.H. Dung, L. Zhang, Z.Q. Ou and E. Brück, From first-order magneto-elastic to magneto-structural transition in $(\text{Mn,Fe})_{1.95}\text{P}_{0.50}\text{Si}_{0.50}$ compounds, *Applied Physics Letters* 99 (2011) 092511.
- [8] R. Fruchart, A. Roger and J.P. Sendteur, Crystallographic and magnetic properties of solid solutions of phosphides M_2P , $\text{M} = \text{Cr, Mn, Fe, Co and Ni}$, *Journal of Applied Physics* 40 (1969) 1250-1257.
- [9] L. Zhang, E. Brück, O. Tegus, K.H.J. Buschow and F.R. de Boer, The crystallographic phases and magnetic properties of $\text{Fe}_2\text{MnSi}_{1-x}\text{Ge}_x$. *Physica B: Condensed Matter* 328 (2003) 295-301.
- [10] D.T. Cam Thanh, *Magnetocalorics and magnetism in MnFe(P,Ge,Si) materials*, PhD thesis, Universiteit van Amsterdam, Chapter 4 and 5 (2009) 27-88.
- [11] L. Zhang, O. Može, K. Prokešc, O. Tegus and E. Brück, Neutron diffraction study of history dependence in $\text{MnFeP}_{0.6}\text{Si}_{0.4}$, *Journal of Magnetism and Magnetic Materials* 290 (2005) 679-681.

- [12] A.M. Tishin and Y.I. Spichkin, *The magnetocaloric effect and its application*, Institute of Physics Publishing, Bristol (2003).
- [13] E. Brück, O. Tegus, X.W. Li, F.R. de Boer and K.H.J. Buschow, Magnetic refrigeration towards room-temperature applications, *Physica B: Condensed Matter* 327 (2003) 431-437.
- [14] W. Dagula, O. Tegus, B. Fuquan, L. Zhang, P.Z. Si, M. Zhang, W.S. Zhang, E. Brück, F.R. de Boer and K.H.J. Buschow, Magnetic-entropy change in $Mn_{1.1}Fe_{0.9}P_{1-x}Ge_x$ compounds, *IEEE Transactions On Magnetics* 41 (2005) 2778-2780.
- [15] M. Bacmann, J.L. Soubeyroux, R. Barrett, D. Fruchart, R. Zach, S. Niziol, R. Fruchart, Magnetoelastic transition and antiferro-ferromagnetic ordering in the system $MnFeP_{1-y}As_y$, *Journal of Magnetism and Magnetic Materials* 134 (1994) 59-67.
- [16] N.H. Dung, L. Zhang, Z.Q. Ou, L. Zhao, L. van Eijck, A.M. Mulders, M. Avdeev, E. Suard, N.H. van Dijk, E. Brück, High/low-moment phase transition in hexagonal Mn-Fe-P-Si compounds, *Physical Review B* 86 (2012) 045134.
- [17] L. Caron, Z.Q. Ou, T.T. Nguyen, D.T. Cam Thanh, O. Tegus and E. Brück, On the determination of the magnetic entropy change in materials with first-order transitions, *Journal of Magnetism and Magnetic Materials* 321 (2009) 3559-3566.

Chapter 7

Structure, magnetism and magnetocalorics of Fe-rich $\text{Mn}_{1.95-x}\text{Fe}_x\text{P}_{2/3}\text{Si}_{1/3}$ compounds

7.1 Introduction

In Chapter 6, we reported the structure, magnetism and magnetocalorics in Fe-rich $(\text{MnFe})_{1.95}\text{P}_{1-x}\text{Si}_x$ compounds, in which the ferromagnetic (FM) – paramagnetic (PM) transition temperature can be easily tuned from 195 to 451 K by varying the P/Si ratio. The thermal hysteresis is strongly reduced from ~61 K for $x = 0.24$ to ~2 K for $x = 0.33$ and the small value is retained up to $x = 0.42$. While on the metal sites, the transition metals substitution (Chapter 5) shows strong effects not only on the magnetic interaction, but also on the thermal and field hysteresis. In this chapter, we show systematic studies on the structure, magnetism and magnetocalorics of Fe-rich $\text{Mn}_{1.95-x}\text{Fe}_x\text{P}_{2/3}\text{Si}_{1/3}$ compounds by varying the Mn/Fe ratio.

7.2 Sample preparation

Polycrystalline Fe-rich $\text{Mn}_{1.95-x}\text{Fe}_x\text{P}_{2/3}\text{Si}_{1/3}$ compounds with $x = 1.0, 1.1, 1.2, 1.3, 1.4, 1.5, 1.6, 1.7, 1.8, 1.9$ and 1.95 were prepared by ball milling technology, followed by a solid-state reaction as described in Chapter 5. The X-ray diffraction patterns were collected at various temperatures with a PANalytical X-pert Pro diffractometer using $\text{Cu K}\alpha$ radiation, a secondary-beam flat-crystal monochromator and a multichannel X'celerator detector. A superconducting quantum interference device (SQUID) magnetometer (Quantum Design MPMS 5XL) with the reciprocating sample option (RSO) mode was employed for magnetic measurements in the temperature range of 5 - 400 K and in magnetic fields up to 5 T. The differential scanning calorimetry (DSC) measurements were carried out using a TA-Q2000 DSC instrument in the temperature range of 90 to 820 K.

7.3 Structure and phase formation

X-ray diffraction patterns show that all the $\text{Mn}_{1.95-x}\text{Fe}_x\text{P}_{2/3}\text{Si}_{1/3}$ compounds with $1.0 \leq x \leq 1.6$ crystallize in Fe_2P -based hexagonal structure. The compounds with higher Fe content show a body-centered orthorhombic (*bco*) to hexagonal (*hex*) structural transition. A phase diagram of the crystal structure and magnetic phase transitions as a function of the temperature and Fe content is shown in Figure 7.1.

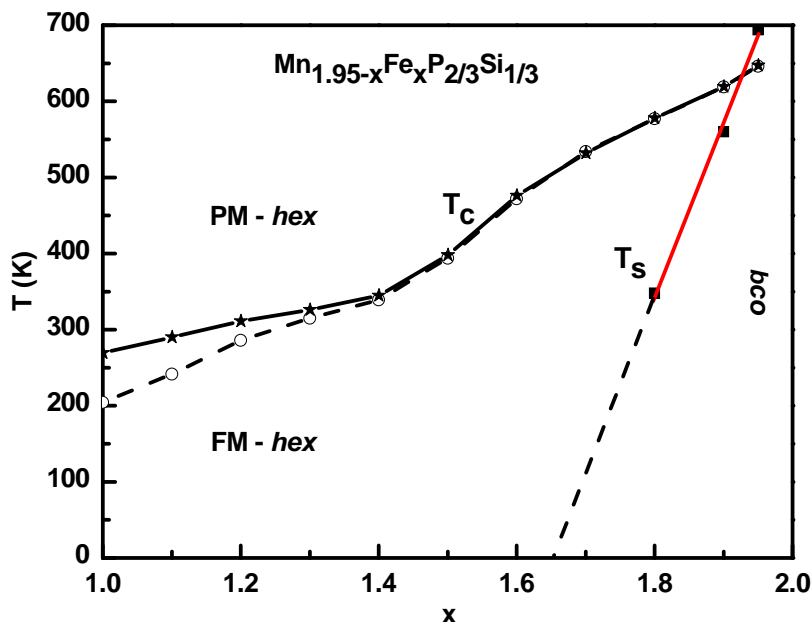


Figure 7.1 Phase diagram of the Fe content dependence of the phase transition temperatures of the $\text{Mn}_{1.95-x}\text{Fe}_x\text{P}_{2/3}\text{Si}_{1/3}$ compounds. T_C is the magnetic ordering temperature upon cooling (open circles) and heating (solid stars), T_S is the *bco* - *hex* structural transition temperature.

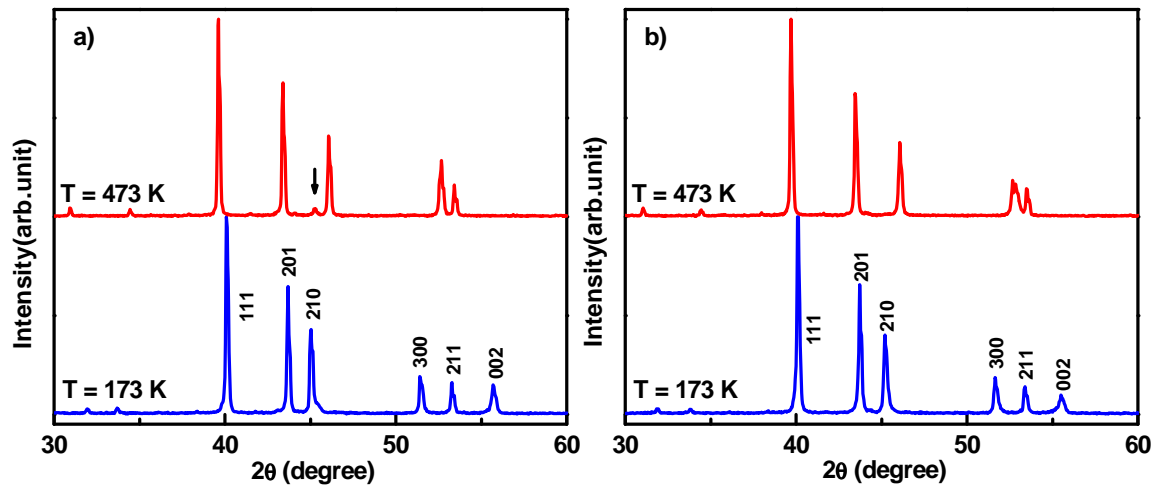


Figure 7.2 X-ray diffraction patterns collected at 173 K (FM) and 475 K (PM) for the $\text{Mn}_{1.95-x}\text{Fe}_x\text{P}_{2/3}\text{Si}_{1/3}$ compounds with $x = 1.0$ (a) and $x = 1.2$ (b).

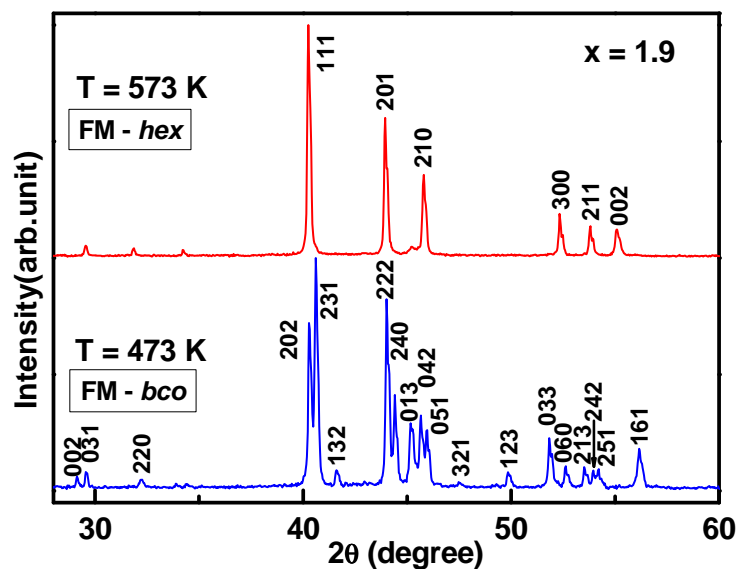


Figure 7.3 X-ray diffraction pattern of the $x = 1.9$ compound collected at 473 K (FM – *bco*) and 573 K (FM – *hex*).

Figure 7.2 shows the X-ray diffraction patterns collected at 173 K (ferromagnetic state) and 475 K (paramagnetic state) for the representative samples $x = 1.0$ (a) and $x = 1.2$ (b). The hexagonal Fe_2P -type structure (space group $P-62m$) is confirmed below and above the FM-PM phase transition. For $x = 1.0$ sample, a minor impurity $(\text{Mn,Fe})_3\text{Si}$ phase ($\sim 0.36\%$) is observed. This phase is only observed in the paramagnetic diffraction pattern, as this reflection peak is overlapping with the (210) peak of the main phase in the FM state [1]. For $x = 1.2$ sample, a single phase pattern is confirmed.

Figure 7.3 shows the X-ray diffraction patterns collected at 473 K (FM - *bco*) and 573 K (FM - *hex*) for the $x = 1.9$ sample, these confirm a *bco-hex* structural transition and a single phase sample. The lattice parameters are listed in Table 7.1.

Table 7.1 Lattice parameters of the $x = 1.9$ compound in FM - *bco* and FM - *hex* crystal structure.

$x = 1.9$						
Temperature (K)	Crystal structure	Space group	Lattice parameters			
			a (Å)	b (Å)	c (Å)	V (Å ³)
473	<i>hex</i>	<i>P-62m</i>	6.0589 ₂	6.0589 ₂	3.33636 ₈	106.070 ₅
573	<i>bco</i>	<i>Imm2</i>	6.5585 ₄	10.4465 ₆	6.1445 ₃	420.98 ₄

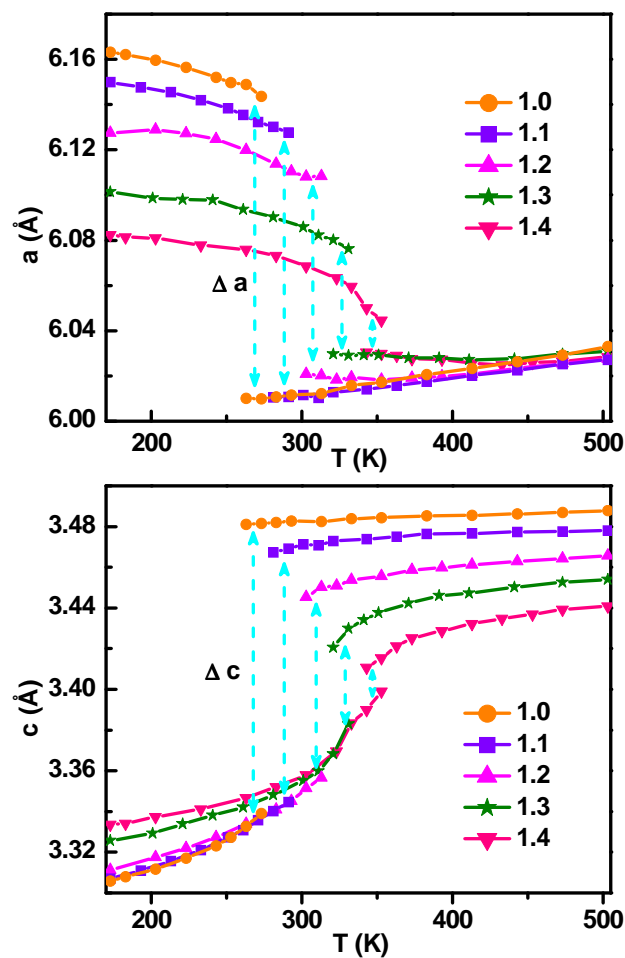


Figure 7.4 Temperature dependence of the lattice parameters a and c of the $\text{Mn}_{1.95-x}\text{Fe}_x\text{P}_{2/3}\text{Si}_{1/3}$ compounds with $x = 1.0, 1.1, 1.2, 1.3$ and 1.4 derived from X-ray diffraction patterns measured upon heating (arrows indicate the jump in lattice parameters in the two-phase coexistent region).

Figure 7.4 shows the temperature dependence of the lattice parameters for the $\text{Mn}_{1.95-x}\text{Fe}_x\text{P}_{2/3}\text{Si}_{1/3}$ compounds with $x = 1.0, 1.1, 1.2, 1.3$ and 1.4 . A discontinuous change of

the lattice parameters a and c is observed at the transition for all the compounds. T_C shifts with about 2 K/%Fe to higher temperature with increasing Fe content.

For increasing temperature, the lattice parameters a and c change abruptly at the transition, while only a small volume expansion ($\Delta V/V$) of $< 0.1\%$ is observed. For all these compositions, the thermal evolution of the lattice parameters a and c show discontinuous changes at the transition, confirming the transition is of first-order. The Δa and Δc values decrease with increasing Fe content (see Figure 7.4). The relative lattice parameter changes $|\Delta a/a|$ and $|\Delta c/c|$ decrease from 2.2% and 4.1% for $x = 1.0$ to 0.24% and 0.54% for $x = 1.4$, respectively (see Table 7.2). Comparing these $|\Delta a/a|$ and $|\Delta c/c|$ values with the ΔT_{hys} , it is found that the magnitudes of the relative lattice parameter changes are correlated with the magnitude of the ΔT_{hys} . However, since both parameters are extrinsic, the relationship is just qualitative.

Table 7.2 Curie temperature (T_C) upon heating and thermal hysteresis (ΔT_{hys}) determined from zero field DSC measurement with a sweeping rate of 20 K/min, $|\Delta a/a|$ and $|\Delta c/c|$ are relative lattice parameter changes at the transition for the Mn_{1.95-x}Fe_xP_{2/3}Si_{1/3} compounds.

Composition	T_C (K)	ΔT_{hys} (K)	$ \Delta a/a $ (%)	$ \Delta c/c $ (%)
$x = 1.0$	269	65	2.2	4.1
$x = 1.1$	290	49	1.9	3.5
$x = 1.2$	311	25	1.4	2.6
$x = 1.3$	326	11	0.77	1.1
$x = 1.4$	345	6	0.24	0.54

7.4 Magnetism and magnetocaloric effect

Figure 7.5 shows the temperature dependence of the magnetization of the Mn_{1.95-x}Fe_xP_{2/3}Si_{1/3} compounds with $1.0 \leq x \leq 1.5$ measured in an applied magnetic field of 1 T. Because the materials are prone to the virgin-effect, all the magnetization curves are plotted from the second or third heating-cooling cycles and thus are repeatable. The existence of thermal hysteresis (ΔT_{hys}) confirms the first-order nature of the transition, which is usually associated with a large MCE [2]. ΔT_{hys} drastically reduces from ~ 65 K for $x = 1.0$ to ~ 4 K for $x = 1.5$. DSC measurements show the ΔT_{hys} is further reduced to ~ 1 K for $x = 1.7$. Very small values of ΔT_{hys} are retained for higher Fe content compounds (see Figure 7.1). All the compounds show a FM-PM phase transition. Their transition temperatures upon heating increase almost linearly from 269 K for $x = 1.0$ to 345 K for $x = 1.4$. For higher Fe contents, a steeper increase in T_C is observed.

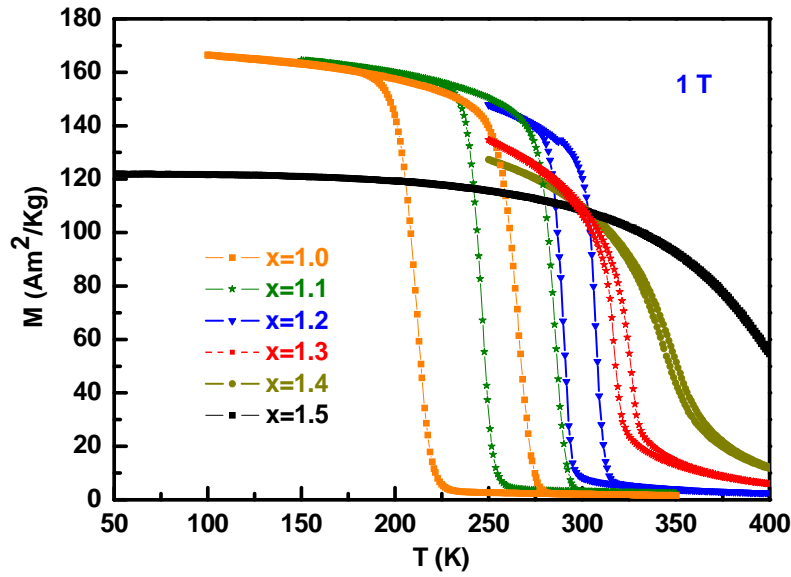


Figure 7.5 Temperature dependence of the magnetization of the $\text{Mn}_{1.95-x}\text{Fe}_x\text{P}_{2/3}\text{Si}_{1/3}$ compounds with $1.0 \leq x \leq 1.5$, measured in a field of 1 T upon cooling and heating.

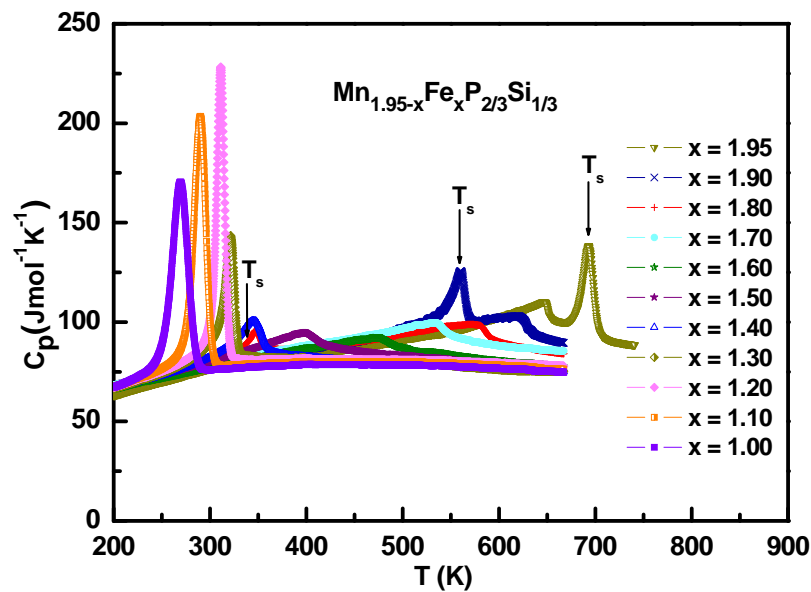


Figure 7.6 Temperature dependence of specific heat of the $\text{Mn}_{1.95-x}\text{Fe}_x\text{P}_{2/3}\text{Si}_{1/3}$ compounds measured in zero field with a sweeping rate of 20 K/min upon heating. T_s indicates the *bco-hex* structural transition temperature.

Since the Fe and Mn atoms favor the $3f$ and $3g$ sites, respectively, in Fe-rich $\text{Mn}_{1.95-x}\text{Fe}_x\text{P}_{2/3}\text{Si}_{1/3}$ compounds, the excess Fe atoms occupy the $3g$ sites. It appears that the ferromagnetic Fe/Mn($3g$)-Fe($3f$) interlayer exchange coupling is enhanced by introducing Fe on the $3g$ sites, as more Fe atoms on the $3g$ sites, strongly enhances T_C (see Figure 7.1 and 7.6). Note that, the T_C of the Mn-free compound is in good agreement with the value reported in reference [3]. For the compounds with $1.0 \leq x \leq 1.2$, the FOMT is pronounced. A further

increase of the Fe content ($1.3 \leq x \leq 1.95$) strongly weakens the first-order nature of transition, as shown in Figure 7.6.

Figure 7.7 shows the magnetic field dependence of the magnetization of the $\text{Mn}_{1.95-x}\text{Fe}_x\text{P}_{2/3}\text{Si}_{1/3}$ compounds with $1.0 \leq x \leq 1.9$ at 5 K. All the compounds are ferromagnetic at 5 K. The saturation magnetic moments (M_s) are between 3.1 and 4.3 $\mu_B/\text{f.u.}$. The moment is independent from the Fe content for the compounds with $1.0 \leq x \leq 1.2$ and decreases with further increasing the Fe content. The M_s of Fe-rich $\text{Mn}_{1.95-x}\text{Fe}_x\text{P}_{2/3}\text{Si}_{1/3}$ compounds are larger than that of Mn-rich Mn-Fe-P-Si compounds [4]. In contrast with the enhancement of the Fe/Mn(3g)-Fe(3f) interlayer exchange coupling, the reduction of the magnetic moment in the Fe-rich $\text{Mn}_{1.95-x}\text{Fe}_x\text{P}_{2/3}\text{Si}_{1/3}$ compounds, suggests that the local electron configuration is dominant to the size of the moment, thus confirming a more localized magnetism on the 3g sites.

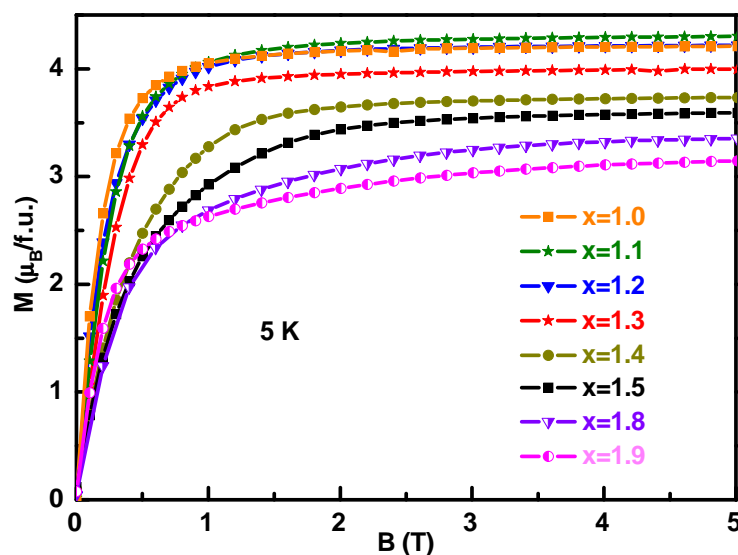


Figure 7.7 Field dependence of the magnetization of the $\text{Mn}_{1.95-x}\text{Fe}_x\text{P}_{2/3}\text{Si}_{1/3}$ compounds measured at 5 K.

Figure 7.8a and 7.8c show the isothermal magnetization loops measured in the vicinity of T_C for the $\text{Mn}_{1.95-x}\text{Fe}_x\text{P}_{2/3}\text{Si}_{1/3}$ compounds with $x = 1.2$ and 1.4, as representatives. Since the compounds show a large ΔT_{hys} , the magnetization data were collected with the loop method as discussed in reference [5]. For the $x = 1.2$ compound, a magnetic-field induced PM-FM transition is reflected in the S-shaped magnetization isotherms, while the field-induced transition is not visible for the compound with the higher Fe content $x = 1.4$. The isothermal magnetic entropy change ($-\Delta S_m$) has been derived from the magnetic isotherms using the

Maxwell equation (2.12). The $-\Delta S_m$ value as a function of temperature for the $Mn_{1.95-x}Fe_xP_{2/3}Si_{1/3}$ compounds with $x = 1.2$ and 1.4 are shown in Figure 7.8b and 7.8d. The lower MCE for the $x = 1.4$ compound is due to lower magnetic moment and the broader FM-PM phase transition that is possibly related to a wider spread in local critical temperature [6].

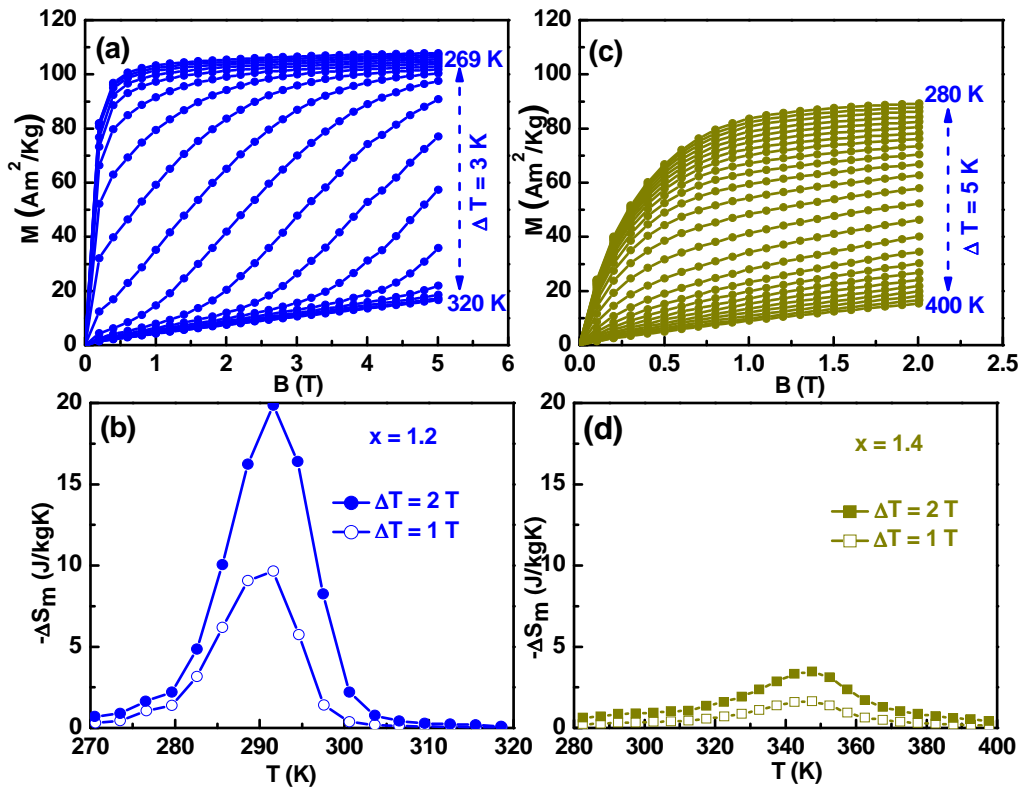


Figure 7.7 Magnetic isotherms of the $Mn_{1.95-x}Fe_xP_{2/3}Si_{1/3}$ compound with $x = 1.2$ and 1.4 in the vicinity of their T_C values (a and c) and the magnetic entropy changes for different magnetic field change (b and d).

7.5 Conclusions

We have synthesized single phase $Mn_{1.95-x}Fe_xP_{2/3}Si_{1/3}$ compounds with $1.0 \leq x \leq 1.95$ using ball-milling technology and solid-state reactions. All the compounds show a FM-PM phase transition. The compounds with $x \leq 1.6$ crystallize in Fe_2P -based hexagonal structure, for the higher Fe content compounds, a *bco-hex* structural transition is observed. In contrast to the Mn-rich Mn-Fe-P-Si system, no coupling between the magnetic and structural transition is found [7].

T_C and ΔT_{hys} in the $\text{Mn}_{1.95-x}\text{Fe}_x\text{P}_{2/3}\text{Si}_{1/3}$ compounds can be easily tuned by adjusting the Fe/Mn ratio. By increasing the Fe content from $x = 1.0$ to 1.95, the T_C increases from ~ 269 to ~ 647 K and the ΔT_{hys} strongly reduces from ~ 65 to ~ 1 K.

The reduction in the magnetic moment of the Fe-rich $\text{Mn}_{1.95-x}\text{Fe}_x\text{P}_{2/3}\text{Si}_{1/3}$ compounds, suggests that the dominant effect on the size of the moment is the change in local electron configuration rather than the interlayer exchange coupling, thus confirming a more localized magnetism on the 3g sites.

References

- [1] L. Zhang, O. Može, K. Prokešc, O. Tegus, E. Brück, Neutron diffraction study of history dependence in $\text{MnFeP}_{0.6}\text{Si}_{0.4}$, *Journal of Magnetism and Magnetic Materials* 290 (2005) 679-681.
- [2] A.M. Tishin and Y.I. Spichkin, *The magnetocaloric effect and its application*, Institute of Physics Publishing, Bristol (2003).
- [3] P. Jernberg, A.A. Yousif, L. Haggstrom, Y. Andersson, A Mössbauer study of $\text{Fe}_2\text{P}_{1-x}\text{Si}_x$ ($x \leq 0.35$), *Journal of Solid State Chemistry* 53 (1984) 313-322.
- [4] N.H. Dung, L. Zhang, Z.Q. Ou, L. Zhao, L. van Eijck, A.M. Mulders, M. Avdeev, E. Suard, N.H. van Dijk, E. Brück, High/low-moment phase transition in hexagonal Mn-Fe-P-Si compounds, *Physical Review B* 86 (2012) 045134.
- [5] L. Caron, Z.Q. Ou, T.T. Nguyen, D.T. Cam Thanh, O. Tegus and E. Brück, On the determination of the magnetic entropy change in materials with first-order transitions. *Journal of Magnetism and Magnetic Materials* 321 (2009) 3559-3566.
- [6] R.P. Hermann, O. Tegus, E. Brück, K.H.J. Buschow, F.R. de Boer, G.J. Long and F. Grandjean, Mössbauer spectral study of the magnetocaloric $\text{FeMnP}_{1-x}\text{As}_x$ compounds. *Physical Review B* 70 (2004) 214425.
- [7] N.H. Dung, L. Zhang, Z.Q. Ou and E. Brück, From first-order magneto-elastic to magneto-structural transition in $(\text{Mn,Fe})_{1.95}\text{P}_{0.50}\text{Si}_{0.50}$ compounds, *Applied Physics Letters* 99 (2011) 092511.

Chapter 8

Neutron diffraction study on the magnetic structure of Fe₂P-based (MnFe)_{1.95}P_{1-x}Si_x melt-spun ribbons

8.1 Introduction

The giant magnetocaloric effect (GMCE), that is associated with a first-order magnetic transition (FOMT), makes near room-temperature magnetic refrigeration attractive as a highly efficient and eco-benign technology [1-7]. We discovered a GMCE in the Fe₂P-type hexagonal (Mn,Fe)₂(P,Si) compounds. Initially a large thermal hysteresis (> 20 K) associated with the FOMT in MnFe(P,Si) hampered the use of this material for cyclic applications [8]. By varying the Mn/Fe ratio well away from 1, the thermal hysteresis has been significantly reduced to about 1 K for specific P/Si ratios while the GMCE is well preserved [9]. The discovery of high-performance and low-cost (Mn,Fe)₂(P,Si) compounds paves the way for commercial applications.

The earlier results show that Mn and Fe preferentially occupy different alternating layers in the Fe₂P structure. A high local magnetic moment is associated with the Mn layer and a lower moment with the Fe layer. For a Mn/Fe ratio that is unequal to 1, the excess Fe or Mn atoms will inevitably occupy the other layer. Consequently, the site disorder will affect the magnetic interactions. Meanwhile, first principle electronic structure calculations suggest that the origin of the GMCE is the coexistence of strong and weak magnetism in alternate atomic layers. The weak magnetism (disappearance of local magnetic moments at the Curie

temperature) is responsible for a strong coupling with the crystal lattice [9]. Knowing how the site disorder affects the local magnetic moment of each layer will help understanding the property-tuning mechanism. With neutron diffraction, the magnetic structure and the distribution of Fe and Mn atoms can be resolved by, while Fe and Mn can hardly be distinguished by X-ray diffraction. The insight obtained from these experiments will provide a handle to further improve this material for applications.

8.2 Experimental details

The Fe-rich compounds $\text{Mn}_{0.66}\text{Fe}_{1.29}\text{P}_{1-x}\text{Si}_x$ ($x = 0.34, 0.37$ and 0.42) were prepared by the melt-spinning technique. The melt-spun ribbons were produced under argon atmosphere at a 40 m/s surface speed of the copper wheel. The as-spun ribbons were subsequently quenched into water after annealing at 1100 °C for 2 hours. The X-ray diffraction patterns were collected at various temperatures in zero field using a PANalytical X-pert Pro diffractometer equipped with an Anton Paar TTK450 low-temperature chamber using Cu $K\alpha$ radiation, a secondary-beam flat-crystal monochromator and a multichannel X'celerator detector. The neutron diffraction data were collected at the Bragg Institute of the Australian Nuclear Science and Technology Organization (ANSTO) on the ECHIDNA high-resolution powder diffractometer with an incident wavelength of 1.622 Å [10]. The sample powder was contained in a vanadium can which was mounted in a cryostat. The measurements were carried out at fixed temperatures in the ferromagnetic and the paramagnetic state in zero field. The refinement of all the diffraction patterns was performed by the Rietveld method [11] using the FullProf program [12]. A superconducting quantum interference device (SQUID) magnetometer (Quantum Design MPMS 5XL) with the reciprocating sample option (RSO) mode was employed for magnetic measurements below 400 K.

8.3 Structural parameters

X-ray diffraction measurements indicate that all the compounds $\text{Mn}_{0.66}\text{Fe}_{1.29}\text{P}_{1-x}\text{Si}_x$ ($x = 0.34, 0.37$ and 0.42) crystallize in the hexagonal Fe_2P -type structure (space group $P-62m$). As shown in Figure 8.1, the contour plots display the thermal evolution of the X-ray diffraction patterns of all the compounds. For the compounds with $x = 0.34$ and 0.37 , a discontinuity of the diffraction peak positions at the transition temperatures indicates a step change in lattice constants. While the compound with the highest Si content ($x = 0.42$) shows a nearly continuous peak shift.

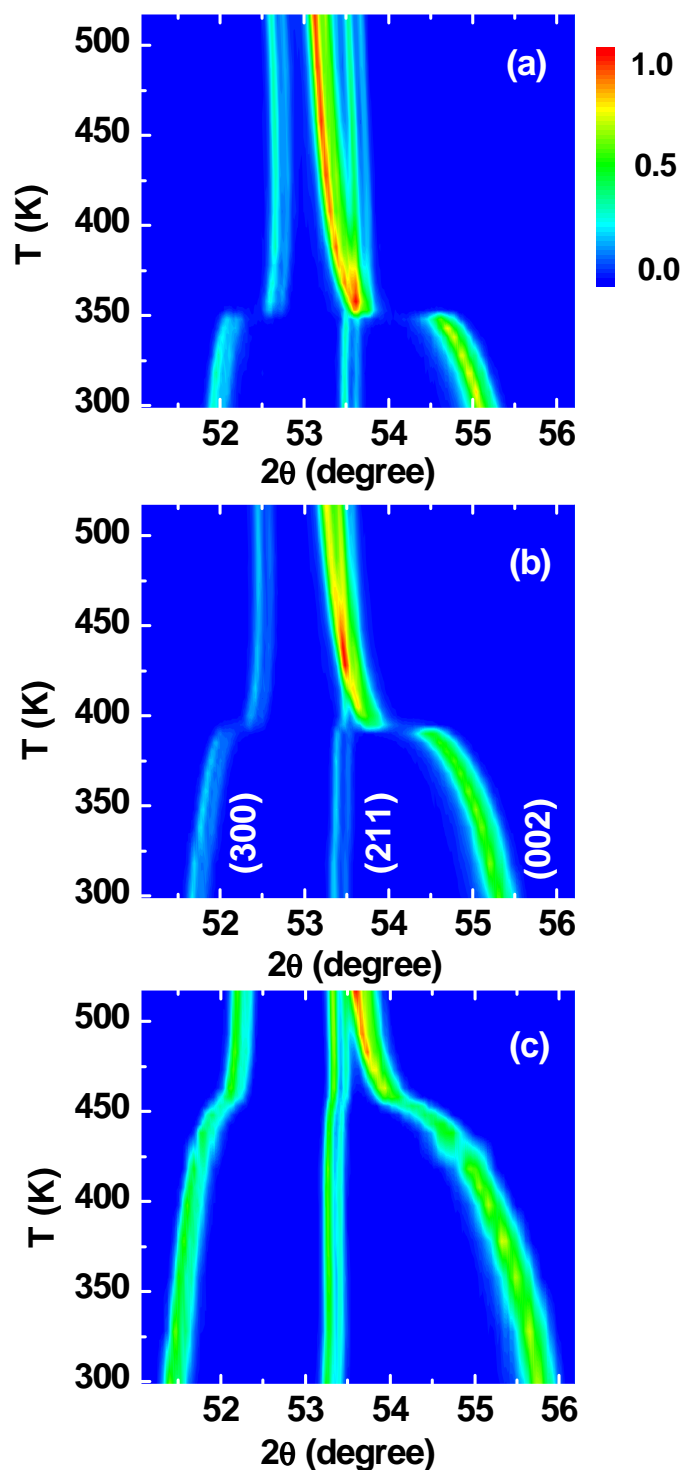


Figure 8.1 Contour plots of the X-ray diffraction patterns for $\text{Mn}_{0.66}\text{Fe}_{1.29}\text{P}_{1-x}\text{Si}_x$ compounds with $x = 0.34$ (a), 0.37 (b) and 0.42 (c) on heating. The bar on the upper-right corner represents the normalized intensity scale.

This variation indicates that the nature of the transition has changed from FOMT towards SOMT (second-order magnetic transition) when the Si content increases from $x = 0.34$ to 0.42 .

The representative (300) and (002) peaks shift in the opposite direction, indicating that the lattice constants a and c change in opposite sense. The lattice constant a decreases and c increases upon heating, resulting in hardly any volume change at the transition for all three compounds. The Curie temperature of all the three compounds can be obtained from the contour plots. The values of T_C are 350, 392 and 451 K for $x = 0.34$, 0.37 and 0.42, respectively. Such high optimal working temperatures combined with the GMCE make the Fe-rich Mn-Fe-P-Si system a good candidate for both magnetic cooling and energy conversion [9].

Table 8.1 Structural parameters of the $\text{Mn}_{0.66}\text{Fe}_{1.29}\text{P}_{1-x}\text{Si}_x$ compounds with $x = 0.34$, 0.37 and 0.42 obtained from the Rietveld refinement of the neutron diffraction patterns measured in the paramagnetic state. Space group: $P-62m$. Atomic positions: $3f\text{-Fe}$ ($x_1, 0, 0$); $3g\text{-Mn/Fe}$ ($x_2, 0, 1/2$); $2c\text{-P/Si}$ ($1/3, 2/3, 0$); $1b\text{-P/Si}$ ($0, 0, 1/2$).

		$x = 0.34$	$x = 0.37$	$x = 0.42$
	Parameters	PM (400 K)	PM (440 K)	PM (475 K)
	$a(\text{\AA})$	6.02284 ₄	6.04228 ₄	6.08222 ₇
	$c(\text{\AA})$	3.43667 ₅	3.42506 ₅	3.39664 ₆
	$V(\text{\AA}^3)$	107.962 ₂	108.293 ₂	108.819 ₃
$3f$	x_1	0.2541 ₂	0.2542 ₂	0.2545 ₂
	$n(\text{Fe})/n(\text{Mn})$	0.246/0.004	0.241/0.009	0.239/0.011
$3g$	x_2	0.619 ₂	0.639 ₃	0.615 ₂
	$n(\text{Fe})/n(\text{Mn})$	0.085/0.165	0.090/0.160	0.092/0.158
$2c$	$n(\text{P})/n(\text{Si})$	0.113 ₃ /0.053 ₃	0.105 ₄ /0.062 ₄	0.089 ₄ /0.078 ₄
$1b$	$n(\text{P})/n(\text{Si})$	0.053 ₃ /0.031 ₃	0.053 ₄ /0.030 ₄	0.056 ₄ /0.027 ₄
	$R_P(\%)$	4.09	4.37	5.29
	$R_{wp}(\%)$	5.33	5.60	7.13
	χ^2	4.88	5.14	4.30

In the paramagnetic state, only nuclear scattering contributes to the neutron diffraction patterns and the site occupancy can be determined by refining these patterns. The refinement of the neutron diffraction patterns confirms the hexagonal Fe_2P -type structure (space group $P-62m$) for all the compounds and shows a minor $(\text{Mn,Fe})_3\text{Si}$ impurity phase (see Figure 8.2a, with $x = 0.34$ as an example). It is found that, for all the compounds $\text{Mn}_{0.66}\text{Fe}_{1.29}\text{P}_{1-x}\text{Si}_x$

($x = 0.34, 0.37$ and 0.42), the Fe and Mn atoms are preferably situated in the tetrahedral $3f$ and the pyramidal $3g$ sites, respectively. The $3f$ site is nearly completely occupied by Fe atoms (Mn atoms occupy about 2 - 4%), while the $3g$ site is occupied by Mn atoms and the excess Fe atoms. Mn and Fe are randomly distributed and the Mn/Fe ratio is about 64.4/35.6, which is in good agreement with the nominal value of 66.0/34.0. We also find that there is no site preference for Si and P: both atoms are randomly distributed (see Table 8.1). This arrangement is the same as the MnFeP_{1-x}As_x compounds [13], but is different from the data reported for the Mn_{1.1}Fe_{0.9}P_{0.8}Ge_{0.2} compound, where Ge has been found to prefer the $2c$ site [14]. The detailed structural parameters are given in Table 8.1.

8.4 Alignment of magnetic moment

In the ferromagnetic state, the magnetic structure can be determined by refining the diffraction patterns. Since earlier studies show that the magnetic moments align along the c -direction in the parent alloy Fe₂P [15] and within the a - b plane in MnFeP_{0.5}Si_{0.5} compound [16], we first assumed that the alignment of the magnetic moments is either along the c -direction or within the a - b plane. By comparing the two refinements, a better fitting is obtained with magnetic moment along the c -direction. This indicates that the alignment of magnetic moment is rather along the c -direction than within the a - b plane for the $x = 0.34$ sample. However, further exploration shows that the best fitting is obtained when the alignment of the magnetic moment is canted $\sim 29^\circ$ away from c -axis (Figure 8.2c). To illustrate the significance of the magnetic contribution to the low temperature neutron diffraction patterns we plot the nuclear and magnetic fits in Figure 8.2. When comparing the refinement with only nuclear scattering (Figure 8.2b) and the refinement with both nuclear and magnetic scattering (Figure 8.2c), there are significant differences between the observed and calculated intensity in the low-angle 2θ range of the neutron diffraction pattern, as expected from the almost compensated nuclear form factor of Mn and Fe on the $3g$ site. Interestingly, by allowing the angle to be free, we obtained an optimized rotation angle of 29° , 46° and 67° with respect to the c -direction for the $x = 0.34, 0.37$ and 0.42 samples, respectively. The refined parameters are listed in Table 8.2. This suggests that the alignment of the magnetic moment strongly depends on the Si content. Note that, such a deviation from the c -direction has previously been reported for the compound MnFeP_{0.7}As_{0.3} [13], where a moment angle of 50° with the c -direction was found. We propose that the magnetic moments are canted away from the c -direction towards the a - b plane for increasing Si contents from $x =$

0.34 to 0.42 in the $\text{Mn}_{0.66}\text{Fe}_{1.29}\text{P}_{1-x}\text{Si}_x$ compounds. The evolution of the alignment is shown in Figure 8.3a-c. The canted magnetic moments indicate a low magnetic anisotropy in the Fe-rich Mn-Fe-P-Si system, which confirms this material is magnetically soft.

Table 8.2 Structural parameters of the $\text{Mn}_{0.66}\text{Fe}_{1.29}\text{P}_{1-x}\text{Si}_x$ compounds with $x = 0.34, 0.37$ and 0.42 in their ferromagnetic state. θ represents the angle between the c -direction and the alignment of the magnetic moment. M_{3f} and M_{3g} are the average magnetic moment at $3f$ and $3g$ site, respectively; M_{Total} is the total moment per formula unit; M_s is the saturation magnetic moment at 5 K determined by magnetization measurements.

Refined parameters		$x = 0.34$	$x = 0.37$	$x = 0.42$
	θ (degree)	29 ₃	46 ₄	67 ₃
	T (K)	10	10	3
<i>Unit cell</i>	a (Å)	6.11886 ₈	6.13672 ₆	6.16703 ₅
	c (Å)	3.29917 ₅	3.28459 ₆	3.26343 ₅
	V (Å ³)	106.974 ₂	107.124 ₂	107.487 ₂
	x_1	0.2557 ₂	0.2564 ₂	0.2557 ₂
<i>3f</i>	M_{3f} (μ_B)	1.71 ₇	1.7 ₁	0.95 ₆
	x_2	0.602 ₁	0.617 ₂	0.615 ₁
	M_{3g} (μ_B)	2.86 ₆	2.33 ₈	2.28 ₅
	M_{Total} (μ_B)	4.57 ₉	4.0 ₁	3.23 ₈
<i>3g</i>	R_p (%)	3.78	5.48	6.85
	R_{wp} (%)	4.81	7.01	5.15
	χ^2	2.96	6.21	3.91
	M_s (μ_B)	4.56	4.47	3.86

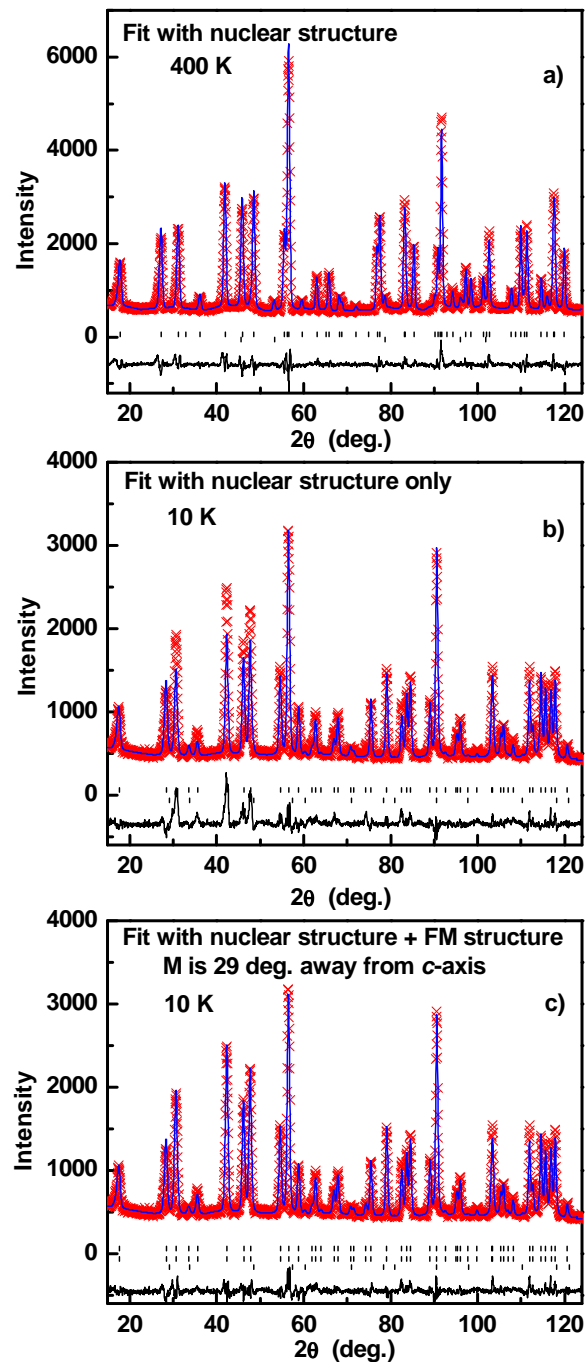


Figure 8.2 Observed (crosses) and calculated (continuous lines) neutron diffraction patterns for sample $x = 0.34$ at 400 K (PM) and 10 K (FM). (a) The fitted neutron diffraction pattern in the paramagnetic state, (b) the fitted neutron diffraction pattern in the ferromagnetic state with a nuclear structure contribution only, (c) the fitted the neutron diffraction pattern in the ferromagnetic state with both nuclear structure and magnetic contributions for moment $\sim 29^\circ$ canted away from c -axis. Differences between observed and calculated patterns are shown in the lower part of the plots. A minor amount of the cubic $(Mn,Fe)_3Si$ impurity phase is detected. Vertical lines indicate the diffraction peaks for the nuclear (top) and the magnetic (middle, if any) structure of the main phase, and the impurity phase (bottom).

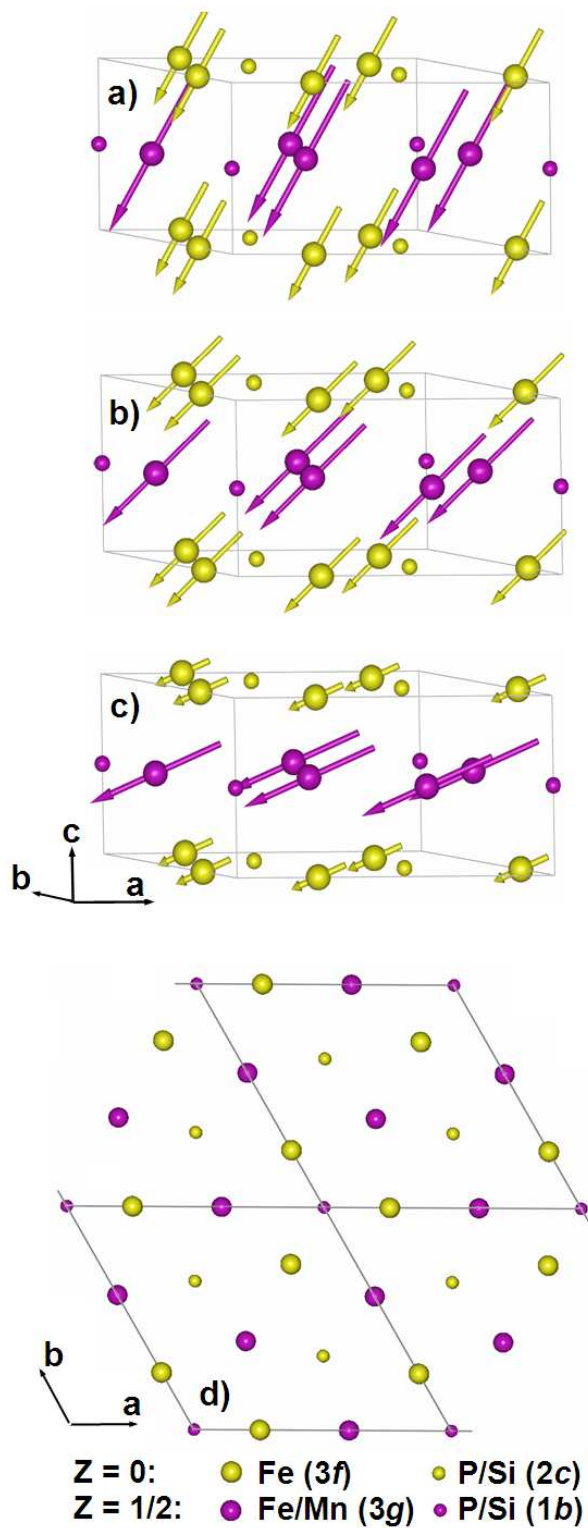


Figure 8.3 Crystal and magnetic structure of $\text{Mn}_{0.66}\text{Fe}_{1.29}\text{P}_{1-x}\text{Si}_x$ compounds with $x = 0.34$ (a), 0.37 (b) and 0.42 (c). The direction and the length of the arrows correspond to the alignment and the magnetic moments.

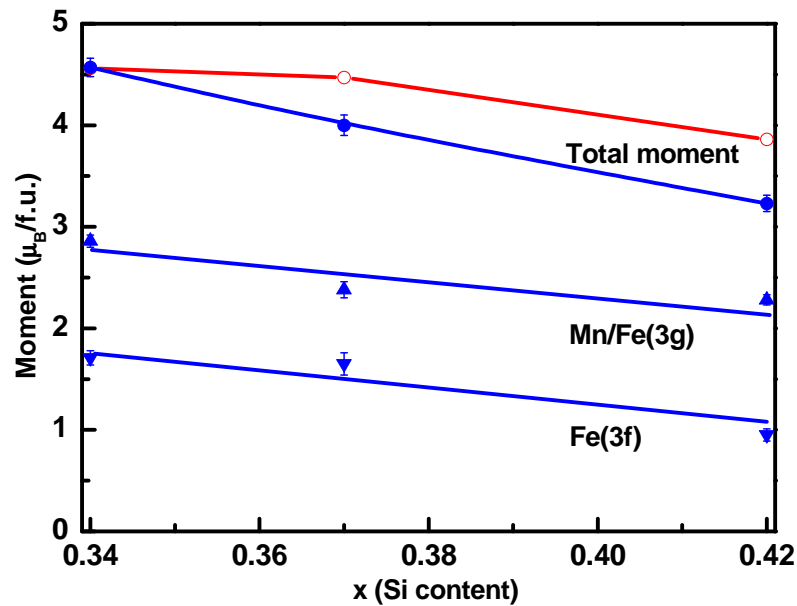


Figure 8.4 Magnetic moment as a function of the Si content derived from the neutron diffraction patterns measured in the ferromagnetic state for the Mn_{0.66}Fe_{1.29}P_{1-x}Si_x compounds with $x = 0.34$, 0.37 and 0.42. The total moments (open circles) are very close ($x = 0.34$) or slightly lower ($x = 0.37$ and 0.42) to those obtained from saturation magnetization measurements at 5 K (solid circles). Note that, the used valences for the metal ions are Fe⁰(3f) and Mn/Fe⁴⁺(3g).

Figure 8.4 shows the Si content dependence of the magnetic moment (total magnetic moment and the average magnetic moment on the 3f and the 3g sites) measured in the ferromagnetic state. The average magnetic moment on the 3f and the 3g sites decrease gradually with increasing Si content. For the sample with $x = 0.34$, the average magnetic moment on the 3g site ($2.86 \mu_B$) is larger than the value on the 3f site ($1.71 \mu_B$). The total moment ($4.57 \mu_B$) is very close to the value obtained from macroscopic measurements of the low-temperature saturation magnetization, as shown in Figure 8.4. The values are much larger than those observed at 5 K/10 K in the Mn-rich Fe₂P-type Mn-Fe-P-Si compounds [17] and slightly larger than the values observed at 296 K in the MnFeP_{0.5}Si_{0.5} compound with a T_c of 382 K [16]. Such high values certainly benefit the GMCE in the Fe-rich Mn-Fe-P-Si system and suggest a high magnetic density.

8.5 Valence state and interatomic distances

The total magnetic moment obtained from the neutron diffraction refinement and the macroscopic measurements are expected to be comparable. The refined total magnetic moment of the compound with $x = 0.34$ is in agreement with the value obtained from the magnetization measurement at low temperature, while the compounds with $x = 0.37$ and 0.42

show a small discrepancy, as shown in Figure 8.4. This discrepancy might be due to the selection of the magnetic form factors when performing the neutron diffraction refinement. All the refinements were performed using magnetic form factors corresponding to the valence states of Fe^0 and Mn/Fe^{4+} on the $3f$ and the $3g$ sites, respectively, based on data from ref. [18]. However, a valence state of Mn/Fe^{2+} ($3g$ site) has also been used/reported in Refs. [13, 19]. The polarized neutron diffraction study on single crystalline Fe_2P shows different spherical magnetic form factors for the free Fe atom state and the Fe^{4+} atom state [18]. Different combinations of valence states for the $\text{Fe}(3f)$ and $\text{Mn/Fe}(3g)$ ions will lead to slightly different magnetic form factors and result in small variations in the refined magnetic moment. To establish exact valence states of $\text{Fe}(3f)$ and $\text{Mn/Fe}(3g)$ ions further experimental evidence, by *e.g.* polarized neutron diffraction and Mössbauer spectroscopy, is required.

Figure 8.5 shows dependence of the lattice parameters and the interatomic distances on the Si content for the $\text{Mn}_{0.66}\text{Fe}_{1.29}\text{P}_{1-x}\text{Si}_x$ compounds in the ferromagnetic state. The detailed values are listed in Table 8.3. The results confirm that the lattice constants change in the opposite sense with increasing Si content: the lattice constant a increases, while c decreases. We find that the intralayer interatomic distances for the ($3f$) positions increase and for the ($3g$) positions decrease with increasing Si content, the opposite changes in the $3g$ and $3f$ layers is likely to destabilize the crystal structure. Introducing Si (up to around 10%) into the Fe_2P compound was previously found to induce a phase transition from the hexagonal (space group $P-62m$) to the body-centered orthorhombic (space group $Imm2$) crystal structure [20]. Introducing Mn into the Fe_2P system, counteracts this destabilizing effects and for 33% Mn the structural transformation is suppressed for Si content up to 42%. Note that, all the compounds solely show a hexagonal crystal structure in the temperature range from 5 to 523 K. Thus, Mn doping, plays an important role in stabilizing the hexagonal crystal structure. The exchange energy between the magnetic atoms, enhanced by partially replacing Fe with Mn, appears to be the driving force behind the stabilization of the hexagonal phase.

Table 8.3 Lattice parameters and interatomic distances of the Mn_{0.66}Fe_{1.29}P_{1-x}Si_x compounds with $x = 0.34, 0.37$ and 0.42 in the ferromagnetic state.

				$x = 0.34$	$x = 0.37$	$x = 0.42$
				($\theta = 29_3^\circ$)	($\theta = 46_4^\circ$)	($\theta = 67_3^\circ$)
Lattice parameters				FM (10 K)	FM (10 K)	FM (3 K)
$a(\text{\AA})$				6.11886 ₈	6.13673 ₆	6.16703 ₅
$c(\text{\AA})$				3.29917 ₅	3.28460 ₆	3.26343 ₅
$V(\text{\AA}^3)$				106.974 ₂	107.124 ₂	107.487 ₂
Metal-metal distances (\AA)						
Fe(3f)-Fe(3f)	Intralayer	$\times 2$		2.710 ₂	2.726 ₂	2.732 ₂
Mn/Fe(3g)-Mn/Fe(3g)	Intralayer	$\times 4$		3.29917 ₅	3.28460 ₆	3.26343 ₅
Mn/Fe(3g)-Fe(3f)	Interlayer	$\times 1$		2.685 ₅	2.757 ₈	2.753 ₆
	Interlayer	$\times 2$		2.700 ₄	2.644 ₆	2.652 ₅
	Mean distance			2.695 ₆	2.68 ₁	2.686 ₆
Metal-nonmetal distances (\AA)						
Fe(3f)-P/Si(2c)	Intralayer	$\times 2$		2.3140 ₈	2.318 ₁	2.3320 ₈
Fe(3f)-P/Si(1b)	Interlayer	$\times 2$		2.2736 ₈	2.275 ₁	2.2694 ₉
	Mean distance			2.294 ₁	2.296 ₁	2.301 ₁
Mn/Fe(3g)-P/Si(2c)	Interlayer	$\times 4$		2.496 ₂	2.521 ₃	2.518 ₂
Mn/Fe(3g)-P/Si(1b)	Intralayer	$\times 1$		2.435 ₆	2.35 ₁	2.372 ₈
	Mean distance			2.484 ₂	2.49 ₁	2.49 ₁

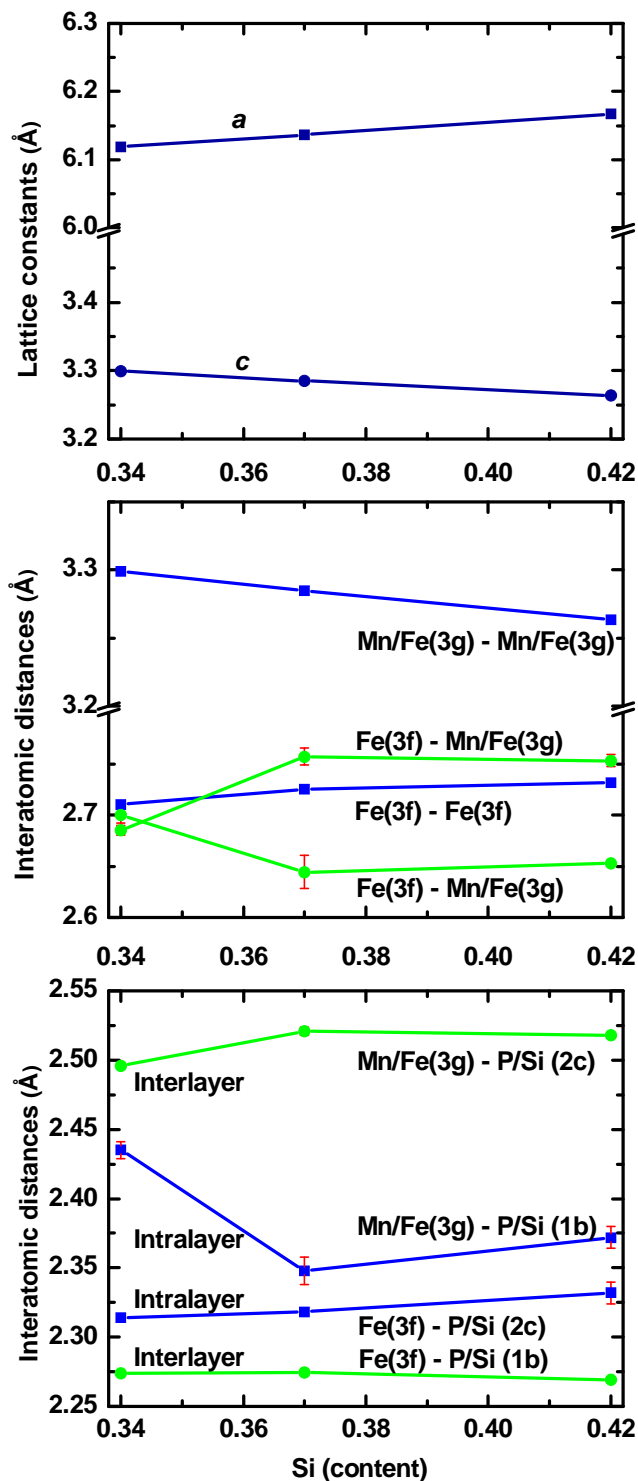


Figure 8.5 Lattice parameters and interatomic distances as a function of the Si content derived from neutron diffraction patterns measured at low temperatures (3 K for $x = 0.34$ and 0.37 , 10 K for $x = 0.42$) for the $\text{Mn}_{0.66}\text{Fe}_{1.29}\text{P}_{1-x}\text{Si}_x$ compounds with $x = 0.34, 0.37$ and 0.42 . The square symbols represent the intralayer interatomic distances; the circle symbols represent the interlayer interatomic distances.

8.6 Conclusions

The Fe-rich Mn-Fe-P-Si compounds are promising materials for high-temperature magnetocaloric applications. A magnetic moment of up to $4.57 \mu_B/\text{f.u.}$ for $x = 0.34$, indicates a high magnetic density in the system, which certainly benefits the GMCE. Introducing site disorder at the 3g site by replacing 1/3 of Fe with Mn appears to enhance the magnetic interaction, while the strong magnetoelastic coupling is maintained. The Mn substitution also shows a stabilizing effect on the hexagonal crystal structure, which is maintained to a high Si content. The moment alignment within the crystallographic unit cell is affected when the Si content increases from $x = 0.34$ to 0.42 in Mn_{0.66}Fe_{1.29}P_{1-x}Si_x compounds, as the canting angle with respect to the *c*-direction increases. The canted magnetic moment alignment confirms a low magnetic anisotropy, which ensures soft magnetic properties of Fe-rich Mn-Fe-P-Si compounds.

References:

- [1] V. K. Pecharsky and K.A.Gschneidner, Giant magnetocaloric effect in Gd₅(Si₂Ge₂), *Physical Review Letters* 78 (1997) 4494-4497.
- [2] F.X. Hu, B.G. Shen, J.R. Sun, Z.H. Cheng, G.H. Rao and X.X. Zhang, Influence of negative lattice expansion and metamagnetic transition on magnetic entropy change in the compound LaFe_{11.4}Si_{1.6}, *Applied Physics Letters* 78 (2001) 3675-3677.
- [3] O. Tegus, E. Brück, K.H.J. Buschow and F.R. de Boer, Transition-metal-based magnetic refrigerants for room-temperature applications, *Nature* 415 (2002) 150-152.
- [4] H. Wada and Y. Tanabe, Giant magnetocaloric effect of MnAs_{1-x}Sb_x, *Applied Physics Letters* 79 (2001) 3302-3304.
- [5] A. Fujita, S. Fujieda, K. Fukamichi, H. Mitamura and T. Goto, Itinerant-electron metamagnetic transition and large magnetovolume effects in La(Fe_xSi_{1-x})₁₃ compounds, *Physical Review B* 65 (2002) 014410.
- [6] E. Brück, Developments in magnetocaloric refrigeration, *Journal of Physics D: Applied Physics* 38 (2005) R381-R391.
- [7] K.G. Sandeman, Magnetocaloric materials: The search for new systems, *Scripta Materialia* 67 (2012) 566-571.
- [8] D.T. Cam Thanh, E. Brück, N.T. Trung, J.C.P. Klaasse, K.H.J. Buschow, Z.Q. Ou, O. Tegus and L. Caron, Structure, magnetism, and magnetocaloric properties of MnFeP_{1-x}Si_x compounds, *Journal of Applied Physics* 103 (2008) 07B318.

- [9] N.H. Dung, Z.Q. Ou, L. Caron, L. Zhang, D.T.C. Thanh, G.A. de Wijs, R.A. de Groot, K.H.J. Buschow and E. Brück, Mixed magnetism for refrigeration and energy conversion, *Advanced Energy Materials* 1 (2011) 1215-1219.
- [10] K.D. Liss, B. Hunter, M. Hagen, T. Noakes and S. Kennedy, Echidna - the new high-resolution powder diffractometer being built at OPAL, *Physica B* 385-86 (2006) 1010-1012.
- [11] H.M. Rietveld, A profile refinement method for nuclear and magnetic structures, *Journal of Applied Crystallography* 2 (1969) 65-71.
- [12] J. Rodríguez-Carvajal, Recent advances in magnetic structure determination by neutron powder diffraction, *Physica B* 192 (1993) 55-69.
- [13] M. Bacmann, J.L. Soubeyroux, R. Barrett, D. Fruchart, R. Zach, S. Niziol and R. Fruchart, Magnetoelastic transition and antiferro-ferromagnetic ordering in the system $\text{MnFeP}_{1-y}\text{As}_y$, *Journal of Magnetism and Magnetic Materials* 134 (1994) 59-67.
- [14] D.M. Liu, M. Yue, J.X. Zhang, T.M. McQueen, J.W. Lynn, X.L. Wang, Y. Chen, J.Y. Li, R.J. Cava, X.B. Liu, Z. Altounian and Q. Huang, Origin and tuning of the magnetocaloric effect in the magnetic refrigerant $\text{Mn}_{1.1}\text{Fe}_{0.9}(\text{P}_{0.8}\text{Ge}_{0.2})$, *Physical Review B* 79 (2009) 014435.
- [15] L. Lundgren, G. Tarmohamed, O. Beckman, B. Carlsson and S. Rundqvist, First order magnetic phase transition in Fe_2P , *Physica Scripta* 17 (1978) 39-48.
- [16] V. Hoglin, M. Hudl, M. Sahlberg, P. Nordblad, P. Beran and Y. Andersson, The crystal and magnetic structure of the magnetocaloric compound $\text{FeMnP}_{0.5}\text{Si}_{0.5}$, *Journal of Solid State Chemistry* 184 (2011) 2434-2438.
- [17] N.H. Dung, L. Zhang, Z.Q. Ou, L. Zhao, L. van Eijck, A.M. Mulders, M. Avdeev, E. Suard, N.H. van Dijk and E. Brück, High/low-moment phase transition in hexagonal Mn-Fe-P-Si compounds, *Physical Review B* 86 (2012) 045134.
- [18] H. Fujii, S. Komura, T. Takeda, T. Okamoto, Y. Ito and J. Akimitsu, Polarized neutron diffraction study of Fe_2P single crystal, *Journal of the Physical Society of Japan* 46 (1979) 1616-1621.
- [19] W.J. Takei, D.E. Cox and G. Shirane, Magnetic structures in the MnSb-CrSb system, *Physical Review* 129 (1963) 2008-2018.
- [20] P. Jernberg, A.A. Yousif, L. Haggstrom and Y. Andersson, A Mössbauer study of $\text{Fe}_2\text{P}_{1-x}\text{Si}_x$ ($x \leq 0.35$), *Journal of Solid State Chemistry* 53 (1984) 313-322.

Chapter 9

Neutron diffraction study on the Fe₂P-type Mn_{1.95-x}Fe_xP_{2/3}Si_{1/3} compounds

9.1 Introduction

Recently, magnetic refrigeration based on the magnetocaloric effect (MCE) has attracted interest as an alternative to the conventional vapor compression cooling techniques due to its high-energy efficiency and low environmental impact. [1-3] We discovered the Giant MCE in Fe₂P-based hexagonal (Mn,Fe)₂(P,Si) compounds, and realized that the undesired thermal hysteresis can be significantly reduced by varying Mn/Fe or/and P/Si ratio(s) while maintaining the GMCE [4, 5].

Careful X-ray diffraction studies show that a large increase in *c/a* ratio occurs through the transition from ferromagnetic to paramagnetic state, while the unit-cell volume is hardly changed. Earlier neutron studies for MnFeP_{0.6}Si_{0.4} [4] show that Mn and Fe occupy the 3*g* and 3*f* sites, respectively, in alternating layers in the Fe₂P structure. First principles electronic structure calculations suggest that at the ferro to paramagnetic transition the spin polarization of the Fe 3*d* electrons at the 3*f* site, presenting a magnetic moment of about 1.5 μ_B, vanishes. In contrast to this, the spin polarization of the Mn 3*d* electrons at the 3*g* site, presenting a magnetic moment of 2.8 μ_B remains almost unaffected through the transition [5].

This unexpected behavior is attributed to the competition between bonding and magnetism. In the paramagnetic state the Fe atoms on the 3*f* site are tetrahedral coordinated, surrounded by 4

metalloid atoms at short distances (~ 2.3 Å). Therefore, the chemical bonding at the $3f$ site is among the strongest in $\text{MnFe}(\text{P},\text{Si})$ compounds. The change in c/a at the phase transition distorts the tetrahedron, weakening or breaking the two intra-layer bonds. The moments developing at the $3f$ sites originate from the electrons freed from the chemical bonding. Meanwhile the $3g$ site is pyramidal, and the Mn atom is surrounded by 5 metalloid atoms at relatively large distances (~ 2.5 Å). Therefore the Mn $3d$ electrons are more localized and less affected by the lattice distortion. Within the layer, the $3g$ sites are interconnected triangularly and antiferromagnetic next nearest neighbor interactions are reported [6]. The exchange field between the $3g$ layers induces moment on the $3f$ sites, leading to the ferromagnetic state. Studying this novel mechanism responsible for the large MCE is the aim of the current study.

In Fe-rich $(\text{Mn},\text{Fe})_2(\text{P},\text{Si})$ compounds, the excess Fe atoms will occupy the $3g$ sites. This will result in a modified electron density on the $3g$ sites, while the symmetry will be less affected as the ionic volumes of Mn and Fe are very similar. The site occupation of Mn and Fe atoms at the two crystallographic sites and the position parameters can only be resolved by neutron diffraction since Mn and Fe are neighbors in the periodic table and can hardly be distinguished by X-ray diffraction. Additionally, we can determine the magnetic moments in the magnetically ordered state on the two magnetic sublattices. The insight obtained with neutron diffraction will certainly deepen our understanding and possibly shed light on how to further improve the material properties for applications.

9.2 Experimental details

The Fe-rich compounds $\text{Mn}_{1.95-x}\text{Fe}_x\text{P}_{2/3}\text{Si}_{1/3}$ ($x = 1.0, 1.1, 1.2, 1.3$ and 1.4) were prepared by the ball-milling technique as described in Chapter 5. The X-ray diffraction patterns were collected at various temperatures in zero field with a PANalytical X-pert Pro diffractometer equipped with an Anton Paar TTK450 low-temperature chamber using $\text{Cu K}\alpha$ radiation. A secondary-beam flat-crystal monochromator and a multichannel X'celerator detector were used to reduce the background and to maintain a reasonable data-collection time. The neutron diffraction data was collected at the Institute Laue-Langevin (ILL) on the D2B high-resolution powder diffractometer [7] with an incident wavelength of 1.595 Å. The sample powder was contained in a vanadium can which was mounted in an Orange cryostat. The measurements were carried out at fixed temperatures in the ferromagnetic and the paramagnetic states in zero field. The refinement of all the diffraction patterns was performed by the Rietveld method [8] using the FullProf program [9]. A superconducting quantum

interference device (SQUID) magnetometer (Quantum Design MPMS 5XL) with the reciprocating sample option (RSO) was employed for magnetic measurements below 400 K.

9.3 Structural parameters

X-ray diffraction measurements indicate that all the compounds $Mn_{1.95-x}Fe_xP_{2/3}Si_{1/3}$ ($x = 1.0, 1.1, 1.2, 1.3$ and 1.4) crystallize in the hexagonal Fe_2P -type structure (space group $P-62m$). As shown in Figure 9.1, the contour plots display the thermal evolution of the X-ray diffraction patterns of all the compounds. For the compounds with $x = 1.0, 1.1, 1.2$ and 1.3 , a discontinuity in the peak positions at the transition temperatures indicates a discontinuous change in lattice constants.

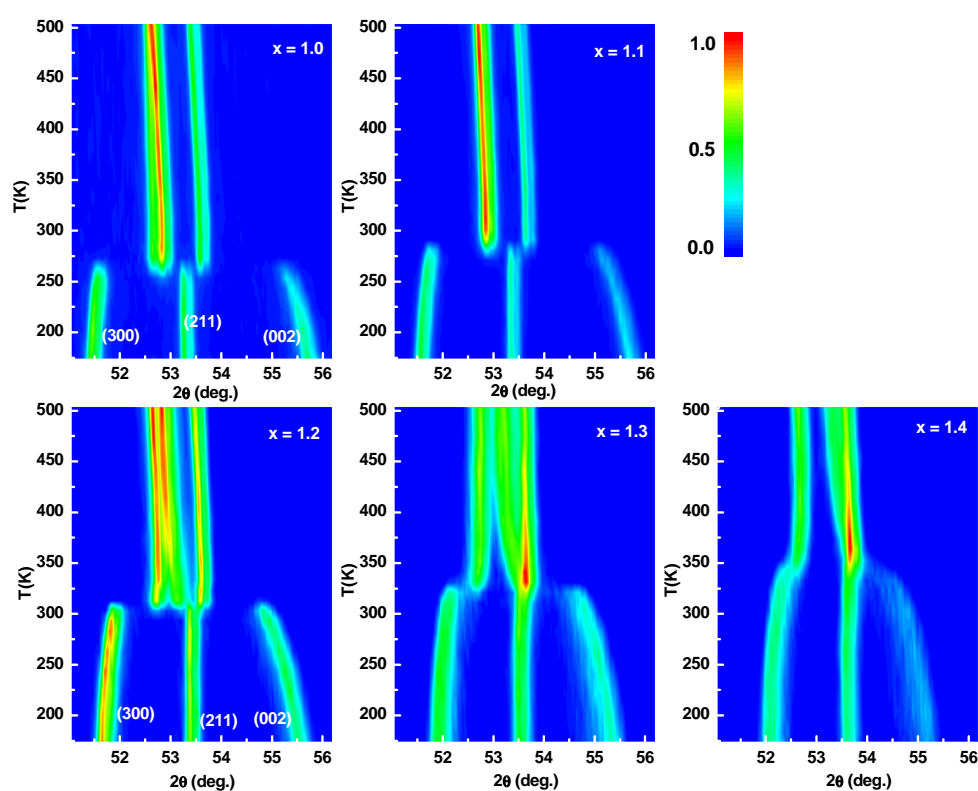


Figure 9.1 Contour plots of the X-ray diffraction patterns for $Mn_{1.95-x}Fe_xP_{2/3}Si_{1/3}$ compounds ($x = 1.0, 1.1, 1.2, 1.3$, and 1.4) on heating. The bar on the upper-right panel represents the normalized intensity scale.

The higher Si content compound ($x = 1.4$), however, shows a more continuous shift of the peaks. This difference in behavior indicates that the nature of the transition changes from FOMT towards SOMT (second-order magnetic transition) when the Fe content increases from $x = 1.0$ to 1.4 . The representative (300) and (002) peaks shift in the opposite direction,

indicating that the lattice constants a and c change in opposite sense. The lattice constant a decreases while c increases upon heating, resulting in only a minute volume change ($< 0.1\%$) at the FOMT for all compounds. Note that, the FOMT is usually accompanied with a sudden change in lattice volume [10]. Due to the strong magnetoelastic coupling present in these compounds, the Curie temperatures can be easily obtained from the X-ray contour plots as shown in Figure 1. The values of T_C are 269, 290, 311, 326 and 345 K for $x = 1.0, 1.1, 1.2, 1.3$ and 1.4, respectively, in good agreement with magnetic measurements.

Table 9.1 Structural parameters of the $\text{Mn}_{1.95-x}\text{Fe}_x\text{P}_{2/3}\text{Si}_{1/3}$ compounds with $x = 1.0, 1.1, 1.2, 1.3$, and 1.4 obtained from the Rietveld refinement of the neutron diffraction patterns measured in the paramagnetic state at 400 K. Space group: $P-62m$. Atomic positions: $3f\text{-Fe}(x_1, 0, 0)$; $3g\text{-Mn/Fe}(x_2, 0, 1/2)$; $2c\text{-P/Si}(1/3, 2/3, 0)$; $1b\text{-P, Si}(0, 0, 1/2)$.

		$x = 1.0$	$x = 1.1$	$x = 1.2$	$x = 1.3$	$x = 1.4$
Parameters		PM (400 K)				
<i>Unit cell</i>	$a(\text{\AA})$	6.01866 ₃	6.01456 ₄	6.01863 ₄	6.02249 ₅	6.02400 ₅
	$c(\text{\AA})$	3.48264 ₃	3.47374 ₃	3.45635 ₃	3.44309 ₅	3.42889 ₄
	$V(\text{\AA}^3)$	109.254 ₁	108.827 ₁	108.429 ₂	108.151 ₂	107.759 ₂
$3f$	x_1	0.2544 ₂	0.2547 ₂	0.2549 ₁	0.2550 ₂	0.2552 ₂
	$n(\text{Fe})/n(\text{Mn})$	0.235/0.015	0.244/0.006	0.248/0.002	0.25/0.00	0.25/0.00
$3g$	x_2	0.5880 ₅	0.5892 ₉	0.581 ₂	0.607 ₃	0.598 ₁
	$n(\text{Fe})/n(\text{Mn})$	0.021/0.229	0.038/0.212	0.06/0.19	0.085/0.165	0.107/0.143
$2c$	$n(\text{P})/n(\text{Si})$	0.124 ₃ /0.042 ₃	0.120 ₃ /0.046 ₃	0.124 ₃ /0.042 ₃	0.125 ₃ /0.041 ₃	0.126 ₄ /0.040 ₄
$1b$	$n(\text{P})/n(\text{Si})$	0.042 ₃ /0.042 ₃	0.046 ₃ /0.038 ₃	0.042 ₃ /0.042 ₃	0.041 ₃ /0.043 ₃	0.040 ₄ /0.044 ₄
	<i>Microstrain (%)</i>	0.03738 ₂	0.04170 ₂	0.08861 ₈	0.1366 ₁	0.1050 ₁
	$R_p(\%)$	4.65	4.73	4.32	4.52	4.94
	$R_{wp}(\%)$	5.99	6.18	5.60	5.81	6.64
	χ^2	4.88	5.52	5.63	4.36	8.22

Since the nuclear scattering cross-section of all 4 elements Fe, Mn, P and Si are markedly different, the neutron diffraction patterns in the paramagnetic state are suited to determine the site occupancy by refining the patterns. The results confirm the hexagonal Fe_2P -type structure (space group $P-62m$) of the main phase for all the compounds and a minor cubic $(\text{Mn,Fe})_3\text{Si}$ impurity phase. Note that, due to the low content of the $(\text{Mn,Fe})_3\text{Si}$ phase ($< 0.4\%$), it is undetectable in some compounds by X-ray diffraction. In all the compounds $\text{Mn}_{1.95-x}\text{Fe}_x\text{P}_{2/3}\text{Si}_{1/3}$ ($x = 1.0, 1.1, 1.2, 1.3$ and 1.4), it is found that the Fe and Mn atoms

preferentially occupy the tetrahedral $3f$ and the pyramidal $3g$ sites, respectively. In the case of our Fe-rich Mn-Fe-P-Si compounds, the excess Fe atoms and Mn atoms share the $3g$ site.

As for the picture of the crystal and magnetic structure, we refer to Figure 8.3. The detailed structural parameters are listed in Table 9.1. Interestingly, at the $3f$ site, a small amount of Mn (about 6%) is observed for the $x = 1.0$ compound and the amount of Mn is gradually reduced to 2% and 1% for $x = 1.1$ and 1.2 compounds, respectively. Eventually, the amount of Mn in the $3f$ site is negligible for compounds with higher Fe content. We find that Si and P show no site preference for all studied compounds and both atoms are randomly distributed. Note that, this arrangement is the same as in $MnFeP_{1-x}As_x$ compounds [11], but is different from that reported for the $Mn_{1.1}Fe_{0.9}P_{0.8}Ge_{0.2}$ compound, where Ge shows a preference for the $2c$ site [12].

9.4 Alignment of the magnetic moment

The magnetic structure can be determined by refining the diffraction patterns in the ferromagnetic state. Earlier studies show that the aligned magnetic moment is along the c -axis in the parent alloy Fe_2P [13], within the a - b plane in $MnFeP_{0.5}Si_{0.5}$ compound [14] and between the a - b plane and the c -axis for other compositions [15]. We have considered all the three possible alignments when refining the neutron data for all the compounds. The detailed refined parameters are listed in the Table 9.2. The significant differences and the contribution of the magnetic reflection to the three possible alignments are shown in Figure 9.2. The $x = 1.0$ sample is selected as an example. Considering the magnetic form factor [16], the magnetic contribution will be dominant in the low-angle range of the neutron diffraction pattern. Thus, by comparing the quality of the refinement, especially in the low-angle range, one can conclude whether the magnetic moments are aligned within the a - b plane, along c -axis or in between.

Table 9.2 Structural parameters of the $\text{Mn}_{1.95-x}\text{Fe}_x\text{P}_{2/3}\text{Si}_{1/3}$ compounds with $x = 1.0, 1.1, 1.2, 1.3,$ and 1.4 at 10 K (in their ferromagnetic state). θ represents the angle between the c -axis and the alignment of the magnetic moment. M_{3f} and M_{3g} are the average magnetic moment at $3f$ and $3g$ site, respectively; M_{Total} is the total moment per formula unit; M_s is the spontaneous magnetic moment per formula determined by magnetization measurements at 5 K.

Parameters		x = 1.0			x = 1.1			x = 1.2			x = 1.3			x = 1.4		
	θ (deg.)	90	0	87 ₅	90	0	83 ₇	90	0	80 ₆	90	0	36 ₃	90	0	26 ₄
<i>Unit cell</i>	a (Å)	6.16647 ₃	6.16648 ₄	6.16647 ₃	6.15627 ₄	6.15634 ₅	6.15628 ₄	6.13747 ₅	6.13760 ₅	6.13754 ₅	6.1038 ₁	6.1039 ₁	6.1039 ₁	6.0798 ₁	6.0801 ₁	6.0799 ₁
	c (Å)	3.29010 ₃	3.29013 ₃	3.29010 ₃	3.29050 ₃	3.29056 ₄	3.29051 ₃	3.29672 ₄	3.29678 ₅	3.29673 ₄	3.3227 ₁	3.3230 ₁	3.3229 ₁	3.3341 ₁	3.3342 ₁	3.3342 ₁
	V (Å ³)	108.346 ₁	108.347 ₁	108.346 ₁	108.001 ₁	108.006 ₂	108.001 ₁	107.545 ₂	107.552 ₂	107.548 ₂	107.206 ₅	107.217 ₅	107.216 ₅	106.731 ₅	106.742 ₅	106.737 ₅
$3f$	x_f	0.2583 ₂	0.2590 ₂	0.2582 ₂	0.2577 ₂	0.2585 ₂	0.2577 ₂	0.2572 ₂	0.2578 ₂	0.2570 ₂	0.2573 ₂	0.2573 ₂	0.2571 ₂	0.2572 ₃	0.2576 ₃	0.2569 ₃
	M_{3f} (μ_B)	1.62 ₇	1.81 ₉	1.55 ₇	1.73 ₈	1.9 ₁	1.63 ₈	1.55 ₆	1.7 ₁	1.36 ₆	1.08 ₇	1.35 ₉	1.27 ₉	0.94 ₇	0.58 ₉	0.86 ₉
$3g$	x_g	0.5938 ₆	0.5922 ₇	0.5940 ₆	0.5952 ₉	0.592 ₁	0.5957 ₉	0.594 ₂	0.584 ₃	0.597 ₂	0.600 ₂	0.596 ₂	0.596 ₂	0.603 ₁	0.602 ₁	0.601 ₁
	M_{3g} (μ_B)	2.78 ₈	2.19 ₈	2.75 ₈	2.74 ₉	2.13 ₉	2.73 ₉	2.74 ₆	1.96 ₈	2.75 ₅	2.85 ₉	2.65 ₇	2.92 ₈	2.76 ₈	2.62 ₆	2.82 ₇
	M_{Total} (μ_B)	4.4 ₁	4.0 ₁	4.3 ₁	4.5 ₁	4.0 ₁	4.4 ₁	4.29 ₉	3.7 ₁	4.11 ₈	3.9 ₁	4.0 ₁	4.2 ₁	3.7 ₁	3.3 ₁	3.7 ₁
	<i>Micros-</i> <i>train</i> (%)			0.05005 ₄			0.05914 ₄			0.10152 ₅			0.2651 ₁			0.2796 ₂
	R_p (%)	5.62	6.34	5.65	5.73	6.34	5.73	5.44	6.01	5.50	6.36	6.19	6.13	6.94	6.68	6.44
	R_{wp} (%)	7.29	8.45	7.32	7.37	8.44	7.38	7.19	8.05	7.22	8.09	7.82	7.80	9.09	8.68	8.48
	χ^2	7.78	10.5	7.86	8.17	10.7	8.20	9.21	11.5	9.28	8.57	8.02	7.97	16.4	14.9	14.2
	M_s (μ_B)		4.23			4.30			4.20			4.00			3.70	

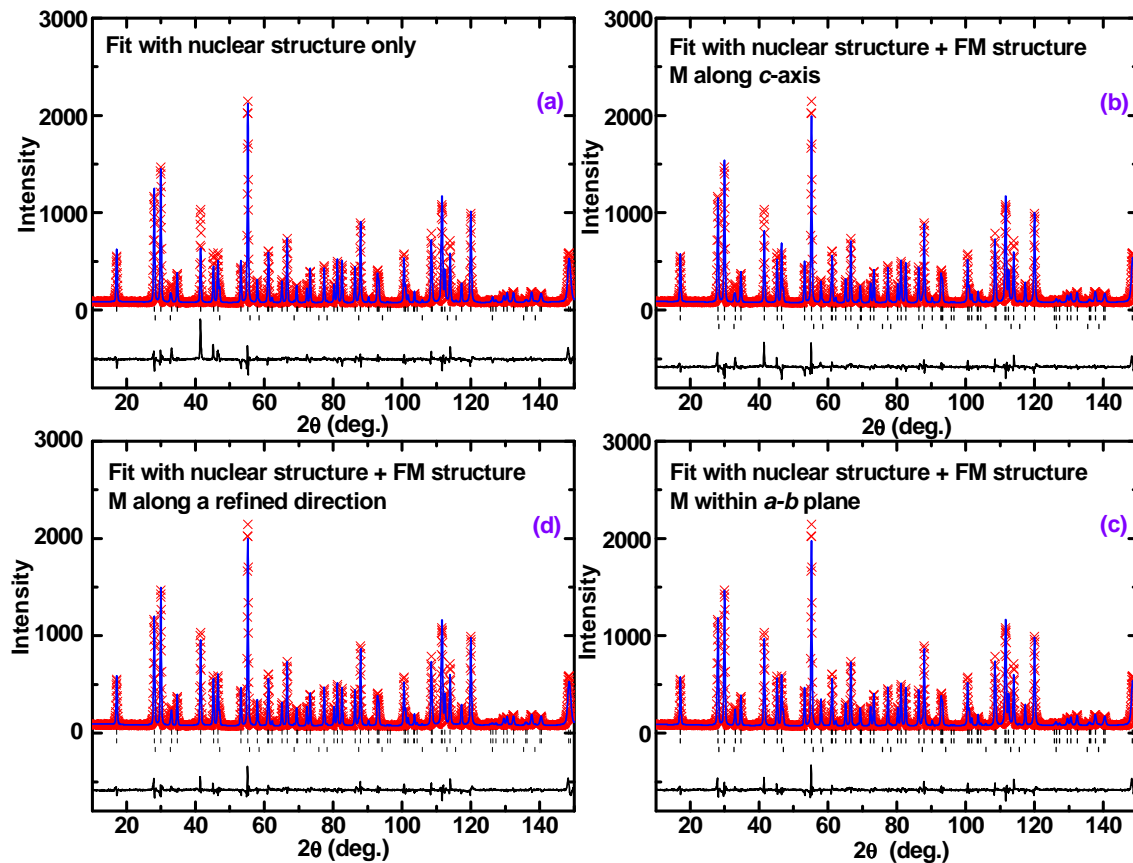


Figure 9.2 Observed (crosses) and calculated (continuous lines) neutron diffraction patterns for sample $x = 1.0$ at 10 K (FM). (a) Neutron diffraction pattern fitted with a nuclear structure contribution only, (b) neutron diffraction pattern fitted with both nuclear structure and magnetic contributions for magnetic moments along the c -axis, (c) neutron diffraction pattern fitted with both nuclear structure and magnetic contributions for magnetic moments within the a - b plane, (d) the fitted neutron diffraction pattern with both nuclear structure and magnetic contributions for magnetic moments along the refined direction. Differences between observed and calculated patterns are shown in the lower part of the plots. A minor amount of the cubic $(Mn,Fe)_3Si$ impurity phase is observed. Vertical lines indicate the diffraction peaks for the nuclear (top) and the magnetic (middle, if any) structure of the main phase, and the impurity phase (bottom).

The alignment angle of the moments in the $Mn_{1.95-x}Fe_xP_{2/3}Si_{1/3}$ compounds obtained is 87, 83, 80, 36 and 26 degrees away from the c -axis for $x = 1.0, 1.1, 1.2, 1.3$ and 1.4, respectively. This indicates that the moment alignments are canted from nearly within a - b plane for $x = 1.0$ towards along c -axis for $x = 1.4$, as listed in Table 9.2. The canted magnetic moments reflect a low magnetic anisotropy of the Mn-Fe-P-Si compounds, which display properties close to that of soft magnets. Interestingly, the alignment angle of the moments in the sample with $x = 1.3$ is about 36 degrees away from the c -axis, in good agreement with that observed for $Mn_{0.66}Fe_{1.29}P_{0.66}Si_{0.34}$ [15] melt-spun ribbon, of about 29 degrees away from the c -axis. Note

that, the magnetic properties of Fe_2P [17] and Fe_2P -based Mn-Fe-P-X ($X = \text{As}, \text{Ge}$ and Si) compounds [18-20] are very sensitive to composition, synthesis method and defects (e.g. vacancies).

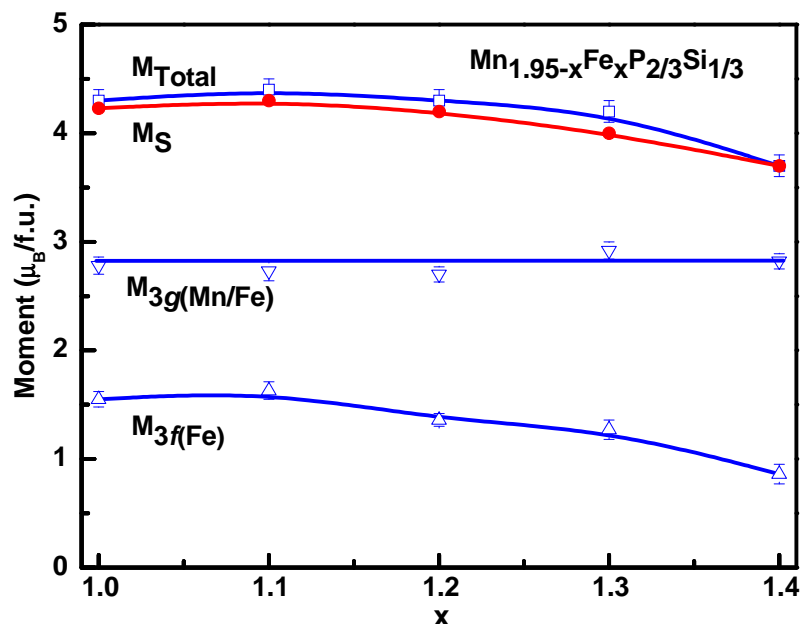


Figure 9.3 Magnetic moment as a function of the Fe content derived from the neutron diffraction patterns measured at 10 K in the ferromagnetic state for the $\text{Mn}_{1.95-x}\text{Fe}_x\text{P}_{2/3}\text{Si}_{1/3}$ compounds with $x = 1.0, 1.1, 1.2, 1.3$ and 1.4 . The total moments are very close to those obtained from saturation magnetization measurements at 5 K (solid circles).

In the Fe-rich $\text{Mn}_{1.95-x}\text{Fe}_x\text{P}_{2/3}\text{Si}_{1/3}$ ($0 \leq x \leq 1.4$) compounds, the Mn/Fe(3g) moments show a constant value of about $2.86 \mu_B$ as a function of Fe content, while the Fe(3f) moments decrease gradually from $1.55 \mu_B$ for $x = 1.0$ to $0.86 \mu_B$ for $x = 1.4$, as shown in Figure 9.3. The total moments are very close to the values obtained from macroscopic measurements of the low-temperature saturation magnetization. The values are much larger than those observed in the Mn-rich Mn-Fe-P-Si compounds [21]. Note that, due to the site preference of the Fe and Mn atoms, the excess Fe will occupy the 3g sites, where Fe(3g) carries a larger magnetic moment than that of Fe(3f). Variation of the Mn/Fe ratio in the Fe-rich $\text{Mn}_{1.95-x}\text{Fe}_x\text{P}_{2/3}\text{Si}_{1/3}$ compounds results in a change of the Mn/Fe ratio only on the 3g sites. Such a variation has hardly any influence on the average Mn/Fe(3g) magnetic moment, suggesting that the Mn(3g) and Fe(3g) have similar magnetic moments and the 3g site moment depends on the adjacent electron configuration of the atoms rather than the type of atom. This finding supports the picture of weak magnetism in the 3f sites, as the 3f moments are affected by replacing Mn by

Table 9.3 Lattice parameters and interatomic distances of the $Mn_{1.95-x}Fe_xP_{2/3}Si_{1/3}$ compounds with $x=1.0, 1.1, 1.2, 1.3$ and 1.4 in the ferromagnetic state at 5 K.

				$x = 1.0$	$x = 1.1$	$x = 1.2$	$x = 1.3$	$x = 1.4$
				($\theta = 87_5^\circ$)	($\theta = 83_7^\circ$)	($\theta = 80_6^\circ$)	($\theta = 36_3^\circ$)	($\theta = 26_4^\circ$)
Lattice parameters								
	$a(\text{\AA})$			6.16647 ₃	6.15628 ₄	6.13754 ₅	6.1039 ₁	6.0799 ₁
	$c(\text{\AA})$			3.29010 ₃	3.29051 ₃	3.29673 ₄	3.3229 ₁	3.3342 ₁
	c/a			0.53355 ₄	0.53450 ₅	0.53714 ₆	0.5444 ₁	0.5484 ₁
	$V(\text{\AA}^3)$			108.346 ₁	108.001 ₁	107.548 ₂	107.216 ₅	106.737 ₅
Metal-metal distances (\AA)								
	Fe(3f)-Fe(3f)	Intralayer	$\times 2$	2.758 ₁	2.7475 ₂	2.732 ₁	2.718 ₂	2.705 ₂
	Mn/Fe(3g)-Mn/Fe(3g)	Intralayer	$\times 4$	3.29010 ₃	3.29051 ₃	3.29673 ₄	3.32292 ₃	3.33419 ₃
	Mn/Fe(3g)-Fe(3f)	Interlayer	$\times 1$	2.644 ₃	2.653 ₄	2.658 ₇	2.655 ₈	2.676 ₅
		Interlayer	$\times 2$	2.743 ₂	2.733 ₃	2.725 ₆	2.725 ₇	2.704 ₄
		Mean distance		2.71 ₄	2.706 ₆	2.703 ₉	2.702 ₈	2.695 ₈
Metal-nonmetal distances (\AA)								
	Fe(3f)-P/Si(2c)	Intralayer	$\times 2$	2.3219 ₇	2.3203 ₇	2.3160 ₆	2.3028 ₉	2.295 ₁
	Fe(3f)-P/Si(1b)	Interlayer	$\times 2$	2.2895 ₇	2.2854 ₈	2.2813 ₇	2.285 ₁	2.285 ₁
		Mean distance		2.306 ₁	2.303 ₂	2.2987 ₉	2.294 ₁	2.290 ₁
	Mn/Fe(3g)-P/Si(2c)	Interlayer	$\times 4$	2.4921 ₈	2.492 ₂	2.492 ₂	2.492 ₃	2.498 ₂
	Mn/Fe(3g)-P/Si(1b)	Intralayer	$\times 1$	2.504 ₃	2.489 ₅	2.475 ₉	2.46 ₁	2.425 ₆
		Mean distance		2.495 ₃	2.491 ₆	2.489 ₉	2.486 ₁	2.483 ₇

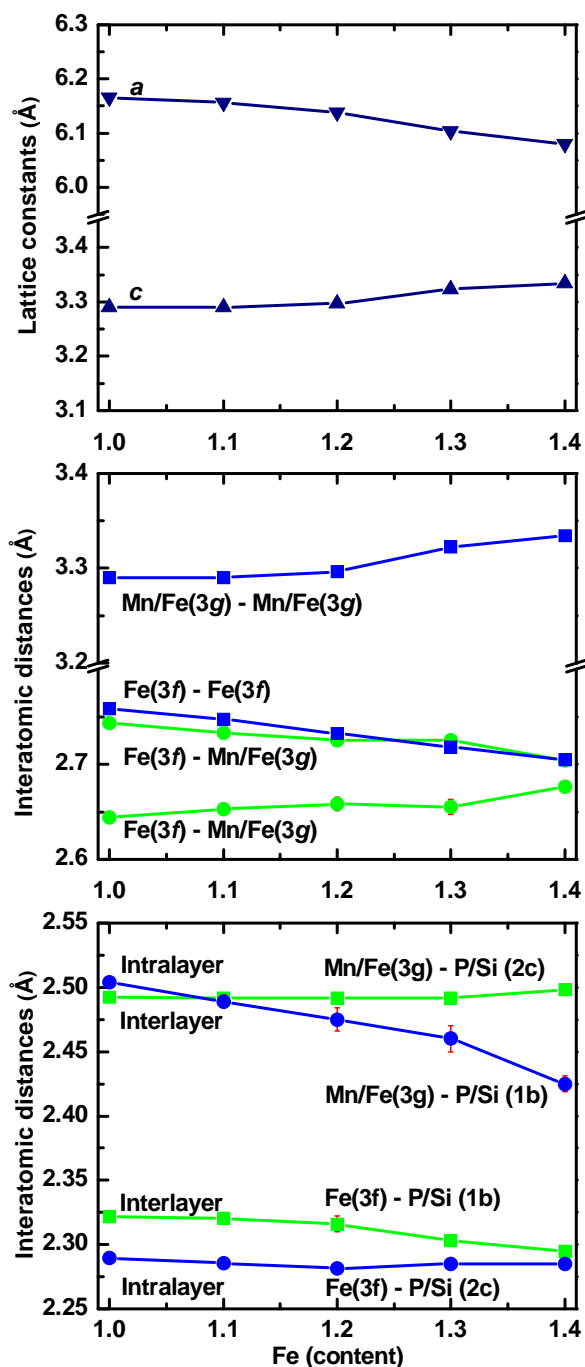


Figure 9.4 Lattice parameters and interatomic distances as a function of the Fe content derived from neutron diffraction patterns measured at 10 K for the Mn_{1.95-x}Fe_xP_{2/3}Si_{1/3} compounds with x = 1.0, 1.1, 1.2, 1.3 and 1.4.

Fe on the 3g sites. We find that the Mn/Fe(3g)-Mn/Fe(3g) interatomic distance is about ~ 3.2 Å and increases with increasing Fe content (see Table 9.3). The Mn/Fe(3g)-Mn/Fe(3g) interatomic distance is larger than the average Mn/Fe atomic radius (1.27 Å for Mn and 1.68 Å for Fe), in agreement with a more localized character of the moments on the 3g site.

The Fe(3*f*)-Fe(3*f*) interatomic distance is about ~ 2.7 Å and decreases with increasing Fe content and the value (see Table 9.3). The Fe(3*f*)-Fe(3*f*) interatomic distance is smaller than the average Fe atomic radius, favoring the itinerant magnetism on the 3*f* sites.

9.5 Influence of site disorder on the stability of the crystal structure

Figure 9.4 shows the variation of the lattice parameters and the distances between the magnetic atoms and the nearest neighbors as a function of Fe content. Replacing Mn(3*g*) with the smaller Fe atom reduces the cell volume (see Table 9.1 and 9.2), decreases the *a* and increases the *c* lattice parameters. The alternating 3*g* and 3*f* layers are parallel to the *a-b* plane of the hexagonal structure. The average interatomic distances within 3*f* and 3*g* layers change in opposite sense with increasing Fe content, the intralayer Fe(3*f*)-Fe(3*f*) distance decreases, while the intralayer Mn/Fe(3*g*)-Mn/Fe(3*g*) distance increases. The lattice parameter *c* increases with increasing Fe content, while the interlayer interatomic mean-distance Mn/Fe(3*g*)-Fe(3*f*) decreases due to the rearrangement of their displacement, which cants the Mn/Fe(3*g*)-Fe(3*f*) bond towards the *c*-axis. Meanwhile, we find that microstrain develops with increasing Fe content and that it is partially released at high temperatures (see Table 9.1 and 9.2). Apparently, introducing Fe atoms into the 3*g* site is not energetically favorable in this layered structure, where the Fe and Mn atoms tend to have different preferred occupancies. Moreover, the mean interlayer interatomic distance Mn/Fe(3*g*)-Fe(3*f*) changes opposite that of the *c* lattice parameter (see Table 9.3). These opposing trends of the atomic displacements are probably the reason for the induced microstrain, the driving force of such a distorted structure. Note that, we find that further increasing the Fe content ($x = 1.8$) leads to a collapse of the hexagonal crystal structure and the formation of the body-centered orthorhombic crystal structure (see Chapter 7). Thus, the role of Mn in the Fe-rich Mn-Fe-P-Si compounds is that of stabilizing the hexagonal crystal structure.

9.6 Conclusions

The high magnetic moments and the easily tunable working temperatures make the Fe-rich Mn-Fe-P-Si compounds promising magnetocaloric materials. The alignment of the magnetic moment is canted from nearly the *a-b* plane towards *c*-axis with increasing Fe content in the Fe-rich $Mn_{1.95-x}Fe_xP_{2/3}Si_{1/3}$ compounds with $1.0 \leq x \leq 1.4$. The canted magnetic moment alignment confirms a low magnetic anisotropy of the Mn-Fe-P-Si compounds, which display properties close to that of soft magnets. The magnetic moments are enhanced on both the 3*f* and 3*g* sites by introducing Mn atoms into the 3*g* sites. Decrease of the Mn/Fe ratio on the 3*g*

sites does not affect the Mn/Fe(3g) magnetic moment, but results in a gradual decrease in the magnitude of the Fe(3f) magnetic moment, supporting the description of the 3f sites as weakly magnetic. Microstrains develop with decreasing Mn content, and are proposed to be caused by the inconsistent change of the intralayer and interlayer interatomic distances with respect to the changes in a and c lattice constants, respectively. Hence, the Mn favors not only the high magnetic moment, but also the hexagonal crystal structure of the Fe-rich Mn-Fe-P-Si compounds.

References

- [1] O. Tegus, E. Brück, K.H.J. Buschow and F.R. de Boer, Transition-metal-based magnetic refrigerants for room-temperature applications, *Nature* 415 (2002) 150-152.
- [2] E. Brück, Developments in magnetocaloric refrigeration, *Journal of Physics D: Applied Physics* 38 (2005) R381-R391.
- [3] V.K. Pecharsky and K.A. Gschneidner, Giant magnetocaloric effect in $Gd_5(Si_2Ge_2)$, *Physical Review Letters*, 78 (1997) 4494-4497.
- [4] L. Zhang, O. Može, K. Prokešc, O. Tegus and E. Brück, Neutron diffraction study of history dependence in $MnFeP_{0.6}Si_{0.4}$, *Journal of Magnetism and Magnetic Materials* 290 (2005) 679-681.
- [5] N.H. Dung, Z.Q. Ou, L. Caron, L. Zhang, D.T.C. Thanh, G.A. de Wijs, R.A. de Groot, K.H.J. Buschow and E. Brück, Mixed magnetism for refrigeration and energy conversion, *Advanced Energy Materials* 1 (2011) 1215-1219.
- [6] E.K. Delczeg-Czirjak, Z. Gercsi, L. Bergqvist, O. Eriksson, L. Szunyogh, P. Nordblad, B. Johansson and L. Vitos, Magnetic exchange interactions in B-, Si-, and As-doped Fe_2P from first-principles theory, *Physical Review B* 85 (2012) 224435.
- [7] A.W. Hewat, D2B, a new high resolution neutron powder diffractometer at ILL Grenoble, *Materials Science Forum* 9 (1986) 69-80.
- [8] H.M. Rietveld, A profile refinement method for nuclear and magnetic structures, *Journal of Applied Crystallography* 2 (1969) 65-71.
- [9] J. Rodriguez-Carvajal, Recent advances in magnetic-structure determination by neutron powder diffraction, *physica B: Condensed Matter* 192 (1993) 55-69.
- [10] K.A. Gschneidner, Y. Mudryk and V.K. Pecharsky, On the nature of the magnetocaloric effect of the first-order magnetostructural transition, *Scripta Materialia* 67 (2012) 572-577.

- [11] M. Bacmann, J.L. Soubeyrou, R. Barrett, D. Fruchart, R. Zach, S. Niziol and R. Fruchart, Magnetoelastic transition and antiferro-ferromagnetic ordering in the system $MnFeP_{1-y}As_y$, *Journal of Magnetism and Magnetic Materials* 134 (1994) 59-67.
- [12] D.M. Liu, M. Yue, J.X. Zhang, T.M. McQueen, J.W. Lynn, X.L. Wang, Y. Chen, J.Y. Li, R.J. Cava, X.B. Liu, Z. Altounian and Q. Huang, Origin and tuning of the magnetocaloric effect in the magnetic refrigerant $Mn_{1.1}Fe_{0.9}(P_{0.8}Ge_{0.2})$, *Physical Review B* 79 (2009) 014435.
- [13] L. Lundgren, G. Tarmohamed, O. Beckman, B. Carlsson and S. Rundqvist, First order magnetic phase transition in Fe_2P , *Physica Scripta* 17 (1978) 39-48.
- [14] V. Hoglin, M. Hudl, M. Sahlberg, P. Nordblad, P. Beran and Y. Andersson, The crystal and magnetic structure of the magnetocaloric compound $FeMnP_{0.5}Si_{0.5}$, *Journal of Solid State Chemistry* 184 (2011) 2434-2438.
- [15] Z.Q. Ou, L. Zhang, N.H. Dung, L. van Eijck, A.M. Mulders, M. Avdeev, N.H. van Dijk and E. Brück, Neutron diffraction study on the magnetic structure of Fe_2P -type $Mn_{0.66}Fe_{1.29}P_{1-x}Si_x$ melt-spun ribbons, *Journal of Magnetism and Magnetic Materials* 340 (2013) 80-85.
- [16] H. Fujii, S. Komura, T. Takeda, T. Okamoto, Y. Ito and J. Akimitsu, Polarized neutron diffraction study of Fe_2P single crystal, *Journal of the Physical Society of Japan* 46 (1979) 1616-1621.
- [17] B. Carlsson, M. Gölin and S. Rundqvist, Determination of homogeneity range and refinement of crystal-structure of Fe_2P , *Journal of Solid State Chemistry* 8 (1973) 57-67.
- [18] E. Brück, J. Kamarad, V. Sechovsky, Z. Arnold, O. Tegus and F.R. de Boer, Pressure effects on the magnetocaloric properties of $MnFeP_{1-x}As_x$, *Journal of Magnetism and Magnetic Materials* 310 (2007) e1008-e1009.
- [19] N.T. Trung, Z.Q. Ou, T.J. Gortenmulder, O. Tegus, K.H.J. Buschow and E. Brück, Tunable thermal hysteresis in $MnFe(P,Ge)$ compounds, *Applied Physics Letters* 94 (2009) 102513.
- [20] M. Hudl, P. Nordblad, T. Bjorkman, O. Eriksson, L. Haggstrom, M. Sahlberg, Y. Andersson, E. K. Delczeg-Czirjak and L. Vitos, Order-disorder induced magnetic structures of $FeMnP_{0.75}Si_{0.25}$, *Physical Review B* 83 (2011) 134420.
- [21] N.H. Dung, L. Zhang, Z.Q. Ou, L. Zhao, L. van Eijck, A.M. Mulders, M. Avdeev, E. Suard, N.H. van Dijk and E. Brück, High/low-moment phase transition in hexagonal Mn-Fe-P-Si compounds, *Physical Review B* 86 (2012) 045134.

Summary

This thesis presents a study of the crystal and magnetic structure, the magnetocaloric effect and related physical properties in Mn-Fe-P-X compounds.

The influences of boron addition in $(\text{Mn,Fe})_2(\text{P,As})$ compounds have been studied. It is found that boron atoms occupy interstitial sites within the basal plane. First-order magnetoelastic phase-transitions with small thermal and magnetic hysteresis are observed in all these compounds. The ferromagnetic ordering temperatures increase by boron addition. The optimal working temperatures can be finely adjusted by varying the boron content without losing the good magnetocaloric properties. Both the maximal magnetic entropy changes and the Relative Cooling Power (RCP) are slightly enhanced. All these features make boron addition a good tool to tune and improve magnetic and magnetocaloric properties in $(\text{Mn,Fe})_2(\text{P,As})$ compounds. (*Chapter 4*)

The effect of transition metal substitution on T_C and ΔT_{hys} has been studied in $(\text{Mn,Fe,T})_{1.95}\text{P}_{0.50}\text{Si}_{0.50}$ ($T = \text{Co, Ni and Cu}$) compounds. X-ray diffraction patterns imply that all the compounds crystallize in the hexagonal Fe_2P type of structure. It is found that all these transition metal substitutions for Mn(3g)/Fe(3f) weaken the ferromagnetic ordering. Ni substitutions reduce the thermal hysteresis, while the Cu substitutions enhance the thermal hysteresis. Moreover, the Co substitutions for Mn(3g) reduce thermal hysteresis, while the Co substitutions for Fe(3f) result in hardly any change in thermal hysteresis. (*Chapter 5*)

Single phase compounds $\text{Mn}_{0.66}\text{Fe}_{1.29}\text{P}_{1-x}\text{Si}_x$ ($0 \leq x \leq 0.42$) have been synthesized using the melt-spinning (rapid solidification) technique. All the compounds form in the Fe_2P -type hexagonal structure, except a Co_2P -type orthorhombic structure of the Si-free $\text{Mn}_{0.66}\text{Fe}_{1.29}\text{P}$ compound. The compounds with $0.24 \leq x \leq 0.42$ present a FM-PM phase transition, while the compounds with lower Si content show an AFM-PM phase transition. By increasing the Si content from $x = 0.24$ to 0.42 , T_C increases from 195 to 451 K and ΔT_{hys} is strongly reduced

from ~ 61 to ~ 1 K. T_C increases and ΔT_{hys} decreases with increasing magnetic field. It is also found that T_C and ΔT_{hys} are not only Si content dependent, but also magnetic field dependent. $\text{Mn}_{0.66}\text{Fe}_{1.29}\text{P}_{1-x}\text{Si}_x$ compounds show large spontaneous magnetic moments with values up to $4.57 \mu_{\text{B}}/\text{f.u.}$. A large MCE with a small thermal hysteresis is obtained simultaneously in Fe-rich $\text{Mn}_{0.66}\text{Fe}_{1.29}\text{P}_{1-x}\text{Si}_x$ melt-spun ribbons. The compounds with a high working temperature may also be useful for other applications, *e.g.* thermomagnetic generators and heat pumps. (*Chapter 6*)

Single phase $\text{Mn}_{1.95-x}\text{Fe}_x\text{P}_{2/3}\text{Si}_{1/3}$ compounds with $1.0 \leq x \leq 1.95$ have been synthesized using ball-milling technology and solid-state reactions. All the compounds show a FM-PM phase transition. The compounds with $x \leq 1.6$ crystallize in Fe_2P -based hexagonal structure, for the higher Fe content compounds, a *bco-hex* structural transition is observed. In contrast to the Mn-rich Mn-Fe-P-Si system, no coupling between the magnetic and structural transition is found. The T_C and ΔT_{hys} in the $\text{Mn}_{1.95-x}\text{Fe}_x\text{P}_{2/3}\text{Si}_{1/3}$ compounds can be easily tuned by adjusting the Fe/Mn ratio. By increasing the Fe content from $x = 1.0$ to 1.95 , T_C increases from ~ 269 to ~ 647 K and the ΔT_{hys} strongly reduces from ~ 65 to ~ 1 K. The reduction in the magnetic moment of the Fe-rich $\text{Mn}_{1.95-x}\text{Fe}_x\text{P}_{2/3}\text{Si}_{1/3}$ compounds, suggests that the dominant effect on the size of the moment is the change in local electron configuration rather than the interlayer exchange coupling, thus confirming a more localized magnetism on the $3g$ sites. (*Chapter 7*)

High-resolution neutron diffraction has been employed to determine the crystal and magnetic structure, the magnetic moment and the interatomic distances in the melt-spun ribbons $\text{Mn}_{0.66}\text{Fe}_{1.29}\text{P}_{1-x}\text{Si}_x$. Introducing site disorder at the $3g$ site by replacing $1/3$ of Fe with Mn appears to enhance the magnetic interaction, while the strong magnetoelastic coupling is maintained. The Mn substitution also shows a stabilizing effect on the hexagonal crystal structure, which is maintained to a high Si content. The moment alignment within the crystallographic unit cell is affected when the Si content increases from $x = 0.34$ to 0.42 in $\text{Mn}_{0.66}\text{Fe}_{1.29}\text{P}_{1-x}\text{Si}_x$ compounds, as the canting angle with respect to the c -direction increases. The canted magnetic moment alignment confirms a low magnetic anisotropy, which ensures soft magnetic properties of Fe-rich Mn-Fe-P-Si compounds. (*Chapter 8*)

The effect of varying the Mn/Fe ratio in the $\text{Mn}_{1.95-x}\text{Fe}_x\text{P}_{2/3}\text{Si}_{1/3}$ compounds has been studied using high-resolution neutron diffraction. The alignment of the magnetic moment is canted from nearly the a - b plane towards c -axis with increasing Fe content in the Fe-rich $\text{Mn}_{1.95-x}\text{Fe}_x\text{P}_{2/3}\text{Si}_{1/3}$ compounds with $1.0 \leq x \leq 1.4$. The canted magnetic moment alignment

confirms a low magnetic anisotropy of the Mn-Fe-P-Si compounds, which display properties close to that of soft magnets. The magnetic moments are enhanced on both the 3*f* and 3*g* sites by introducing Mn atoms into the 3*g* sites. Decrease of the Mn/Fe ratio on the 3*g* sites does not affect the Mn/Fe(3*g*) magnetic moment, but results in a gradual decrease in the magnitude of the Fe(3*f*) magnetic moment, supporting the description of the 3*f* sites as weakly magnetic. Microstrains develop with decreasing Mn content, and are proposed to be caused by the inconsistent change of the intralayer and interlayer interatomic distances with respect to the changes in *a* and *c* lattice constants, respectively. Hence, the Mn favors not only the high magnetic moment, but also the hexagonal crystal structure of the Fe-rich Mn-Fe-P-Si compounds. (*Chapter 9*)

Samenvatting

Dit proefschrift presenteert een studie van de kristal- en magnetische structuur, het magneto-calorisch effect en gerelateerde fysische eigenschappen in Mn-Fe-P-X verbindingen.

De effecten van boriumadditie in $(\text{Mn,Fe})_2(\text{P,As})$ verbindingen zijn bestudeerd. Gevonden werd, dat boriumatomen interstitiële sites binnen het grondvlak innemen. Eerste-orde magnetoelastische faseovergangen met kleine thermische en magnetische hysteresis zijn waargenomen in al deze verbindingen. De ferromagnetische ordeningstemperaturen verhogen door boriumadditie. De optimale werktemperaturen kunnen fijn worden afgestemd door het boriumgehalte te variëren zonder de goede magnetocalorische eigenschappen te verliezen. Zowel de maximale magnetische entropieveranderingen als het Relatieve Koel-Vermogen (RKV) zijn licht verbeterd. Al deze eigenschappen maken boriumtoevoeging een goed instrument om de magnetische and magneto-calorische eigenschappen in $(\text{Mn,Fe})_2(\text{P,As})$ verbindingen af te stemmen en te verbeteren. (*Hoofdstuk 4*)

Het effect van overgangsmetaalsubstitutie op T_C en ΔT_{hys} werd bestudeerd in $(\text{Mn,Fe,T})_{1.95}\text{P}_{0.50}\text{Si}_{0.50}$ ($T = \text{Co, Ni and Cu}$) legeringen. Röntgendiffractiepatronen impliceren dat al deze verbindingen in de hexagonale structuur van het Fe_2P type kristalliseren. Er werd gevonden dat deze substituties door overgangsmetalen voor Mn(3g)/Fe(3f) de ferromagnetische ordening verzwakken. Ni substituties verlagen de thermische hysteresis, terwijl Cu substituties de thermische hysteresis verhogen. Verder verlagen Co substituties voor Mn(3g) de thermische hysteresis, terwijl Co substituties voor Fe(3f) nauwelijks enige verandering in thermische hysteresis bewerkstelligen. (*Hoofdstuk 5*)

Éénfasige verbindingen $\text{Mn}_{0.66}\text{Fe}_{1.29}\text{P}_{1-x}\text{Si}_x$ ($0 \leq x \leq 0.42$) werden gesynthetiseerd met de smelt-spinnen (snelle stolling) techniek. Alle verbindingen worden gevormd in de Fe_2P -type hexagonale structuur, behalve het Si-vrije $\text{Mn}_{0.66}\text{Fe}_{1.29}\text{P}$. dat een orthorhombische structuur van het Co_2P -type krijgt. De stoffen met $0.24 \leq x \leq 0.42$ laten een FM-PM faseovergang zien,

terwijl die met lager Si gehalte een AFM-PM faseovergang vertonen. Door het Si gehalte te verhogen van $x = 0.24$ tot 0.42 , stijgt T_C van 195 naar 451 K en wordt ΔT_{hys} sterk verlaagd van ~ 61 naar ~ 1 K. T_C verhoogt en ΔT_{hys} verlaagt met toenemend magnetisch veld. Eveneens werd gevonden dat de T_C en ΔT_{hys} niet alleen afhankelijk zijn van het Si gehalte, maar ook van het magnetisch veld. $\text{Mn}_{0.66}\text{Fe}_{1.29}\text{P}_{1-x}\text{Si}_x$ verbindingen laten hoge spontane magnetische momenten zien met waarden tot aan $4.57 \mu_B/\text{f.u.}$. Een hoog MCE met simultaan een kleine thermische hysteresis is verkregen in Fe-rijk uit smelt gesponnen lint van $\text{Mn}_{0.66}\text{Fe}_{1.29}\text{P}_{1-x}\text{Si}_x$. De verbindingen met een hoge werkt temperatuur kunnen ook bruikbaar zijn voor andere doeleinden, b.v. thermomagnetische generatoren en warmtepompen. (Hoofdstuk 6)

Enkefasige $\text{Mn}_{1.95-x}\text{Fe}_x\text{P}_{2/3}\text{Si}_{1/3}$ samenstellingen met $1.0 \leq x \leq 1.95$ zijn gesynthetiseerd met de kogelmolentechnologie en vaste-stof reacties. Alle verbindingen vertonen een FM-PM faseovergang. De verbindingen met $x \leq 1.6$ kristalliseren in de Fe_2P -gebaseerde hexagonale structuur, voor de verbindingen met hoger Fe gehalte, werd een *bco-hex* structurele overgang waargenomen. In contrast met het Mn-rijke Mn-Fe-P-Si systeem, werd geen koppeling tussen de magnetische en de structurele overgang gevonden. De T_C en ΔT_{hys} in de $\text{Mn}_{1.95-x}\text{Fe}_x\text{P}_{2/3}\text{Si}_{1/3}$ verbindingen kan gemakkelijk worden afgestemd door de Fe/Mn ratio in te stellen. Door het Fe gehalte te verhogen van $x = 1.0$ tot 1.95 , gaat T_C van ~ 269 naar ~ 647 K en de ΔT_{hys} verkleint van ~ 65 naar ~ 1 K. De reductie in het magnetisch moment van de Fe-rijke $\text{Mn}_{1.95-x}\text{Fe}_x\text{P}_{2/3}\text{Si}_{1/3}$ verbindingen, suggereert dat het dominante effect op de grootte van het moment de verandering in lokale elektronenconfiguratie is, veeleer dan de uitwisselingskoppeling tussen lagen, en hiermee wordt een meer gelokaliseerd magnetisme op de 3g sites bevestigd. (Hoofdstuk 7)

Hoge-resolutie neutronendiffractie werd toegepast om de kristal- en magnetische structuur, het magnetisch moment en de interatomaire afstanden te bepalen in de uit smelt gesponnen linten $\text{Mn}_{0.66}\text{Fe}_{1.29}\text{P}_{1-x}\text{Si}_x$. Het introduceren van wanorde op de 3g site door vervanging van $1/3$ van Fe door Mn lijkt de magnetische interactie te versterken, waarbij de sterke magneto-elastische koppeling behouden blijft. De Mn substitutie laat ook een stabiliserend effect op de hexagonale kristalstructuur zien, welke behouden blijft tot een hoog Si gehalte. De momentoriëntatie binnen de kristallografische eenheids cel wordt beïnvloed als het Si gehalte stijgt van $x = 0.34$ naar 0.42 in $\text{Mn}_{0.66}\text{Fe}_{1.29}\text{P}_{1-x}\text{Si}_x$ verbindingen, waarbij de hoek ten opzichte van de *c*-richting toeneemt. De scheve oriëntatie van de momenten bevestigd een lage

magnetische anisotropie, die de zachte magnetische eigenschappen van Fe-rijk Mn-Fe-P-Si verzekert. (*Hoofdstuk 8*)

Het effect van variaties in de Mn/Fe verhouding in de $\text{Mn}_{1.95-x}\text{Fe}_x\text{P}_{2/3}\text{Si}_{1/3}$ verbindingen werd bestudeerd met hoge-resolutie neutronendiffractie. De oriëntatie van het magnetisch moment verandert van bijna in het a - b vlak naar meer langs de c -as met toenemend Fe gehalte in de Fe-rijke $\text{Mn}_{1.95-x}\text{Fe}_x\text{P}_{2/3}\text{Si}_{1/3}$ verbindingen met $1.0 \leq x \leq 1.4$. De scheve oriëntatie van de magnetische momenten bevestigt een lage magnetische anisotropie van de Mn-Fe-P-Si verbindingen, welke eigenschappen laten zien in overeenstemming met zachte magneten. De magnetische momenten zijn versterkt op zowel de $3f$ en $3g$ sites door Mn atomen te introduceren op de $3g$ sites. Verlaging van de Mn/Fe ratio op de $3g$ sites beïnvloedt niet het Mn/Fe($3g$) magnetisch moment, maar resulteert in een graduele afname in de grootte van het Fe($3f$) magnetisch moment, wat de beschrijving van de atomen op de $3f$ sites als zwak magnetisch ondersteunt. Microspanningen ontwikkelen zich bij afnemend Mn gehalte. Zij worden mogelijk veroorzaakt door de inconsistente verandering van de atoomafstanden binnen en tussen de atoomlagen in vergelijking tot de veranderingen respectievelijk in de a en c roosterconstanten. Aldus veroorzaakt het Mn niet alleen het hoge magnetische moment, maar ondersteunt het ook de hexagonale kristalstructuur van de Fe-rijke Mn-Fe-P-Si verbindingen. (*Hoofdstuk 9*)

List of publications

Publications related to the work presented in this thesis:

- [1] Z.Q. Ou, L. Zhang, N. H. Dung, L. van Eijck, A. M. Mulders, M. Avdeev, N.H. van Dijk and E. Brück, Neutron diffraction study on the magnetic structure of Fe₂P-based Mn_{0.66}Fe_{1.29}P_{1-x}Si_x melt-spun ribbons, *Journal of Magnetism and Magnetic Materials* 340 (2013) 80-85. (Chapter 8)
- [2] Z.Q. Ou, L. Caron, N.H. Dung, L. Zhang and E. Brück, Interstitial boron in MnFe(P,As) giant-magnetocaloric alloy, *Results in Physics* 2 (2012) 110-113. (Chapter 4)

Other publications:

- [3] N.H. Dung, L. Zhang, Z.Q. Ou and E. Brück, Magneto-elastic coupling and magnetocaloric effect in hexagonal Mn-Fe-P-Si compounds, *Scripta Materialia* 67 (2012) 975-978.
- [4] N.H. Dung, L. Zhang, Z.Q. Ou, L. Zhao, L. van Eijck, A.M. Mulders, M. Avdeev, E. Suard, N.H. van Dijk and E. Brück, High/low-moment phase transition in hexagonal Mn-Fe-P-Si compounds, *Physical Review B* 86 (2012) 045134.
- [5] E. Brück, N.T. Trung, Z.Q. Ou and K.H.J. Buschow, Enhanced magnetocaloric effects and tunable thermal hysteresis in transition metal pnictides, *Scripta Materialia* 67 (2012) 590-593.
- [6] N.H. Dung, L. Zhang, Z.Q. Ou and E. Brück, From first-order magneto-elastic to magneto-structural transition in (Mn,Fe)_{1.95}P_{0.50}Si_{0.50} compounds, *Applied Physics Letters* 99 (2011) 092511.
- [7] N.H. Dung, Z.Q. Ou, L. Caron, L. Zhang, D.T. Cam Thanh, G.A. de Wijs, R.A. de Groot, K.H.J. Buschow and E. Brück, Mixed magnetism for refrigeration and energy conversion, *Advanced Energy Materials* 1 (2011) 1215-1219.
- [8] X.G. Liu, S.W. Or, B. Li, Z.Q. Ou, L. Zhang, Q. Zhang, D.Y. Geng, F. Yang, D. Li, E. Brück and Z.D. Zhang, Magnetic properties of Dy nanoparticles and Al₂O₃-coated Dy nanocapsules, *Journal of Nanoparticle Research* 13 (2011) 1163-1174.

- [9] X.G. Liu, Z.Q. Ou, D.Y. Geng, Z. Han, H. Wang, B. Li, E. Brück and Z.D. Zhang, Enhanced absorption bandwidth in carbon-coated supermalloy FeNiMo nanocapsules for a thin absorb thickness, *Journal of Alloys and Compounds* 506 (2010) 826-830.
- [10] X.G. Liu, Z.Q. Ou, D.Y. Geng, Z. Han, J.J. Jiang, W. Liu and Z.D. Zhang, Influence of a graphite shell on the thermal and electromagnetic characteristics of FeNi nanoparticles, *Carbon* 48 (2010) 891-897.
- [11] N.T. Trung, Z.Q. Ou, T.J. Gortenmulder, O. Tegus, K.H.J. Buschow and E. Brück, Tunable thermal hysteresis in MnFe(P,Ge) compounds, *Applied Physics Letters* 94 (2009) 102513.
- [12] L. Caron, Z.Q. Ou, T.T. Nguyen, D.T. Cam Thanh, O. Tegus, and E. Brück, On the determination of the magnetic entropy change in materials with first-order transitions, *Journal of Magnetism and Magnetic Materials* 321 (2009) 3559-3566.
- [13] X.G. Liu, Z.Q. Ou, D.Y. Geng, Z. Han, Z.G. Xie and Z.D. Zhang, Enhanced natural resonance and attenuation properties in superparamagnetic graphite-coated FeNi₃ nanocapsules, *Journal of Physics D: Applied Physics* 42 (2009) 155004.
- [14] G.F. Wang, L. Song, F.A. Li, Z.Q. Ou, O. Tegus, E. Brück and K.H.J. Buschow, Magnetocaloric effect in the La_{0.8}Ce_{0.2}Fe_{11.4-x}Co_xSi_{1.6} compounds, *Journal of Magnetism and Magnetic Materials* 321 (2009) 3548-3552.
- [15] L. Song, G.F. Wang, Z.Q. Ou, Hashaolu, Hunusitu, X. W. Li, O. Tegus, E Brück and K.H.J. Bushow, Magnetic properties and magnetocaloric effect of MnFeP_{0.5}Ge_{0.5-x}Si_x compounds, *Journal of Alloys and Compounds* 474 (2009) 388-390.

Patent

1. Ekkehard BRÜCK, Zhiqiang Ou, Lian Zhang and Luana Caron, Magnetocaloric materials, International Publication Number: WO 2011/111004 A1.

Acknowledgements

The realization of this thesis would not have been possible without helps and supports of many people. I would like to take this opportunity to express my gratitude.

First of all, I am deeply indebted to Prof. Ekkes Brück, my promoter, for giving me the opportunity to work in FAME group as a PhD candidate; for his enthusiastic and patient guidance and supports in my research; for the valuable advice and constructive remarks through the whole thesis work. I would like to give my special thanks to Dr. Niels van Dijk, my copromoter, for his supervision, valuable discussion, revision of manuscripts and supports in neutron diffraction measurements and data analysis.

I am very grateful to Prof. K.H. Jürgen Buschow for his valuable discussion during my PhD study and even before. Special thanks to Dr. Lian Zhang and Dr. Luana Canon, for their guidance and valuable suggestions.

I am especially grateful to Anton J.E. Lefering, Michel P. Steenvoorde and Bert Zwart for their supports in my experiments. Special thanks go to Nicole Banga, Ilse van der Kraaij and Annette Bor, who are always willing to help with arranging administrative work. Special thanks to Jouke Heringa for his support in computer and network-related issues.

I would like to thank Cam Thanh, Trung, Dung, Jose and Francois Guillou, for the great experience of working together as a team. I thank Leon, Kee and Deepak for grouping me into their “food” events. I acknowledge Theo, Kees, Lucas, Jie Yang, Anna, Anca, Romain, Shangming, Xianguo, Swapna, Kun, Xiaoyu, Shasha, Zhouzhou, Yibole, Miao, Fengjiao, Wenqin and all the other people of FAME and NPM2, for interesting conversations and pleasant atmosphere. You made my day.

Special thanks go to my dear friends from the badminton club (USSR). We had so much enjoyable time on and off courts. If you counted how much of my spare time that I had spent on badminton, you will know how much you mean to me.

I would like to give my special and deepest gratitude to Tegusi, Dagula, Song Lin, Nuomin, Lili, Yuncang Wu, Hailan and Yiliqi. Whenever I stay with you, you make me feel like that I am home again.

Last but no least are my wife Juanjuan and my parents. Love you so much.

Curriculum Vitae

Zhiqiang Ou was born on March 28th 1982 in Inner Mongolia, China.

He studied in the Inner Mongolia Normal University and received his BSc degree in science with honour in 2004. In the same year, he followed the master program in the same college and worked on the magnetocaloric material in Inner Mongolian Key Laboratory for Physics and Chemistry of Functional Materials under the supervision of Prof. Dr. O. Tegusi and Prof. L. Song. During the third year of his master study, he joined the Exchange Programme between China and the Netherlands and worked in the Van der Waals-Zeeman Institute under the supervision of Prof. Dr. E.H. Brück. He received his MSc degree in science in 2007.

After finishing his master study, he worked at Inner Mongolian Key Laboratory for Physics and Chemistry of Functional Materials as a guest research fellow.

In November 2008, he joined the research group of Fundamental Aspects of Materials and Energy at Delft University of Technology and worked on the Novel Magnetocaloric materials under the supervision of Prof. Dr. E.H. Brück. The outstanding results during his PhD research are presented in this thesis.